Effect of Post-Rolling Surface Condition on the Corrosion Resistance of UNS 32205 Stainless Steel Rebar

by

Fook Yee Yang

A thesis

presented to the University of Waterloo

in fulfillment of the

thesis requirement for the degree of

Master of Applied Science

in

Civil Engineering

Waterloo, Ontario, Canada, 2022

Author's Declaration

I hereby declare that I am the sole author of this thesis. This is a true copy of the thesis, including any required final revisions, as accepted by my examiners.

I understand that my thesis may be made electronically available to the public.

Abstract

During the winter season, ice accumulation on roads and sidewalks is a major problem and poses a hazard to road users. The most common method of addressing this issue is by applying de-icing salts or spraying a brine solution on road surfaces. Unfortunately, the use of de-icing salts and anti-icing brines has a detrimental effect on concrete infrastructure by causing corrosion of steel reinforcement and deterioration of the concrete matrix.

The issue of corrosion can be addressed by using more corrosion resistant material as reinforcement (rebar), such as stainless steel. Currently, the manufacturing process of stainless steel rebar involves a hot rolling process followed by shotblasting to remove mill scale formed during the high temperature rolling process and then acid pickling to remove the chromium depleted layer below the mill scale. Since this process is generally required by many authorities, there is little literature on the effect of mill scale on the corrosion resistance of stainless steel.

The main goal for this project is to determine the effect of surface condition due to post-rolling processes on the corrosion performance of UNS 32205 duplex stainless steel rebar. Furthermore, this project examines the condition of the mill scale after exposure to the high pH environment in concrete for an extended time. Four different surface conditions of rebar were tested as part of this project: as-rolled (no treatment), shotblasted-only, pickled-only, and both shotblasted-and-pickled.

This project is divided into three parts: rebar surface characterization, a rapid corrosion screening test, and a longer-term corrosion exposure test. Firstly, surface characterization was carried out by optical microscopy, scanning electron microscope (SEM) paired with energy-dispersive X-ray spectroscopy (EDX), and secondary ion mass spectrometry (SIMS).

The rapid screening test provides only a qualitative comparison of the corrosion resistance. For this test, six replicate lengths of rebar of each type of surface condition were cast into concrete cylinders. Sodium chloride was dissolved in the mixing water to induce active corrosion. The concrete cylinders were cured for 24 hours before being demoulded and immersed in saturated calcium hydroxide solution. The open circuit potential of the bars was monitored for 24 hours;

after which, they were anodically polarized for 96 hours. The current response in the rebar was recorded during this time. Only two of the 30 specimens exhibited active corrosion during the 96 hours of polarization. These were two of the six shotblasted-only bars. There are several possible reasons for the corrosion found in only these bars. Firstly, the shotblasting process was done using carbon steel chips as a medium. Any embedded carbon steel in the mill scale would be more susceptible to corrosion. Secondly, microscopy showed incomplete removal of mill scale from these bars. This would lead to a galvanic effect between areas with mill scale remaining and areas where mill scale had been removed, further aggravating any corrosion.

The as-rolled and pickled-only bars exhibited similar corrosion rates to those which were fully treated, i.e., shotblasted-and-pickled bars. This was unexpected because the mill scale was cracked in many places and still had a chromium depleted layer in the underlying steel. These results show that, at least in this test, as-rolled UNS 32205 rebar performs as well as those with conventional post-rolling treatments.

For more quantitative data, a modified version of the ASTM A955 macrocell corrosion test was used. In this test, rebar specimens were cast in concrete mortar rectangular blocks with a ponding well. Four replicates of each surface condition were prepared. Saturated calcium hydroxide was added to the ponding well to prevent calcium hydroxide from leaching out and maintaining a high pH environment. After 200 days, 15% sodium chloride solution was added to the ponding well of three replicates in an attempt to initiate corrosion. One replicate of each surface condition was kept without exposure to chlorides to allow observation of the effect of the high pH on the mill scale. Throughout this time, the macrocell potential of the bar was measured. Electrochemical tests were performed periodically to monitor for any corrosion activity. After 440 days, two of the three replicates exposed to chlorides were autopsied to examine the condition of the rebar. None of the bars exhibited active corrosion rates and there were no visible signs of corrosion on the autopsied bars. It was concluded from this test that a 15% sodium chloride solution is insufficient to initiate corrosion in UNS 32205 rebar in any of the surface conditions.

Acknowledgements

Firstly, I would like to thank my supervisor Dr. Carolyn Hansson for taking me on as a student, and patiently guiding me through the world of materials, metallurgy, and the *stochastic* world of corrosion. She is a source of encouragement and support not only in this research project but towards my physical and mental health throughout the COVID-19 pandemic. She has made me a better researcher, engineer, and person.

I would like to thank past and current members of my research group: Dr. Ibrahim Ogunsanya, Dr. Colin van Niejenhuis and Shelley Yang for help and advice with my various tests. In addition, Dr. Ogunsanya and Dr. van Niejenhuis have been role models as researchers and their sense of curiosity inspires me to continue to explore and learn in the field of materials and beyond.

I would like to thank the various lab technologists and technicians who had helped me with my experiments. Thank you to Richard Morrison for his guidance with fabricating formwork, specimens, and making sure I was always working safely in the lab. Thanks to Neil Griffett for his assistance with the setup of the data acquisition multimeter; Dr. Yuquan Ding for help with scanning electron microscopy, as well as Doug Hirst and Mark Griffett for their assistance in the lab. Thank you to Joseph Jessy from the Waterloo Advanced Technology Laboratory (WATLab) for his assistance with the secondary ion mass spectrometry analyses.

My research was made possible by the supply of materials from Max Aicher North America Ltd., Vector Corrosion Technologies, financial assistance from the Natural Sciences and Engineering Research Council of Canada (NSERC), and a bursary from the Department of Civil and Environmental Engineering at the University of Waterloo.

Thank you to Graeme Milligan for his countless advice on teaching and life in graduate school. Special thanks to Felix Hou, Kevin Honsberger, Mike Murage, and Nick Karl – I am lucky to have them as friends. Finally, thank you to my parents and sister for their love and support throughout all my endeavours.

Table of Contents

List of Figures

List of Tables

1 Background

Concrete is one of the most widely used materials in the world. Every year, over 10 billion tonnes of concrete are used [1]. Concrete has various advantages as a construction material. It is strong in compression, high fire resistance, low cost and can be formed into various shapes. However, concrete is weak in tension. Hence, steel reinforcing bars (rebar) are cast in the concrete to resist tensile forces in the structural member.

Southern Ontario experiences a continental climate with four distinct seasons. During the colder months, snow, and ice accumulation on roads lead to hazardous conditions for road users. This occurs approximately between November and April, that is, from late fall until early spring season. In 2017, about 30% of all vehicle collisions were reported to have occurred on wet, snowy or icy roads [2]. Hence, winter maintenance strategies are implemented by the authorities in order to reduce the formation of ice on the road. Information stations monitor road conditions and maintenance crews are deployed when a winter storm is forecasted.

Figure 1-1: Snowplows clearing snow and salting road during a winter storm [3]

Generally, maintenance crews remove by plowing and prevent ice build-up by applying de-icing salts on road surfaces. These are applied either as rock salt, pre-wetted rock salt or in the form of a brine sprayed from moving trucks, as shown in Figure 1-1. The use of pre-wetted salt or

brines allow for better coverage across the surface of the road. The salt used in the brine can be either sodium chloride, calcium chloride, magnesium chloride, or a combination of all three in a multi-chloride brine. The salt dissolves into the ice and lowers the freezing point of water, causing it to melt.

Unfortunately, the use of salts has a detrimental effect on concrete infrastructure. The brines are applied for nearly six months in a year, which causes deterioration of the concrete matrix as well as corrosion of steel reinforcement within the concrete. This damage leads to decreased service life and increased maintenance cost. The service life of a typical concrete bridge in Ontario is specified to be 75 years [4]. However, the damage from salt usage results in heavy maintenance needed after only one or two decades – far less than what is expected from the structure. Thus, the durability of reinforced concrete structures needs to be addressed in order to achieve the intended service life.

Figure 1-2: Corroded rebar causing cracking and spalling of concrete on a bridge pier [5]

The work in this project is focused on the corrosion of rebar in concrete. One solution to address the corrosion of rebar is by replacing typical carbon steel rebar with more corrosion resistant materials. There are different rebars of alternative materials available, with one option being stainless steel rebar. However, stainless steel is often overlooked due to its higher

initial cost. Given the excellent performance of stainless steel rebar in resisting corrosion, a reduction in the cost would encourage its use in public infrastructure.

One method being considered is eliminating shotblasting and pickling after the hot-rolling process. This process removes the oxide layer formed at high temperature during hot-rolling, as well as the chromium depleted layer underneath. However, it is unclear as to what extent partial or no removal of mill scale affects corrosion performance. If removal of mill scale is not necessary, this would help reduce cost of manufacturing as well as eliminate a hazardous manufacturing step. It should be noted that the mill scale on conventional carbon steel rebar is not removed before use, i.e., it is used in the “as-rolled” condition.

This project has several goals. Firstly, this project aims to determine the effect of surface condition, including removal of the mill scale and of the chromium depleted layer, on the corrosion performance of duplex UNS 32205 stainless steel rebar in concrete. Secondly, the project considers whether or not surface treatment is necessary for this grade of rebar. Finally, this project will investigate the condition of the mill scale after exposure to the high pH environment of concrete over a period of time. The performance of two different rebar lug geometries will also be compared.

2 Literature Review

2.1 Corrosion of rebar

Corrosion is an electrochemical process, which involves the oxidation of a metal leading to loss of material. Jones describes it as “a destructive result of a reaction between a metal or metal alloy and its environment” [6]. Metals naturally tend to revert to form oxides or hydroxides as a more stable compound. A complete electrical circuit is needed for corrosion to occur, where the movement of electrons and ions between the anode and cathode connects the circuit. In an electrochemical system, the anode is the location where oxidation occurs, while the cathode is the site where reduction occurs.

The fluid found in the pores within concrete have a high pH due to the presence of calcium hydroxide formed as a hydration product of cement, as well as sodium and potassium hydroxide. The high pH (>12.5) results in the formation of a passive protective oxide layer on the steel. A reduction in pH will result in the breakdown of this passive film, which causes the bar to become more susceptible to active corrosion. The stability of iron, its ions and oxides as a function of pH of the environment and electrochemical potential is shown in Figure 2-1 [7].

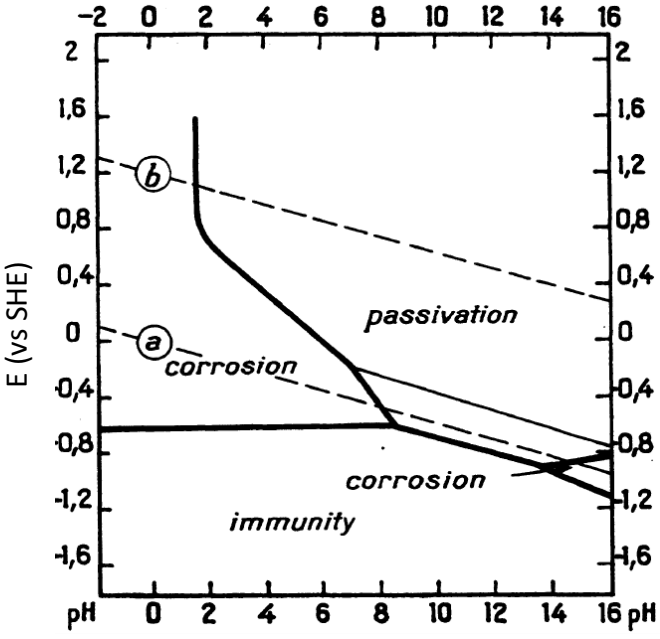

Figure 2-1: Thermodynamic conditions for passivity, immunity and corrosion of iron, Fe, at 25°C assuming passivation by films of Fe_2O_3 and Fe_3O_4 [7]

For steel rebar cast in concrete, a number of different oxidation products may be produced at the anode [8]. These are shown on Table 2-1. Where the pH of the environment surrounding the rebar remains high, oxides form a thin protective layer over the base metal, limiting the corrosion rate to a negligible level. However, when the pH decreases, these oxides are produced more rapidly, leading to severe loss of rebar cross-section as well as spalling of the concrete due to the expansive corrosion products. Furthermore, an acidic pH leads to the dissolution of iron metal into iron ions. At the cathode, water and oxygen are converted into hydroxide ions. Where oxygen supply is limited, hydrogen gas is produced.

Table 2-1: Reactions at the anode and cathode [8]

Anodic	**Cathodic**
$3Fe + 4H_2O \rightarrow Fe_3O_4 + 8H^+ + 8e^-$	$2H_2O + O_2 + 4e^- \rightarrow 4OH^-$
$2Fe + 3H_20 \rightarrow Fe_2O_3 + 6H^+ + 6e^-$	$2H^+2e^- \rightarrow H_2$
$Fe + 2H_2O \rightarrow HFEO_2^- + 3H^+ + 2e^-$	
$Fe \rightarrow Fe^{2+} + 2e^-$	

When considering the corrosion of rebar, macrocell or microcell corrosion may occur.

Microcell corrosion occurs when the anode and cathode are located on the same bar. In other words, the site of active corrosion and cathodic reaction are nearby each other. At the anode, electrons are produced from oxidation which feed the cathodic reaction. Microcell corrosion is difficult to determine directly without destructive testing (i.e., exposing the rebar in the concrete), and is often neglected. However, this may be problematic since it is easier for the anodic and cathodic reactions to occur on the same bar. This is because the distance travelled by the electron is much shorter on the same bar compared to a cathode on a different bar [9].

Macrocell corrosion occurs when the anodic and cathodic reactions occur on different rebars. This occurs when there is a grid or a rebar mat present, where rebars are laid perpendicular to each other. The rebars are in contact which allows for electron flow between separate bars. An example of macrocell corrosion can be illustrated by a bridge deck. The highest concentration of chlorides is often found at top layer of rebar on a bridge girder, having diffused through the

surface. Hence, the top layer of rebar would begin corroding as the anode while the chloride-free rebar at the bottom mat becomes the cathode, being electrically connected by stirrups. Macrocell corrosion measurements are increasingly popular since they are simpler and could be performed without the expensive equipment needed for microcell measurements [9].

2.2 Deleterious effect of chlorides on corrosion

As discussed earlier, steel rebar is protected by a passive layer when embedded in concrete. This passive layer is formed by oxidation of the metal substrate on the surface. However, this passive layer can be broken down when chlorides are present. If there is a high enough anodic potential on the film, ferrous (Fe^{2+}) and ferric ions (Fe^{3+}) are produced from the hydrated passive film. The ions attract negatively charged chloride ions to the surface of the film. The chloride ions react with the oxide to produce $FeCl_2$ or FeOCl, which subsequently dissociates in water, releasing the chloride ions to "recycle" and repeat the above process to displace and destroy the passive film [10].

Marcus et.al. [11] proposed a model for the breakdown of the passive film at the grain boundaries of the film. Chloride ions, Cl^- in the electrolyte compete with hydroxyl ions, OH^- for adsorption on the surface of the passive film. This lowers activation energy for transfer of metal cations, leading to faster local thinning of the passive layer. The authors suggested that grain boundaries are less resistive to ion transfer, leading to local depassivation around the grain boundary. This causes a depressed surface topography in that local area which leads to pitting corrosion.

2.3 Manufacturing of stainless steels

Stainless steels are defined as iron-based alloys that contain at least 11% of chromium [12]. Additional alloying elements are often added to control the structure and mechanical properties and to further enhance the corrosion resistance. Iron-chromium alloys were observed to show resistance to oxidizing agents in experiments as early as the 19th century [13]. Their superior corrosion resistance led to the increasing use of these alloys in a wide variety of applications from turbines blades in power stations to bridges and household cutlery. Stainless

steels can be classified into several categories, including austenitic, duplex, ferritic, and martensitic.

The manufacturing of stainless steel rebar involves several stages. Firstly, the steel is melted in an electric arc furnace and cast into billets. The billets are then hot-rolled until they reach the appropriate diameter of bar required. The ribs or deformations on the bar are also created at this stage by the rollers. After that, typically the stainless steel will undergo shotblasting and pickling to remove the oxide layer that forms during the high temperature processes. This process and the oxide layer will be further discussed in upcoming sections.

2.4 Use of stainless steel for rebar

Austenitic stainless steels are most commonly used for reinforcement in concrete. Experimental testing has shown that the corrosion resistance of stainless steel rebar is far superior compared to carbon steel rebar [14] as well as carbon steel with coatings [15]–[17]. Table 2-2 shows several grades of stainless steel commonly used for rebar:

Table 2-2: Typical alloys used in rebar and their alloying elements [18]

UNS Designation	Type	Composition %						
		Carbon, C	Manganese, Mn	Chromium, Cr	Nickel, Ni	Molybdenum, Mo	Nitrogen, N	Other Elements
Austenitic Grades								
S24100	XM-28	0.15	11.00-14.00	16.50 - 19.50	0.50 - 2.50	-	0.20-0.45	S 0.03, Si 1.00
S31600	316	0.08	2.00	16.00 - 18.00	10.00-14.00	2.00-3.00	0.10-0.16	P 0.045, S 0.03, Si 1.00
Duplex (Austenitic-Ferritic)								
S32205	2205	0.03	2.00	22.00 - 23.00	4.50 - 6.50	3.00-3.50	0.14-0.20	P 0.04, S 0.04, Si 1.00
S32304	2304	0.03	2.50	21.50 - 24.50	3.00 - 5.50	0.05-0.60	0.05-0.20	P 0.04, S 0.04, Si 1.00, Cu 0.05-0.60

However, different alloys of stainless steel have varying levels of corrosion performance, depending on the alloying elements. Nickel has been shown to improve corrosion resistance, where austenitic stainless steels such as AISI 316 and 304 outperforms stainless steel alloys with lower or no nickel content [19]–[21]. Next, an increased proportion of chromium also improves corrosion resistance [22], [23]. It is important to consider this in terms of stainless steel alloys, since high chromium alloys alone does not perform as well as stainless steels [24], [25] as their levels of chromium are lower compared to stainless steel.

Meanwhile, molybdenum was observed to provide increased resistance to pitting corrosion [26]–[28]; however, this effect may not be as pronounced for austenitic alloys as the pH of the surrounding increases [19], [28], [29]. The beneficial effect of molybdenum was observed to be more prominent in ferritic alloys compared to austenitic grades, even in high pH environments. This was also observed in duplex alloys, where molybdenum present in the less resistant ferrite phases improve their resistance to corrosion [28], [29].

Although carbon steel reinforcement is typically used in concrete, the use of stainless steel rebar has been documented as far back as the early 20th century. One such example is the Progreso Pier in Yucatán, Mexico which was completed in 1941. In the 1980s, an extension was added to the pier to accommodate increasing commercial activity, making it the longest pier in the world at 6.5km long. It was reinforced using 30 mm diameter UNS 30400 stainless steel rebar, which was novel at the time of construction. After 80 years in service, the pier was reported to be in good shape, with minimal deterioration despite having no maintenance in its lifetime [30].

More recently, various other projects have utilized stainless steel rebar as shown in Table 2-3.

Table 2-3: Recent projects utilizing stainless steel reinforcement
[*courtesy of the International Zinc Association*]

Project	Location	Amount (tonnes)	Alloy
New Champlain Bridge	Montréal	17,000	AISI 2304
Hong Kong-Zhuhai-Macau Bridge	Hong Kong	11,000	AISI 2304
Sakonnet River Bridge	Rhode Island	800	AISI 2205
Daniel Hoan Bridge	Wisconsin	5,000	AISI 2304
Sitra Causeway Bridge	Bahrain	6,400	AISI 2205, 2304
Kenaston Overpass	Manitoba	200	AISI 2304
Gardiner Expressway	Ontario	5,000+	AISI 2205

2.5 Mill scale on stainless steel

During the hot rolling process, a mill scale forms on bare stainless steel. Mill scale is the general term used to describe the oxide layer that forms on the surface of steel at high temperature as the steel billet is hot rolled into the shape of a cylindrical bar. These oxides are not perfect and may contain an excess or deficit of metal or oxygen ions [6].

The mill scale on stainless steel is made up of primarily haematite Fe_2O_3, magnetite Fe_3O_4, chromium (III) oxide Cr_2O_3, and the $FeCr_4O_3$ spinel [31], [32]. The distribution of these compounds varies with depth of the mill scale. Li et. al. [33] described it as an external layer of haematite and magnetite, and a more dense internal layer of $(FeCr)_3O_4$ spinel. This was observed on duplex steels as well as ferritic and austenitic grades [33], [34]. Hamadou [35] reports that FeOOH is also present close to the surface of the mill scale. Meanwhile, if the alloy contains nickel and molybdenum, small amounts of each may be found in the inner layer.

Chromium oxidizes preferentially compared to iron and nickel, which creates a chromium depleted layer immediately underneath the oxide. In austenitic and duplex grades, this layer becomes a nickel-enriched austenitic layer [34]. Around austenitic grains, “nodules” of oxide form since austenite oxidizes more easily compared to ferrite. This is a consequence of the higher concentration of chromium in ferrite phases [28], which form a thin, dense layer of

chromium oxide at the start, limiting further oxidation while oxide thickness around austenite phases grow further. However, this was found to be mainly prevalent in a mixed methane and air environment compared to air alone [33].

It is important to differentiate between a passive layer and the oxide layer that forms at high temperatures. A passive layer is a 3 – 20 nanometer-thick oxide layer formed when exposed to oxygen in air or hydroxide ions in solution [36], [37]. On the other hand, mill scale, which forms at high temperatures, is much thicker at about 10 micrometers [31]. This thickness depends on the temperature at which the oxidation occurs, where increased temperature leads to increased thickness [32].

Oxide layers are described as resembling a semiconductor due to the presence of vacancies and interstitial ions. This is crucial since it helps describe how electrons and ions move through the oxide layer, directly affecting corrosion behaviour of the base metal. Consequently, the multilayer composition of stainless steel mill scale has also been described as a semiconductor. A study by Hakiki et. al. [38] involved growing oxide films on AISI 304 stainless steel at temperatures between 50- and 450°C. Auger analysis depth profiles revealed an inner layer of mixed iron-chromium oxide region, and an outer iron oxide region. Capacitance measurements revealed similar behaviour to that of passive films on stainless steel. In other words, the inner layer behaved like a p-type semiconductor, while the outer layer is similar to an n-type semiconductor. These observations were echoed by Hamadou et. al. [35]. Hence, from these observations, it can be postulated that the electronic behaviour of passive films can also be attributed to mill scale layers.

Meanwhile, different alloying elements will affect the defect structure of the oxide. Montemor et. al. [32] found that molybdenum reduces the number of electron donors in the outer iron oxide layer. This effectively reduces the conductivity of the oxide layer, effectively reducing the dissolution of the base metal.

2.6 Effect of mill scale on corrosion

The mill scale has been shown to affect corrosion resistance of carbon steel in high pH. If the mill scale layer is flawless and undisturbed, it is a protective layer which prevents the metal underneath from oxidizing. This is because it forms a physical barrier which blocks the loss of electrons from the bare metal. Hamadou et. al. [35] reports that stainless steel with a thermally formed oxide film had a current density an order-of-magnitude lower than that of samples without the film, showing that the film had a protective influence on the oxidation of the base metal.

Marcotte et.al. [39] studied corrosion products on carbon steel plates immersed in cement paste. It was found that corrosion initiated on surfaces with an adherent mill scale before surfaces which had the mill scale removed. Observations showed that the surface of the mill scale was irregular and uneven, with many small pits. These small pits were hypothesized to be sites where crevice corrosion could initiate.

Ghods et. al. studied the properties of mill scale on carbon steel rebar, and its effect on depassivation of the rebar [40]. Similar to Marcotte and Hansson's work above, the surface of the mill scale contained defects and crevices, which can lead to crevice corrosion. The authors observed that numerous voids and crevices were present at the interface between steel and mill scale. In addition, the mill scale was found to be varied in thickness, uniformity, and microstructure. This is to be expected since it is a by-product of the manufacturing process. This study also showed that corrosion often initiated in the crevices between the mill scale and steel. The authors speculated that the composition of the solution in crevices would have initially resembled pore solution, but over time they evolve using a process similar to crevice corrosion. It may be concluded that without these voids, corrosion would not have initiated.

However, Pillai and Trejo showed some contrasting results with their study on carbon steel and stainless steel rebars [41]. Their tests showed that low alloy carbon steel rebar (ASTM A706) had a lower critical chloride threshold (i.e., less chloride is needed to initiate corrosion) when the mill scale is present compared to bars which had the mill scale removed. In other words, rebar with mill scale present performed worse compared to rebar with mill scale removed.

However, the ASTM A615 carbon-steel rebar performed better in the as-received condition. There were several explanations put forward for the results. Firstly, it was hypothesized that the A615 rebar had a much more homogeneous mill scale in the as-received condition compared to the A706 rebar. This allowed the mill scale on the A615 rebar to perform well as a protective barrier and reduce movement of chlorides to the steel substrate.

Hurley and Scully investigated the chloride thresholds of different rebar alloys in concrete with different surface conditions [42]. In their tests, UNS 32101 and Fe-9%Cr rebar were tested with mill scale present and compared with as-received carbon steel. They reported that the alloyed rebars with mill scale present performed equally with carbon steel bars in saturated calcium hydroxide, $Ca(OH)_2$, negating the beneficial effect of alloying elements. This was attributed to the formation of a chromium depleted layer under the mill scale. Chromium oxidizes preferentially at high temperatures, causing a decrease in chromium composition at the outer depths of the metal substrate.

2.7 Shotblasting and pickling of stainless steel rebar

As described previously, the mill scale is removed from stainless steel rebar by shotblasting and then pickling. Shotblasting is done by firing small projectiles to physically remove oxide layers. The materials used include stainless steel chips or sand. Shotblasting improves the effectiveness of the subsequent pickling process since some of the less adherent scale can be removed physically without requiring a chemical reaction to break them down. Surface defects can be induced from the impact of the projectiles, and work hardening may occur.

Shotblasting as a technique to remove mill scale has been shown to affect corrosion performance of rebar. Ding and Poursaee showed that the corrosion performance of carbon steel rebar increased as sandblasting time increased [43]. After removal of the mill scale, stainless steel is pickled in an acid bath in order to remove the chromium-depleted steel surface [44]. The pickling process involves immersing the bars in concentrated hydrofluoric acid, HF, and nitric acid, HNO_3. Both acids play a distinct role in the pickling process. HF performs several

functions including being a complexing agent to form complex ions with Fe^{3+}, destroying the passive layer. The addition of HF also increases the rate of dissolution of the metal [44]. Meanwhile, HNO_3 acts as the main dissolution agent for oxide scales, as well as a passivating agent and a source of hydrogen ions. This acid removes the chromium depleted layer, with the following reactions [44]:

$$Fe + 4H^+ + NO_3^- \rightarrow Fe^{3+} + NO + 2H_2O$$
$$Cr + 4H^+ + NO_3^- \rightarrow Cr_3^+ + NO + 2H_2O$$
$$3Ni + 8H^+ + 2NO_3^- \rightarrow 3Ni^{2+} + 2NO + 4H_2O$$

The reactions involving HNO_3 seen above will result in the release of nitrous oxide gas, NO. This gas is then oxidized in air to form nitrogen dioxide. This gas is a contributor to acid rain and harms the human respiratory tract. In addition, both acids used in this process are themselves hazardous to human health.

Furthermore, in some cases, the pickling of stainless steels could negatively affect corrosion resistance if not performed correctly, especially if they are immersed for too long. Ogunsanya et. al. [45] conducted tests with several randomly selected batches of stainless steels from three different manufacturers. Some batches were received with micropits on the surface, which were hypothesized to be a result of over-pickling and a lack of quality control. They acted as corrosion initiation sites on subsequent exposure to chlorides. Thus, it would be an advantage to avoid pickling if it is not necessary to achieve the required level of corrosion performance.

In closing, studies have shown how mill scale affects corrosion resistance of stainless steel in general; however, few studies have been made on the mill scale of stainless steel rebar specifically when cast in concrete (as opposed to testing in pore solution). Most tests seen in literature, such as those described above, have been conducted on thermally formed oxides which were deliberately grown, rather than a specimen with mill scale forming randomly during the hot rolling process.

There is also little information on the state of the mill scale after being in a high pH environment for an extended period of time. Typically, the mill scale (and chromium-depleted layer) on stainless steel is removed by the producer before delivery to the end user. Hence, most users often make use of stainless steel without considering any beneficial effects of the mill scale that may have been present.

3 Materials and Experimental Procedure

In order to evaluate the influence of post-rolling surface treatments, the experimental procedure included a rapid screening test which provided a relative measure of corrosion resistance and a longer-term test which provided more quantitative corrosion data.

3.1 Rebar types

The work in this thesis was conducted using UNS32205 stainless steel rebar. As shown on Table 2-3 in Chapter 2, this is a common alloy of stainless steel used in recent construction projects. The rebar samples received from the manufacturer was analyzed by X-ray fluorescence to verify the composition of the alloy against those specified by AISI. The results are shown in Table 3-1.

Table 3-1: Composition of stainless steel rebar as-received

Element	**Composition (wt. %)**	**Range specified by SAE/AISI** [18]
Iron, Fe	67.81	n/a
Chromium, Cr	21.91	22.0-23.0
Nickel, Ni	5.15	4.50-6.50
Molybdenum, Mo	3.00	3.00-3.50
Manganese, Mn	1.68	2.00 max

The results show that the composition of chromium is narrowly below the range specified for UNS 32205. All other major requirements are met for the alloy. The composition of carbon was not determined since XRF is not able to quantitatively identify elements smaller than nitrogen (atomic number 7) accurately.

Bars with four different surface treatments were used in this test. One of them, the shotblasted-and-pickled bar, had two sets with different lug or rib patterns. All the bars are identified in Table 3-2 and shown in Figure 3-1 and Figure 3-2.

Table 3-2: Type of surface treatment and rib type for each rebar sample

Specimen Label	Treatment	Rib Type
AR	As-rolled – no treatment	Threaded
PK	Pickled only	Classic
SBO	Shotblasted only	Threaded
PKSB	Shotblasted and pickled	Classic
PKSBT	Shotblasted and pickled	Threaded

The as-rolled rebar was tested as received from the supplier. The shotblasted-only rebar received a shotblasting treatment using chips of carbon steel. The pickled-only rebar received an acid bath treatment which contained a mixture of hydrofluoric acid, HF and nitric acid, HNO_3. Meanwhile, the shotblasted-and-pickled are first shotblasted and then pickled, as per typical stainless steel treatment procedure [44].

Figure 3-1: Rebar with different surface treatments – (from top) as-rolled, shotblasted-only, pickled-only, pickled-and-shotblasted

The two lug types are shown in Figure 3-2 below. The classic lug type features a diagonal rib pattern on each half of the bar, and a rectangular longitudinal rib with sharp edges. This rib pattern is the most commonly found pattern available in North America. The threaded lug, which was developed in Europe, features a repetitive rectangular rib with rounded edges and no longitudinal rib. The lug is not continuous along the entire circumference; rather they are present on each half of the circumference with a slope down to the surface of the bar.

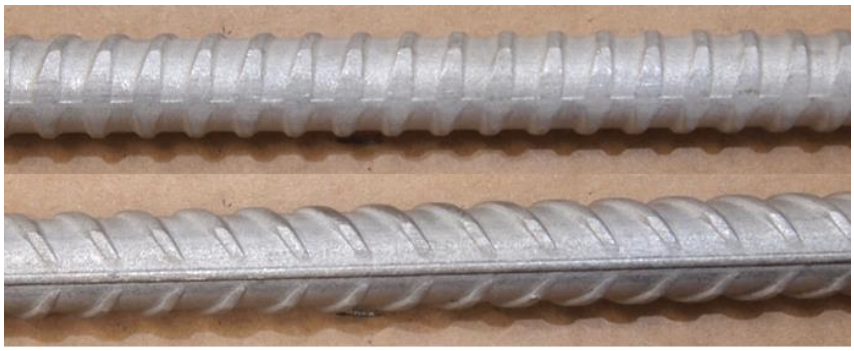

Figure 3-2: Threaded lug (top) and classic lug (bottom) on rebar

3.2 Experimental procedure

3.2.1 Surface characterization

Surface characterization involved the use of microscopy and spectroscopy techniques to examine the physical surface and analyze chemical composition of the rebar. Each technique is described in further detail in the following sections.

3.2.1.1 Optical microscopy

Optical microscopy was used to examine the curved surface of the rebar. The rebar specimens were prepared by cutting the rebar into two-inch lengths. The rebar was then cut in the longitudinal plane such that a length of rebar with a hemisphere cross-section was obtained. The curved surface was cleaned using isopropanol.

The curved surface was observed under a stereo microscope and the condition of surfaces of rebar with different surface treatments were compared, and micrographs of the different surfaces were taken. The condition of the surface was noted, specifically considering the consistency of any mill scale and presence of deformities or cracking on the surface.

Figure 3-3: Rebar longitudinal sections for microscopy

3.2.1.2 Scanning electron microscopy and energy-dispersive spectroscopy

Following optical microscopy, the surface of the bars were further characterized by scanning electron microscopy (SEM) and energy dispersive X-ray spectroscopy (EDS). They were observed and analyzed in two different geometries: as the longitudinal sections shown above and as cross-sections mounted in resin, shown in Figure 3-4.

Figure 3-4: Mounted rebar cross-section in resin

A scanning electron microscope creates an image of the specimen by focussing a beam of electrons at the specimen in a vacuum chamber. Specimens are placed in a vacuum chamber for SEM so that there are minimal foreign atoms which could interfere with the electron beam. These electrons collide with atoms of the specimen, and the energy transmitted to the atom

during the collision results in the emission of electrons from the atom known as “secondary electrons”. These electrons could be from the outermost (or valence) shell of the atom, or inner shells. The secondary electrons emitted from the sample are received by a detector. Software calibrated with the detector analyzes the change in energy of the electrons to produce an image.

Energy dispersive X-ray spectroscopy is an analysis, which can be conducted as part of SEM. EDS is integrated as part of the SEM instrument and is used to identify composition of elements of a specimen. While SEM imaging requires the detection of secondary electrons, EDS makes use of emission of X-rays from the specimen. In the emission of secondary electrons from the specimen, some are a result of electrons being displaced from the inner shell of atoms of the specimen. When these electrons are displaced, the electrons in the outer shell (or valence shell) move to fill vacated space in the inner shell with a lower energy level. This movement result in the emission of X-rays. An EDS detector contains a crystal which detects and absorbs the emitted X-rays. The absorbed energy produces electrons which are read as electrical charge signals. Individual elements will produce X-rays of different magnitudes depending on size of the atom and distance travelled by electrons from outer to inner shell.

The longitudinal sections used for SEM and EDS were the same specimens that had been used for optical microscopy as shown earlier in Figure 3-3. EDS was performed to identify the composition of mill scale on the surface of the specimen.

Mounted cross-sections were prepared by cutting a one-inch length of bar at a 45-degree angle. The angled surface was hot mounted in a carbon-based conductive resin. Each specimen was then ground with silicon carbide paper of increasing grit from 120 to 800 grit. Fine polishing was continued with diamond polishing suspension up to 1 micrometer in size. The specimens were then cleaned with soap and water and degreased with isopropanol. Similar to the longitudinal sections, these specimens were examined using SEM and EDS.

3.2.1.3 Stereoscopic image analysis

Stereoscopy is a technique used to simulate stereo or binocular vision using overlapping two-dimensional images. This technique improves the spatial awareness obtained from images, allowing depth perception or topography of a surface to be distinguished. In the context of this project, stereoscopic image analysis was used on micrographs of the longitudinal specimens taken by SEM to identify possible holes on the surface of the rebar.

In order to analyze the SEM images, the tilt method of stereo recording was used [46]. Firstly, a micrograph was taken at a location of interest on the specimen. A prominent feature on the surface (for example, a crack) was selected as a coordination point. Then, the sample was tilted by 7° in the vacuum chamber. Using the prominent feature selected previously, the image was realigned using the coordination point such that the prominent feature is in the same location as in the previous micrograph. Then, a second micrograph was taken of the specimen. The size of the micrographs was digitally adjusted so that the width of each image is equivalent to the distance between the lenses on a stereoscope and printed. Both micrographs were placed next to each other as shown in Figure 3-5 and viewed through the stereoscope.

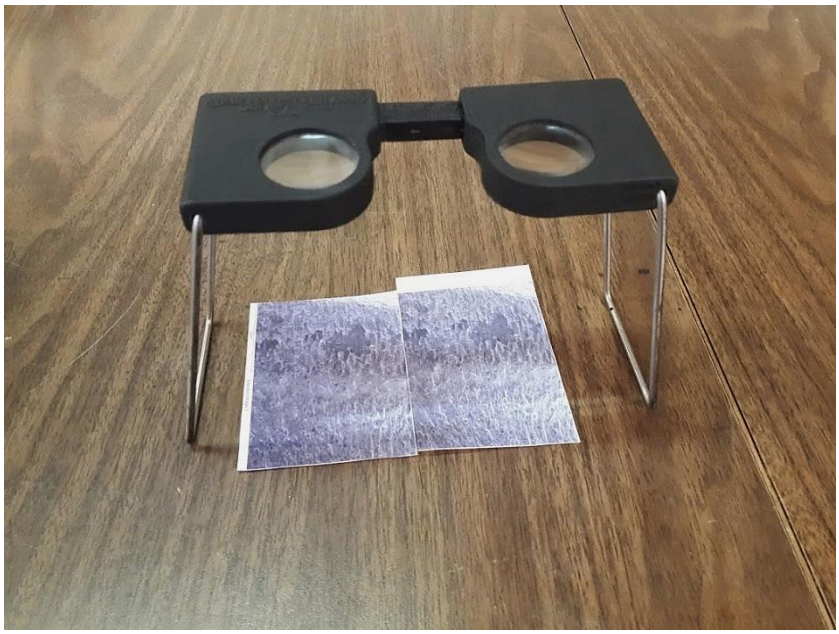

Figure 3-5: Pair of micrographs under a stereoscope

3.2.1.4 Determination of mill scale thickness from cross-section samples

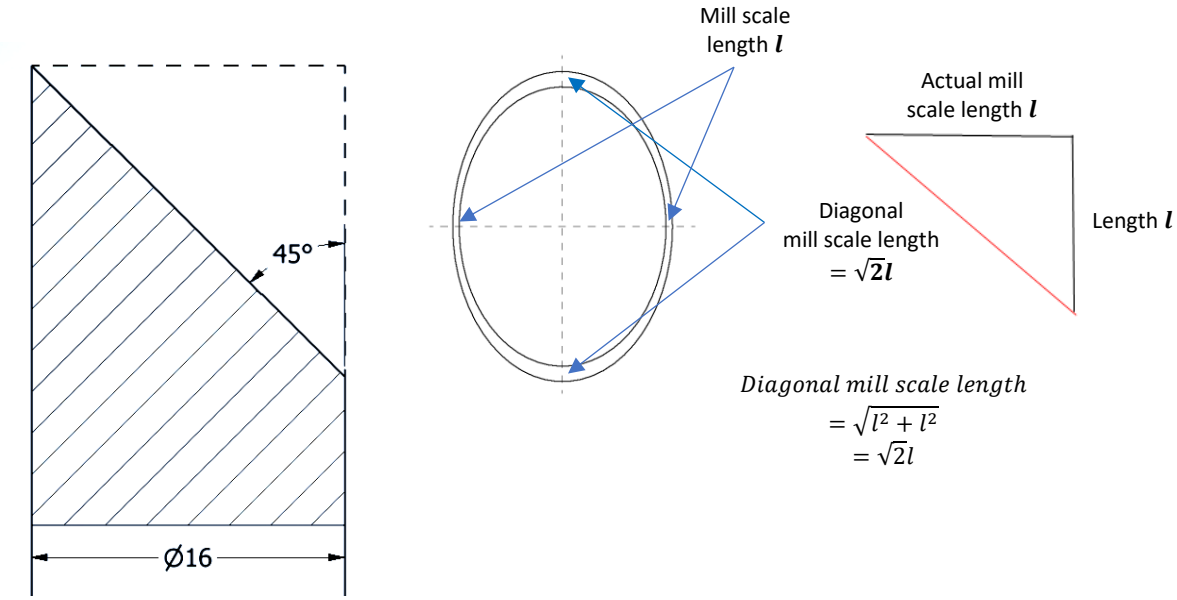

Figure 3-6: (Left) Section view showing 45-degree cut on rebar, (Middle) Diagonal cross-section with mill scale, and trigonometry used to calculate actual mill scale length

The thickness of the mill scale was measured at two points, at the tip and middle of the diagonal cross-section, as shown on Figure 3-6. At the tip of the cross-section, the mill scale is parallel to the long axis of the cut face. Using trigonometry, the 45° cut angle means that the mill scale at the tip of the cross section would be extended by a factor of $\sqrt{2}$. This was accounted for in the measurement. Meanwhile, the mill scale at the middle is perpendicular to this axis, and so the thickness of the mill scale measured is the actual thickness.

3.2.1.5 Secondary ion mass spectroscopy analysis of surface layer

A separate test was conducted to determine the composition of the surface layer with increasing depth starting with the outer surface of mill scale. This was conducted using secondary ion mass spectrometry (SIMS). The technique revolves around the interactions of a primary ion beam fired at the surface of a sample. The energy from the ions bombarding the sample surface is transferred to the atoms, which leads to emission of ions from the surface.

The emission of ions from the surface is also known as “sputtering” since the surface atoms are ionized and projected from the surface.

The emitted ions, which are known as “secondary ions”, are then analyzed for information on the surface. Generally, the ion beam has an opposite charge to the ions of interest in the sample. For example, if identification of cations is of interest in the sample, a negative ion such as O^- is used in the ion beam. If anions on the surface are of interest, then a positive ion such as Cs^+ is fired at the sample.

In this analysis, Time-of-Flight SIMS (ToF-SIMS) instrumentation was used in which the secondary ions sputtered from the surface are accelerated in an electric field towards a detector [47], [48]. The “time-of-flight”, or time taken by the ions to travel to a detector in a vacuum tube is measured. The detector forms part of the spectrometer which distinguishes between the energy spectrum of the ions and hence identifies the emitted ions.

This technique has various purposes ranging from surface imaging to trace element analysis. One application of SIMS is depth analysis of a sample, which was carried out in this project. The primary ion beam was used to sputter or remove several layers of atoms. This allows the atoms beneath the surface to be analyzed so that a local depth profile is established, where the composition of atoms with increasing depth can be obtained. However, this only provides information on elemental composition rather than molecular [47], as the bombardment of ions can cause changes in the molecular composition and distort results.

The SIMS analysis done in this project was performed by the Waterloo Advanced Technology Laboratory (WATLab) in the Department of Chemistry at the University of Waterloo. A rebar sample of dimensions 1 cm by 1 cm was prepared by cutting the cross section of a rebar into four pieces as shown in Figure 3-7. The tip of a single “quarter-section” was then ground such that a flat surface is obtained, with the curved surface with mill scale facing upwards. The sample was then thoroughly cleaned with an ultrasonic cleaner and degreased in isopropanol. Only the as-rolled and shotblasted-and-pickled specimens were examined using SIMS to consider the difference in composition at the surface of each specimen.

Figure 3-7: (from left) rebar cut into half-hemispheres; top view of curved surface of a single specimen; and isometric of specimen with sharp corner ground flat

3.2.1.6 X-ray fluorescence spectrometry

X-ray fluorescence spectrometry is a non-destructive technique used for elemental analysis of a sample. XRF involves the emission of X-rays from an emitter towards a sample. The X-rays excite atoms of the specimen and dislodges electrons from the inner shells of the atom which releases characteristic X-rays. These are specific to each element since they vary depending on the size of the atom. A detector senses the emitted radiation and the likely element in the sample.

The way in which XRF functions is similar to EDS, in that X-rays are released by the atom of the specimen in both cases. However, EDS fires a beam of electrons at the specimen rather than X-rays. XRF does not require the specimen to be placed in a vacuum chamber which can allow larger samples to be analyzed as-is without physically modifying it (such as cutting it up). EDS allows analysis of a smaller area (up to a few microns) identified using SEM compared to XRF.

For this project, a ThermoScientific Niton XRF gun was used to analyze specimens where necessary. The composition of the various components and test specimens were identified using XRF, shown in Section 3.1.

3.2.2 Rapid screening test

The rapid screening test is based on the test developed by Schönning and Randström [49] which had origins from the EN 480-14:2006 test. Further modifications were implemented based on work by Loudfoot [50] and van Niejenhuis et.al [51].

Specimens of each of the bars listed in Table 3-2 were cut into 5 inch (127 mm) lengths. A 5 mm diameter hole was drilled into the cross-section at one end of the bar, where a solid copper wire was inserted and soldered into the bar to create an electrical connection. Both ends of the specimens were then coated in an electroplating stop lacquer. This prevents corrosion of the exposed ends and limits exposure to the electrolyte to a 3 inch (76 mm) length. The bars were degreased using isopropanol and photographed to document their pre-test condition. The bars were cast into the centre of concrete cylinders. The cylinders were 65 mm in diameter and 140 mm tall. Thus, 25 mm of concrete cover is provided all around the bar.

The concrete mix used for the cylinders complies with the Ontario Provincial Standard Specifications 1002 and 1350, with the exception of maximum aggregate size and curing time [52], [53]. The maximum aggregate size used in the mix was reduced to 13 mm due to the limited cover, while curing time was adapted to the Rapid Screening Test procedures. The concrete mix is shown in Table 3-3.

Table 3-3: Concrete mix design per cubic metre of concrete

Material	Amount	Unit
13 mm Gravel	1045	kg
Sand	705	kg
Portland Cement (Type GU)	297	kg
Blast Furnace Slag	98	kg
Air Entrainment	0.237	L
Plasticizer	0.900	L
Water	158	L

In addition, sodium chloride, NaCl was added directly to the fresh concrete, by dissolving it in the mixing water. 7.5% by mass of cementitious material of chlorides (equivalent to 24% sodium chloride solution) was added to the fresh concrete. This corresponds to the maximum solubility of chloride in porewater of this concrete mix as demonstrated in work by van Niejenhuis et. al. [54]. In other words, the greatest amount of chloride is provided in order to encourage breakdown of the passive layer and initiate corrosion on the rebar.

The fresh concrete was cast into moulds in two lifts. They were vibrated after each lift on a shake table. This ensures that the concrete is consolidated and there are no large air voids in the specimen. The cylinders were then cured in a humidity room for 24 hours, after which the specimens were demoulded and placed in individual containers with saturated calcium hydroxide solution. Each container was set up as shown in Figure 3-8.

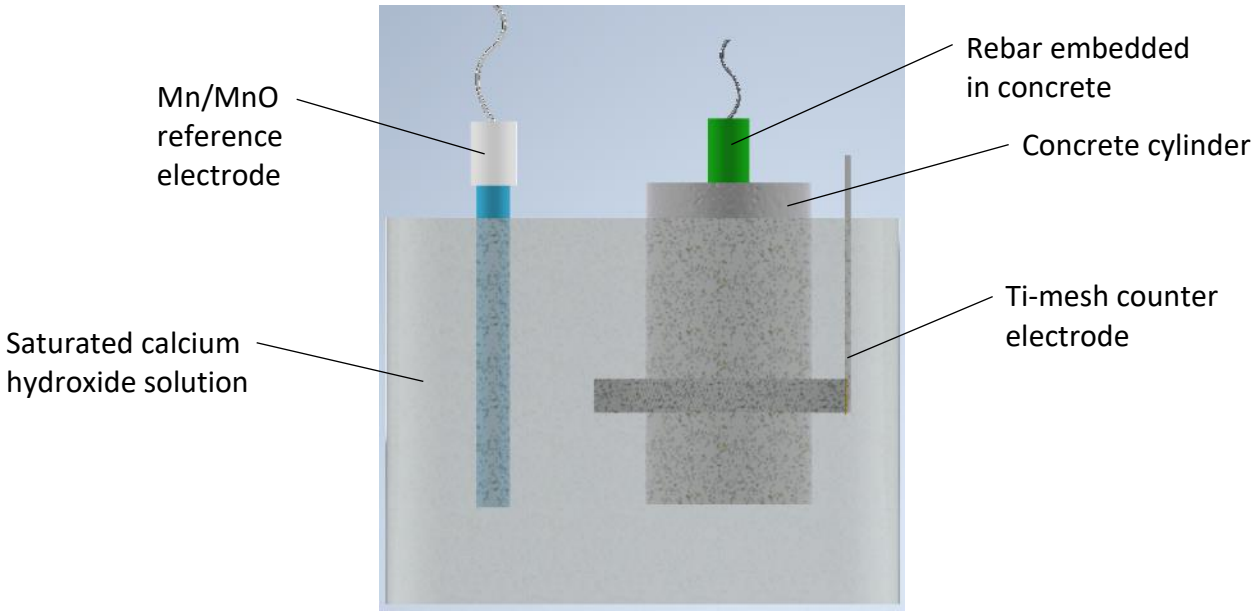

Figure 3-8: Rapid screening test setup

A titanium mesh with a mixed-metal oxide coating was used as a counter electrode. The concrete cylinders were positioned such that the counter electrode is at the same distance away from the cylinder all around. A manganese-manganese oxide, Mn/MnO reference electrode was used for this test. This reference electrode is more durable and provides stable

readings in a high pH environment compared to other more common reference electrodes such as a saturated calomel reference electrode.

The specimens were allowed to immerse in the calcium hydroxide solution for 24 hours. During this time, the open circuit potential (OCP) was monitored using a Biologic potentiostat. After 24 hours, an anodic polarization of 300 mV was applied to each specimen for 96 hours continuously. The current response in the rebar was recorded during this time.

Figure 3-9: Rapid screening test specimens connected to potentiostat

3.2.3 Longer term exposure test

The long-term exposure test is intended to consider the effect of longer-term exposure in high pH and exposure to chlorides to the oxide layer on the rebar. The specimens are based on those used for the ASTM A955 test [55], with modifications to suit available materials and test restraints. The modified specimen is shown in Figure 3-10.

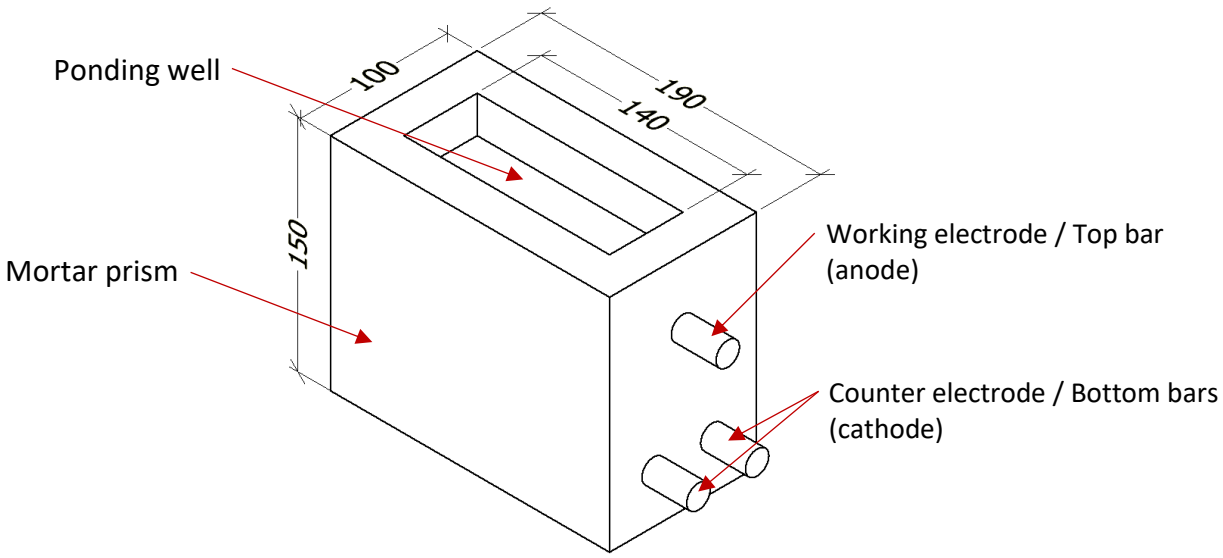

Figure 3-10: Modified ASTM G955 test specimen (measurements in mm)

Rebar with the same treatments and lug patterns and of the same batch and heat with those used tested in the Rapid Screening Test were used. 10 inch (254 mm) rebar lengths were used instead of 15 inches (381 mm) specified in the standard. This length was selected due to the amount of rebar available for testing, as well as reducing the weight of each single specimen. Next, a ponding well was cast in the specimen, rather than installing a tank or dam on top of the prism. This creates a more compact specimen which is more easily stored. The solution in the ponding well is also less likely to leak or spill due to improper sealing of the dam. The concrete specified in the standard was substituted with mortar. Mortar has higher permeability compared to concrete [56], which would accelerate the diffusion of chlorides to the anode and speed up the test. For this reason, the cover between the bottom of the ponding well and anode was reduced to 10 mm. Cover elsewhere was maintained at 25 mm.

The counter electrodes used in the specimen consist of UNS 32205 rebar from a different manufacturer. Carbon steel was considered initially; however, stainless steel was used instead given concerns that the cathode may preferentially corrode before the anode given the exposure to chlorides. The counter electrodes were connected to the anode with a 10 ohm resistor installed in series between the anode and counter electrode. The resistor allows for the

current in the system to be monitored by measuring the potential difference across the resistor.

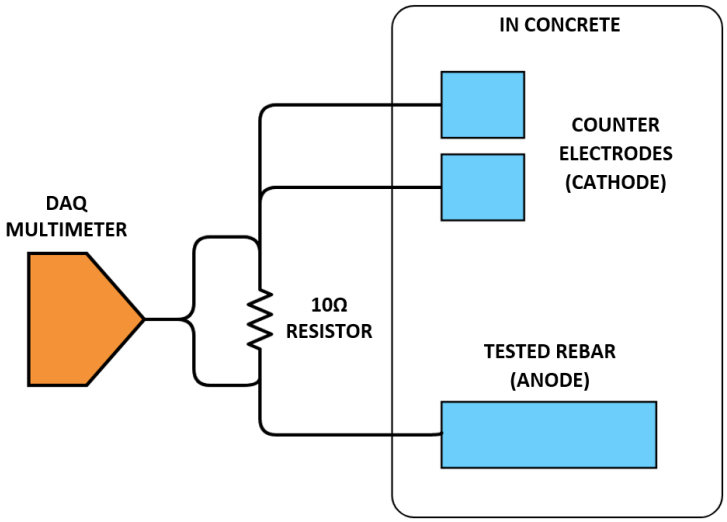

Figure 3-11: Electrical schematic of wiring between rebar, resistor, and multimeter

Formwork for the specimens were built using 13/16" formply. A piece of extruded polystyrene (XPS) foam was placed at the bottom of the form to create the ponding well. Figure 3-12 shows the layout of rebar and ponding well in the specimen. The specimens were demoulded after 72 hours and the foam removed. The ponding wells were then filled with calcium hydroxide solution in order to maintain moisture in the specimen but avoid calcium hydroxide in the porewater from leeching out. This ensures that the pH of the porewater was maintained to keep the rebar in a passivated state. Four replicates of each type of surface condition were fabricated. After six months, 15% by weight sodium chloride solution was added to the ponding well of three replicates, with one replicate kept free of chlorides. Chlorides were added in order to initiate corrosion on the rebar.

ASTM A955 is specifically applicable for stainless steel rebar and recommends the use of 15% by weight sodium chloride solution. However, this test specifies an artificial crack created by casting a steel shim in the bottom of the ponding well to allow chlorides to reach the rebar more quickly. However, this is unrealistic since the artificial crack is a direct path to the rebar. This would lower the pH around the rebar, which eliminates the protective environment present in typical concrete. This presents a different environment than that which a rebar

would likely experience in a naturally cracked concrete, in which the cracks follow a longer, tortuous path with many bottlenecks [57] Therefore, the artificial crack was not included in the specimen.

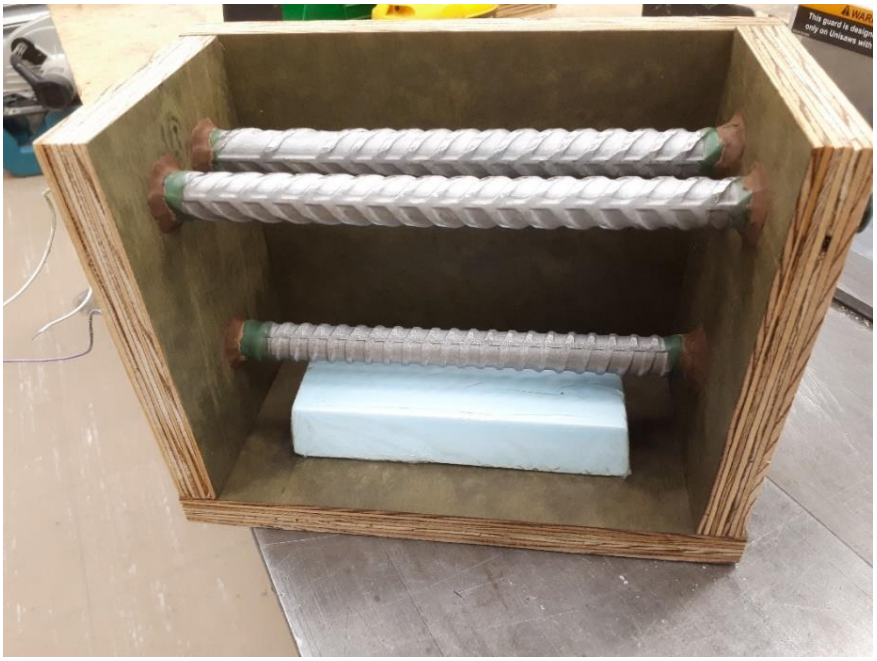

Figure 3-12: Layout of rebar inside formwork

Figure 3-13: Cured mortar specimens connected to resistor

3.2.3.1 Autopsy of specimens

The specimens were cut open at the end of the project in order to examine the condition of the rebar. The specimens were cut open using a concrete saw. A specimen clamp frame was designed and fabricated in order to safely restrain the specimen while cutting with the saw. The design and construction of the frame were carried out in collaboration with Richard Morrison and Shelley Yang. The completed jig is shown with the concrete saw on Figure 3-14.

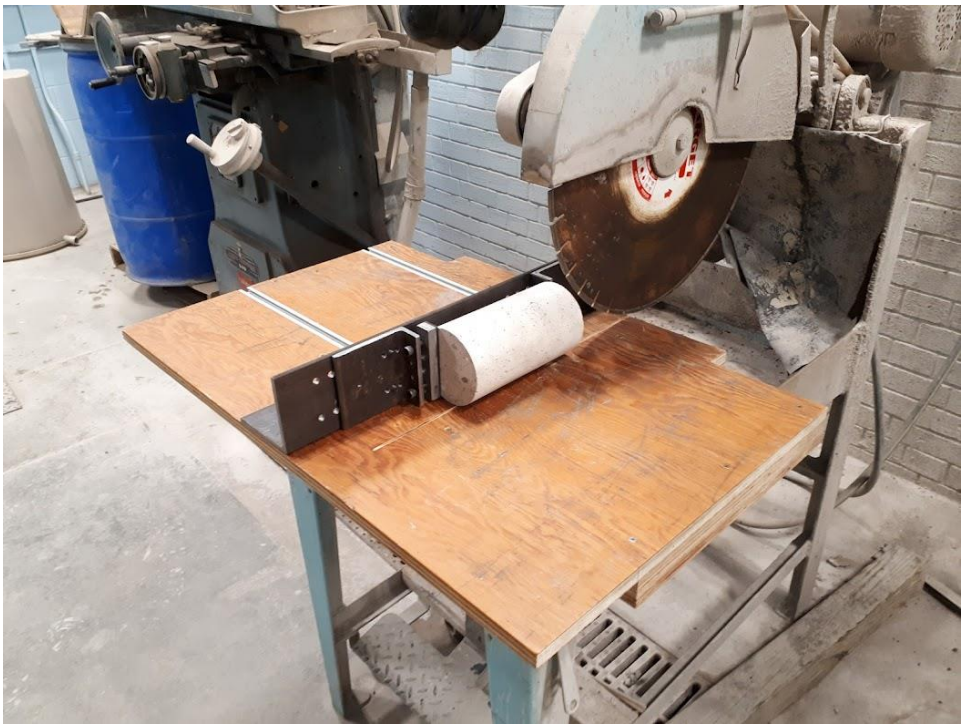

Figure 3-14: Specimen clamp frame for concrete saw, with a concrete cylinder as a cutting sample

A wet cut method with water as a lubricant was used as it limited dust dispersal into the air. The specimens were split open one at a time and photographed immediately to avoid documenting oxidation of the rebar in atmosphere.

3.2.4 Electrochemical measurements and testing

Electrochemical tests are based on the principle that the movement of electrons and ions in a corrosion process can be represented by an electrical circuit. The basic circuit is known as Randle's circuit, shown on Figure 3-15. In the circuit, R_s (or R_Ω in other literature) represents the

resistance of the electrolyte. R_{ct} (also represented as R_p) is the polarization resistance, which represents the ability of the steel in the concrete to ionize. C_{dl} represents the capacitor-like behaviour which is attributed to the Hemholtz double layer. This phenomenon occurs when a metal is placed into a polar solution. In an electrochemical cell, the anode oxidizes and releases electrons, hence the surface is negatively charged with electrons. The polar molecule in the electrolyte becomes dielectric by becoming attracted to the surface and adsorbing to the surface. This forms the inner Hemholtz layer. An outer layer is formed by anions in the polar molecule attracting cations in the electrolyte (which completes the "double layer"). Meanwhile, Z_w represents the Warburg impedance. This represents the influence of diffusivity of ions to the electrode on the rate of redox reactions on the electrode. For instance, the reduction of oxygen on a cathode requires diffusion of oxygen through the electrolyte. If this diffusion is limited, then the reduction reaction will slow down.

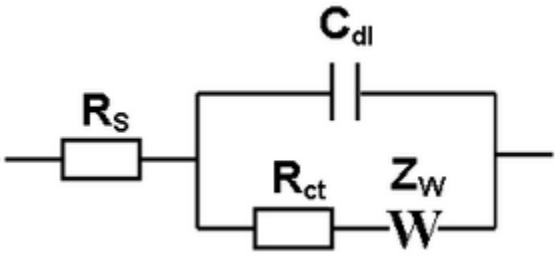

Figure 3-15: Randle's circuit schematic

3.2.4.1 Microcell potential measurement

Microcell readings were taken to measure the open circuit potential (OCP) of the individual rebar compared to a reference electrode. A saturated calomel reference electrode was used for these measurements. The reference electrode was placed in the ponding well, and a multimeter was used to measure the potential difference between the electrode and the rebar.

3.2.4.2 Macrocell current determination

Macrocell measurements were taken by monitoring the current flowing from the anode (rebars being tested) to the cathode (counter electrode rebars). A Keithley data acquisition (DAQ) multimeter was connected to each specimen to periodically measure the potential across the

10-ohm resistor joining the anode bar to the cathodes. Using Ohm's Law, the current in the system can be calculated based on the voltage measurements obtained from these readings, shown in Equation 3-1. The DAQ was set up to take a reading every four hours.

$$I_{corr} = \frac{V_{measured}}{R}, R = 10\Omega \quad \text{Equation 3-1}$$

3.2.4.3 Linear polarization resistance (LPR) test

Next, linear polarization resistance tests was periodically conducted on each specimen. The test was carried out in accordance with ASTM G59 [58]. The polarization resistance, R_p is the electrical resistance in an electrochemical system as a result of polarization in the system. Stern and Geary [59] demonstrated a linear relationship between potential and current at low magnitudes of polarization. When potential and current is plotted on a graph, at low polarization, R_p is defined as the slope of the graph at the origin:

$$R_p = \frac{\Delta E}{\Delta I} \quad \text{Equation 3-2}$$

In the same study, the following equation was derived to relate experimental measurements for R_p described above with the steady state corrosion measurement in a system. At the linear region, the following equation represents the relationship between corrosion current, i_{corr} and R_p. B represents the Stern-Geary constant, where 26 mV is generally used for rebar in concrete [60]. The corrosion current density, i_0 can then be calculated using the area of exposed rebar in the specimen.

$$R_p = \frac{B}{i_{corr}} \quad \text{Equation 3-3}$$

$$i_0 = \frac{i_{corr}}{A_{rebar}} \quad \text{Equation 3-4}$$

For the LPR test, a titanium mesh with a mixed-metal oxide was used as the counter electrode, and a saturated calomel electrode used as the reference electrode. The top rebar, counter electrode and reference electrodes were connected to a Biologic potentiostat. The open circuit

potential of the rebar was measured for three minutes. After that, a -30 mV polarization was applied on the specimen and held for 60 seconds. Then, a +30 mV potentiodynamic polarization was applied. In accordance with the standard [58] the potential was increased at a rate of 10 mV per minute to +30 mV above open circuit potential, and reversed at the same rate to the open circuit potential. As the bar was polarized, the current response was recorded. The current response was plotted against the potential polarization applied on the bar. The polarization resistance, R_p was calculated using the slope of this graph. The corrosion current and corrosion current density were then calculated using the equations above.

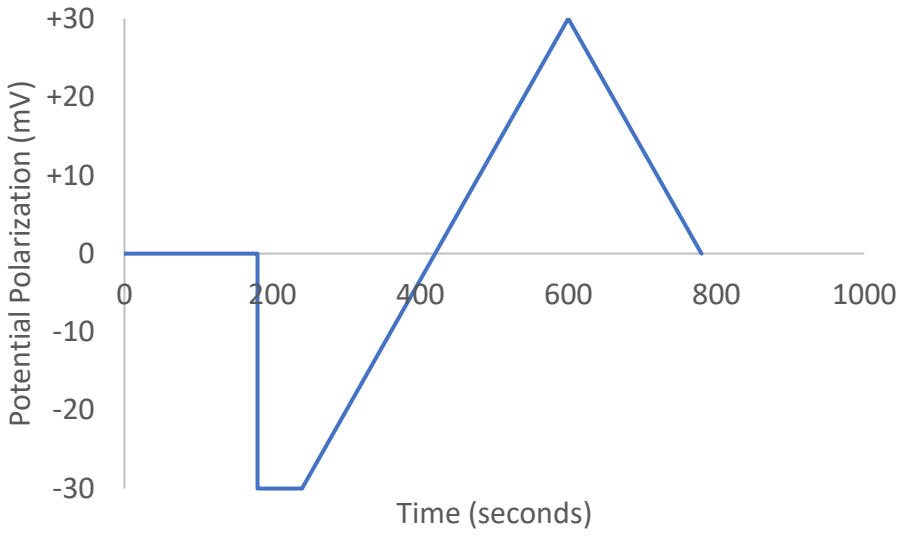

Figure 3-16: Polarization applied on top rebar during LPR test

3.2.4.4 Galvanostatic pulse (GP) test

The galvanostatic pulse procedure was performed based on work by Newton and Sykes [61]. In this test, a constant 150 µA current was applied to the top bar for 180 seconds. The potential response was measured throughout this time. Similar to the LPR test, a titanium mesh with a mixed metal oxide was used as the counter electrode.

Compared to LPR, the GP test is useful since the measurement indicates the resistance of the electrolyte R_c. In the context of this project, this would be the resistance of the cement mortar surrounding the rebar. Hence, the potential drop caused by the mortar can be subtracted from

the change in potential measured from the polarization. This presents a more accurate value of polarization resistance of the rebar sample. Equation 3-3 and Equation 3-4 were used to calculate the polarization resistance and subsequently corrosion current density.

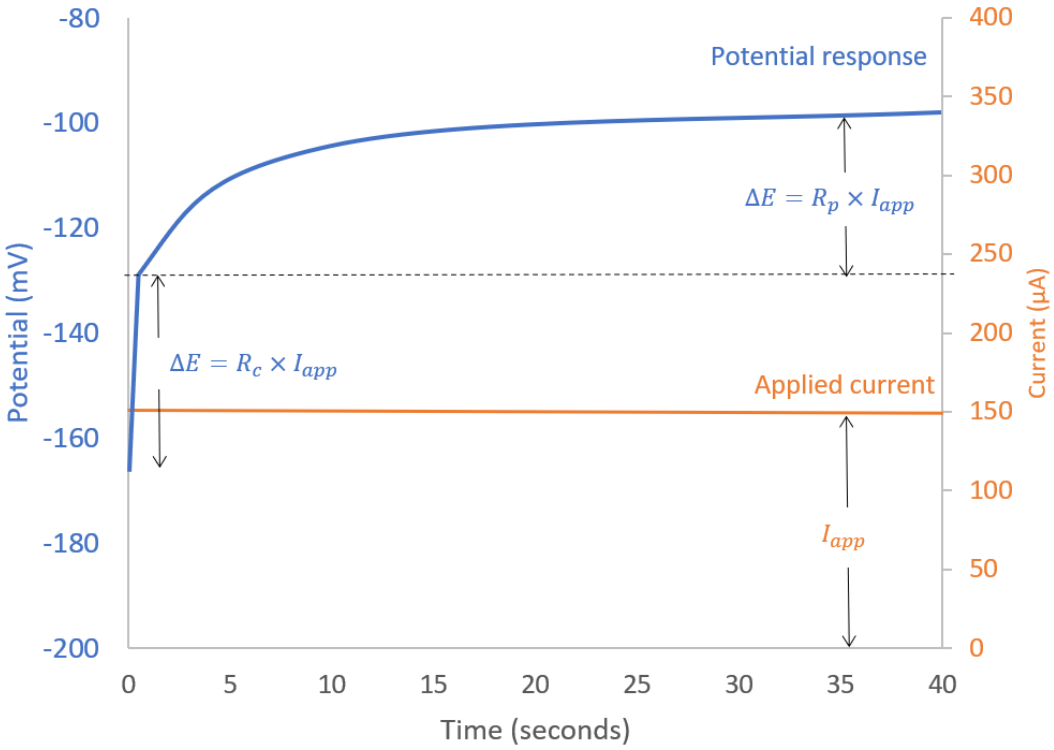

Figure 3-17: Theoretical galvanostatic pulse polarization and response

Initially, the anode was only polarized with a 10 µA current, similar to that performed in work on carbon steel by Hunt [62] and Ogunsanya [63]. However, the resulting current response did not plateau as shown in Figure 3-17. This meant that the polarization resistance, R_p was being underestimated. Following the work by Newton and Sykes [61], the galvanostatic current was increased in order to induce the plateauing, such that an accurate R_p was being measured.

4 Results

4.1 Surface characterization

4.1.1 Optical microscopy

The external surfaces described in Chapter 3 were observed under a stereoscope to determine if there were any visible differences in surface topography between different specimens. Of particular interest were specimens with mill scale still present (as-rolled) or those partially removed (shotblasted-only and pickled-only).

The micrograph in Figure 4-1 shows the rough surface of an as-rolled sample. The mill scale forms randomly during the hot rolling process, while the bar is being deformed into the appropriate bar size. The mechanical action leads to a rough finish on the surface. There are regions on the sample which appear brighter and shinier compared to the dull and dark-colour finish shown in Figure 4-1. These are more prevalent on the rebar lug than on the areas between the lugs. They appear to be locations where mill scale had been removed, which is an artifact from handling and transportation of the rebar.

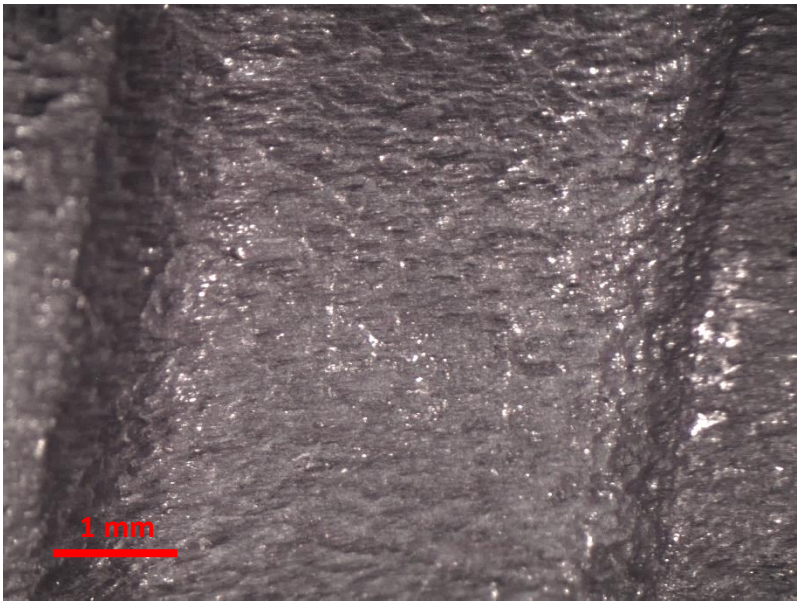

Figure 4-1: Surface of as-rolled rebar

Meanwhile, shown in Figure 4-2, the surface of the shotblasted-only specimen is much more undulating and less uniform than the as-rolled sample. The dimpled surface is consistent with impressions of projectiles impacting the surface of the mill scale. This is unsurprising since the surface had been subjected to additional mechanical deformation by the shotblasting process after hot-rolling. The bright spots on the shotblasted-only specimen are more polished surfaces of the mill scale allowing it to better reflect light.

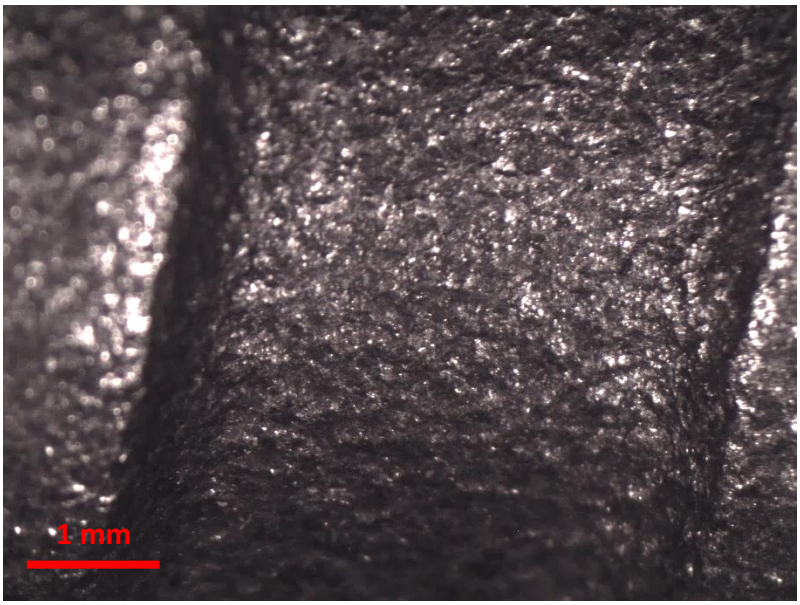

Figure 4-2: Surface of shotblasted-only rebar

The shotblasted-and-pickled specimen, shown in Figure 4-3, appears smoother than the previous specimens observed. This rebar has received the conventional post-rolling treatments for removing mill scale and the chromium-depleted surface layer of the underlying metal, and has the typical light grey colour associated with stainless steel. There are faint dark lines along the length of the specimen (and the whole length of the rebar, as shown previously in Figure 3-1). These are believed to be the remnants of mill scale which have become embedded in the rebar during the rolling process. The shotblasting and pickling appears to not remove these oxides from the rebar.

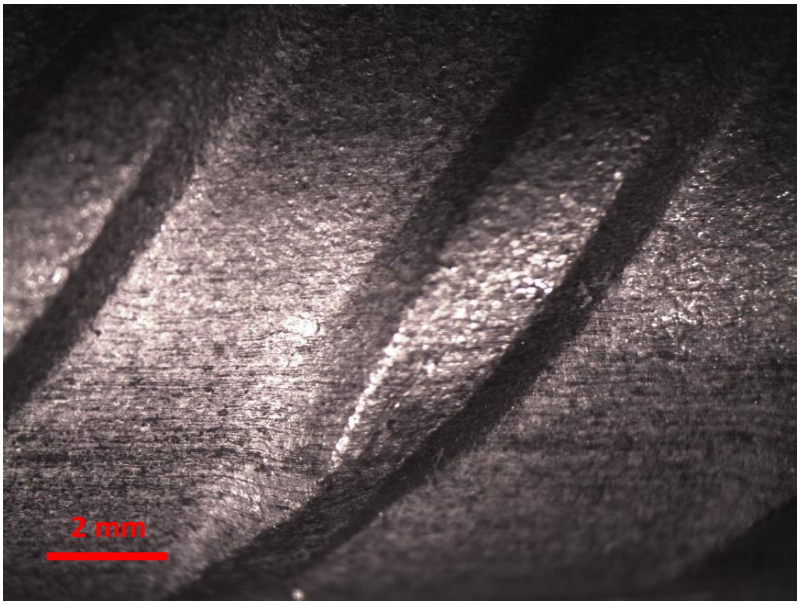

Figure 4-3: Surface of shotblasted-and-pickled rebar

The surface on the pickled-only specimen, shown on Figure 4-4, appears smooth and more consistent. The surface has the characteristic light grey colour associated with stainless steel. There are areas of dark lines running along the length of the specimen similar to the pickled-and-shotblasted specimen. However, they are more numerous in quantity compared to the previous specimen.

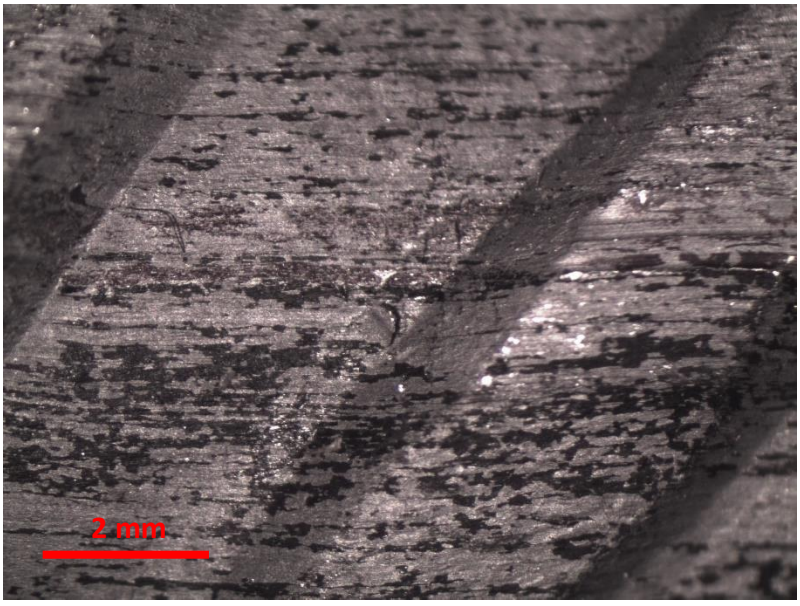

Figure 4-4: Surface of pickled-only rebar

4.1.2 Scanning electron microscopy (SEM)

4.1.2.1 External surface

The longitudinal specimens of the as-rolled and shotblasted-only bars were further observed using SEM. Only these specimens were included to examine the mill scale at a greater magnification and consider whether the shotblasted-only sample had any mill scale remaining.

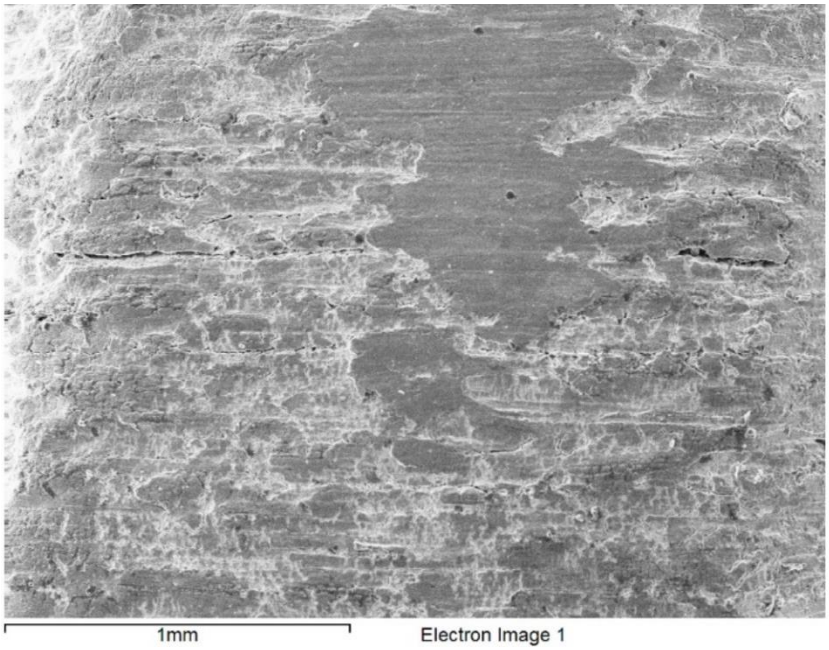

Figure 4-5: SEM micrograph of as-rolled rebar surface

As observed in the stereo microscope, a rough surface is present on the surface of the as-rolled rebar. Horizontal markings as shown in Figure 4-5 are observed along the length of the rebar. These are attributed to the motion of the rebar in the rolling mill during the hot-rolling process. Some areas on the as-rolled rebar showed cracks in the mill scale, particularly on the lug as shown in Figure 4-5. Due to the brittle nature of the mill scale, the cracks could have formed during the rolling process as stress is applied on the bar, or after hot-rolling where the surface of the rebar cools quicker than the inner area of steel.

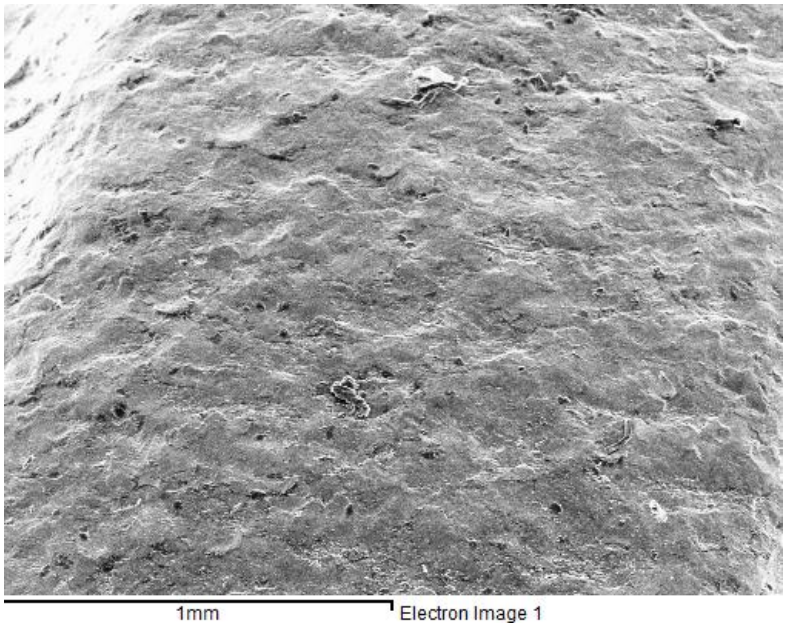

Figure 4-6: SEM micrograph of shotblasted-only rebar

Similarly, the micrograph of the shotblasted rebar in Figure 4-6 reveals a rough surface. However, the horizontal markings seen on the as-rolled rebar was not observed on the shotblasted-only rebar since further mechanical work was done on the surface by the shotblasting process. This is shown by the indentations seen in Figure 4-6. The surface of the shotblasted-only rebar did not show any cracks in the mill scale. However, mill scale at some areas had been loosened from the surface but not completely detached as seen in Figure 4-7.

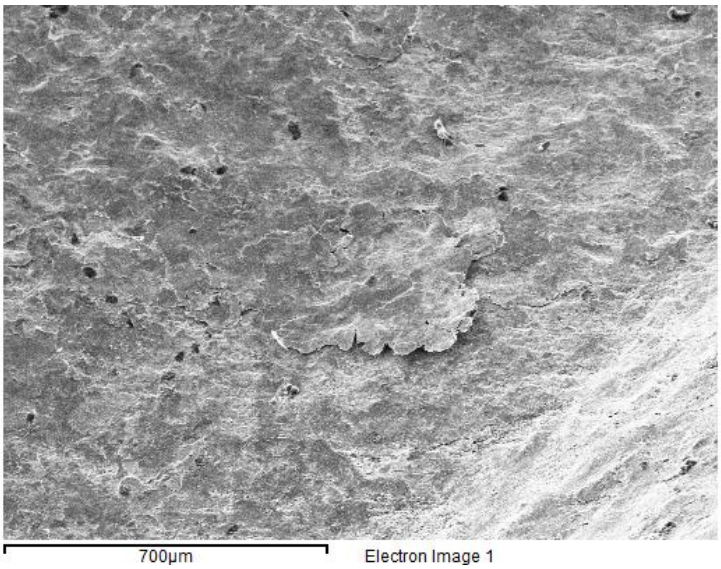

Figure 4-7: Shotblasted-only rebar with mill scale partially detached

Meanwhile, dark irregular spots were observed on the surface of both specimens. Further analysis using stereoscopic images showed that the spots are holes in the mill scale. EDS analysis revealed the presence of oxygen in those locations, which suggest that the holes are not continuous pits up to the surface of the base steel.

4.1.2.2 Cross-section specimens

The cross-sections of rebar were examined in a scanning electron microscope. Observations from SEM imaging reveal a varying mill scale thickness around the circumference of the as-rolled rebar. From the SEM micrographs, the mill scale was found to be between 4 and 13 µm in thickness. Cracks and gaps were observed in the mill scale; however, none was observed to be a continuous path from the surface to the base steel. The mill scale appears to have two distinct layers, with a top "loose" layer and an adjacent layer which appears denser and more closely adherent to the base metal. An EDS analysis, shown in Figure 4-9, indicates a higher concentration of chromium in the inner region.

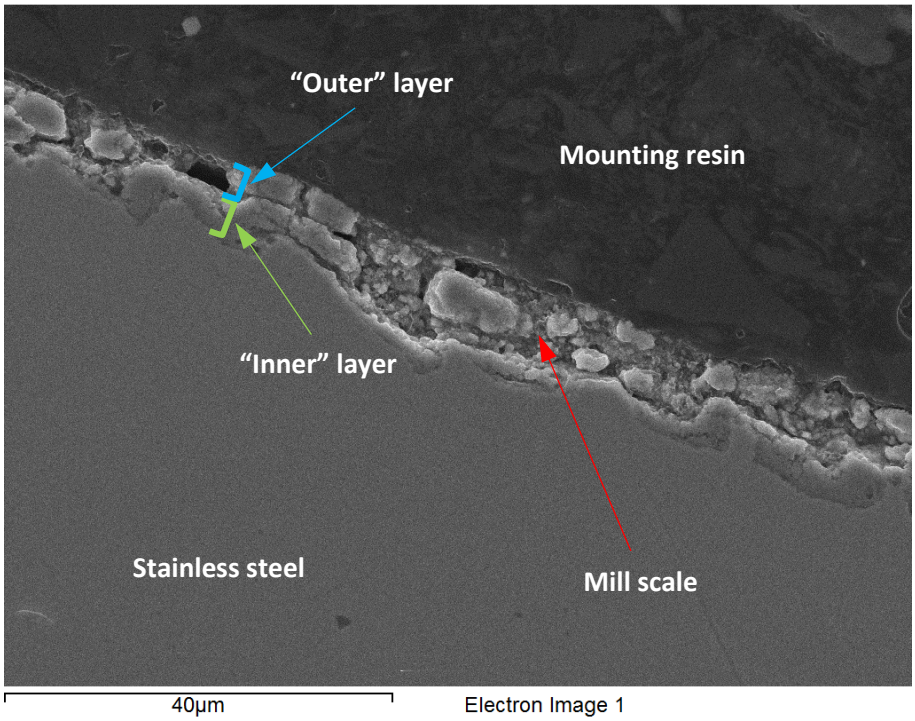

Figure 4-8: SEM micrograph of as-rolled rebar cross-section

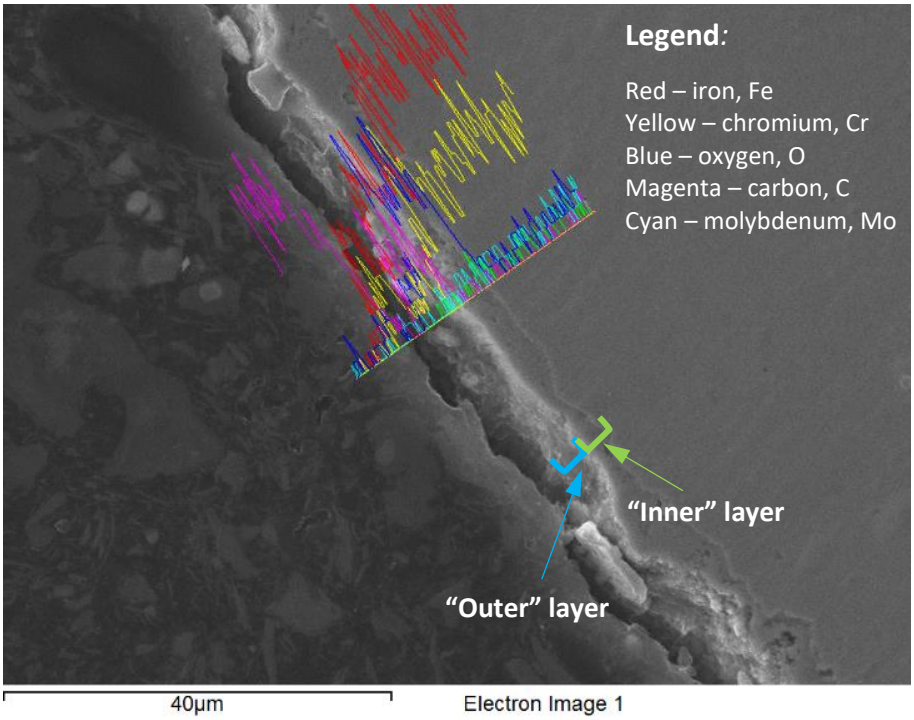

Figure 4-9: SEM micrograph of as-rolled rebar cross-section with elemental composition overlay

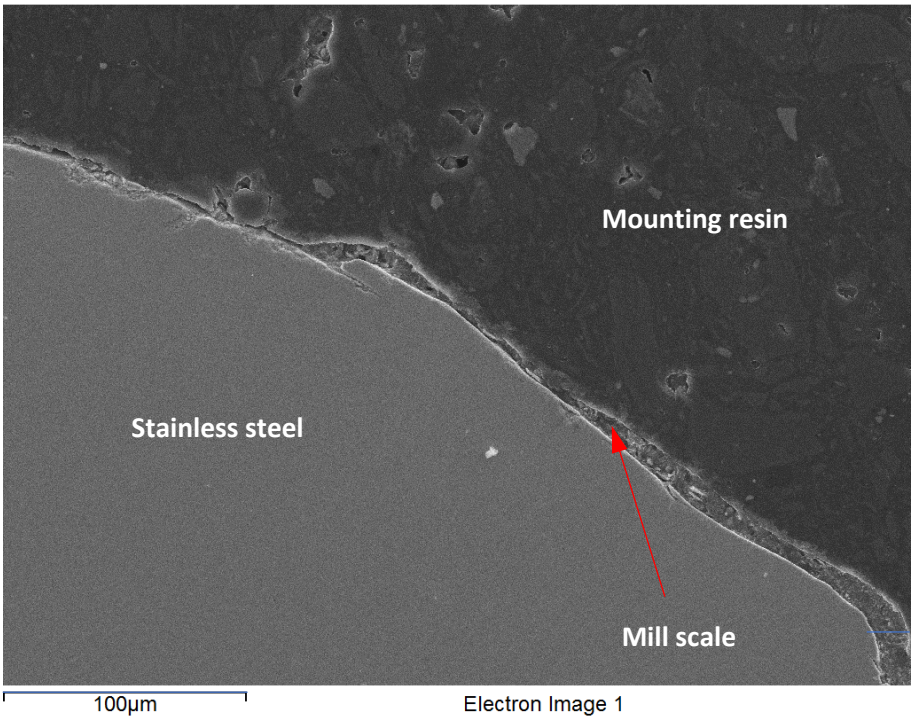

Figure 4-10: SEM micrograph of shotblasted-only rebar cross-section. Top-left corner shows less mill scale compared to bottom-right corner

Shotblasting is intended to remove the mill scale. However, the shotblasted-only specimens exhibited mill scale with thicknesses ranging from 0 to 10 µm. It is clear that the mill scale in some locations was almost completely removed; however, in others, very little had been removed. This can also be observed from the micrograph in Figure 4-10. The mill scale is clearly more prominent towards the bottom-right of the image compared to the top-right area.

The shotblasted-and-pickled rebar had no significant mill scale layer on the surface. However, micro-pits of oxides were observed as shown in Figure 4-11. These correlate with the dark lines observed on the rebar surface in Figure 4-3. EDS analysis confirms the presence of oxygen in these locations which indicates that they are area of entrapped mill scale. However, the surface was not smooth and had micropits without any mill scale. These micropits have been observed in work by others and are attributed to the pickling process [45]. The micropits observed on this sample were much fewer and not as severe those as seen in other studies.

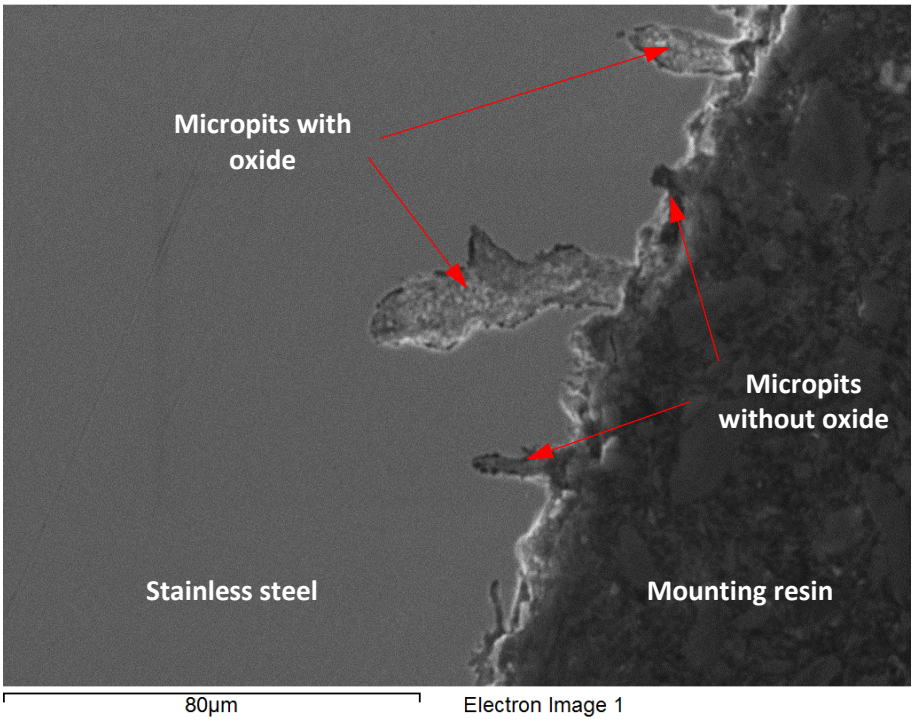

Figure 4-11: SEM micrograph of shotblasted-and-pickled rebar with micropits containing oxide and micropits without oxide

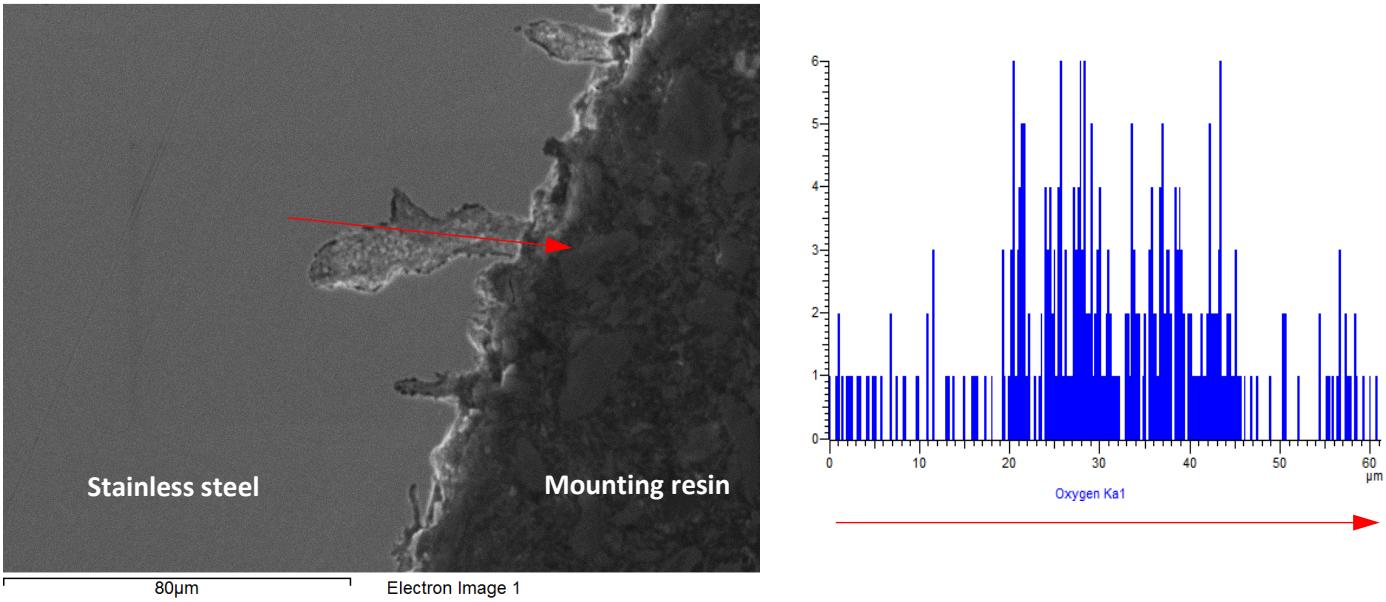

Figure 4-12: SEM micrograph of shotblasted-and-pickled rebar cross-section. Plot shows relative oxygen content along scanned length represented by the red arrow using EDS

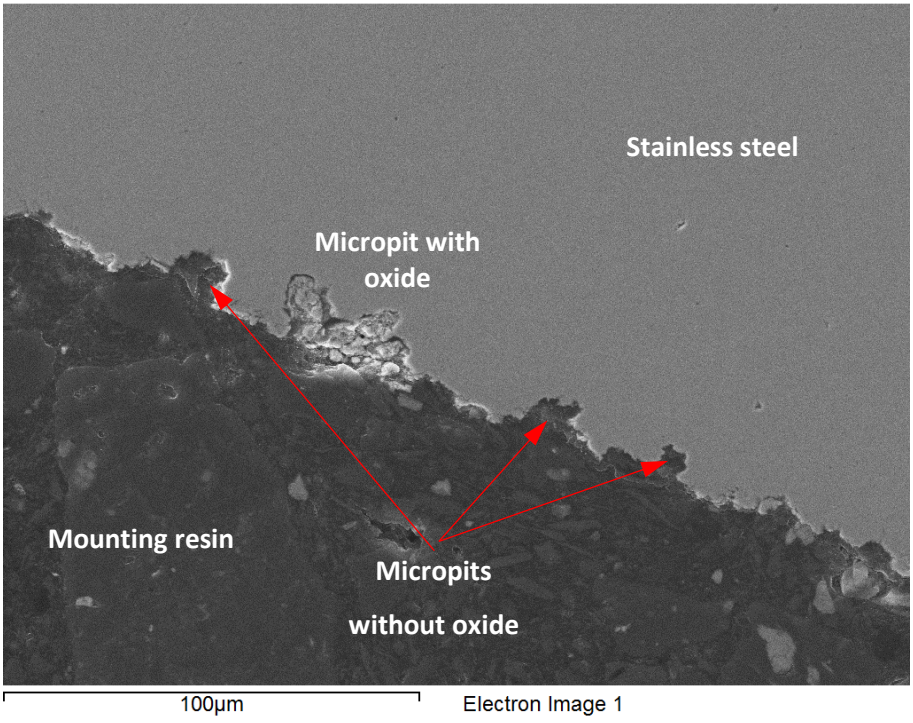

Figure 4-13: SEM micrograph of pickled-only rebar cross-section showing micropits at the rebar surface

Similarly, the pickled-only rebar did not show a distinct layer of mill scale on the surface. Furthermore, micropits with and without oxides were found at the surface of the rebar. In this sample, the micropits with oxides were more numerous and tended to accumulate in a group. This can be seen in Figure 4-14. This correlates to the numerous dark lines observed on the pickled-only surface in Figure 4-4.

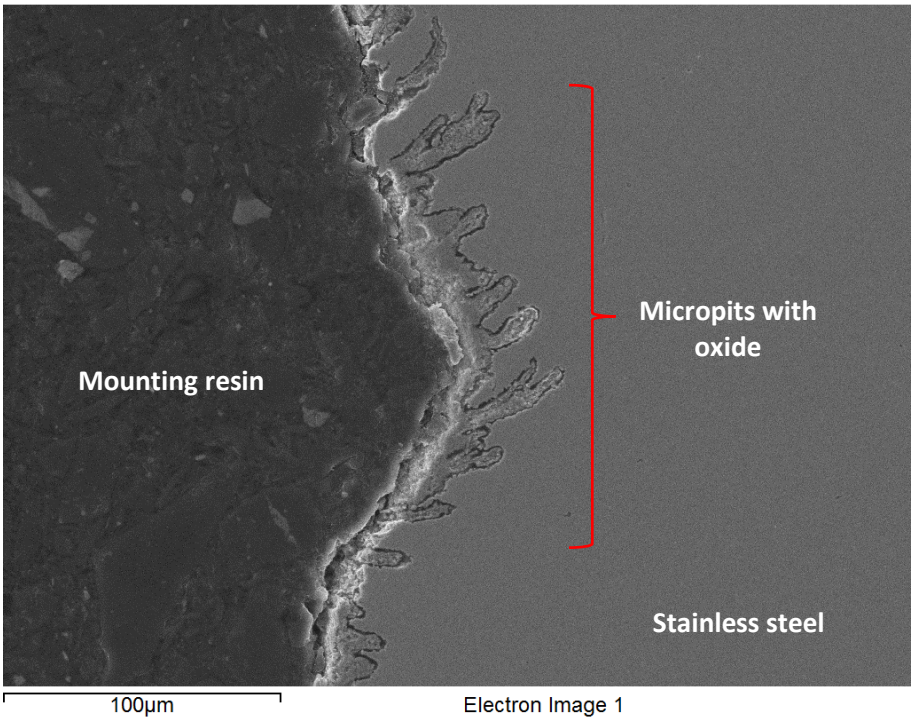

Figure 4-14: SEM micrograph of pickled-only rebar cross-section showing micropits containing oxide

4.1.3 Secondary ion mass spectroscopy (SIMS)

Depth profiles of the mill scale of an as-rolled bar and the passive film of a shotblasted-and-pickled bar were obtained using secondary ion mass spectrometry (SIMS). The graphs in Figure 4-15 and Figure 4-16 show the relative composition of the major constituent elements with increasing depth from the surface. The vertical axis indicates the relative intensity of specific ions received by the detector, while the horizontal axis shows the length of time sputtering was applied, representing depth from the external surface. The intensity of other constituents, such as molybdenum were below the detection limit.

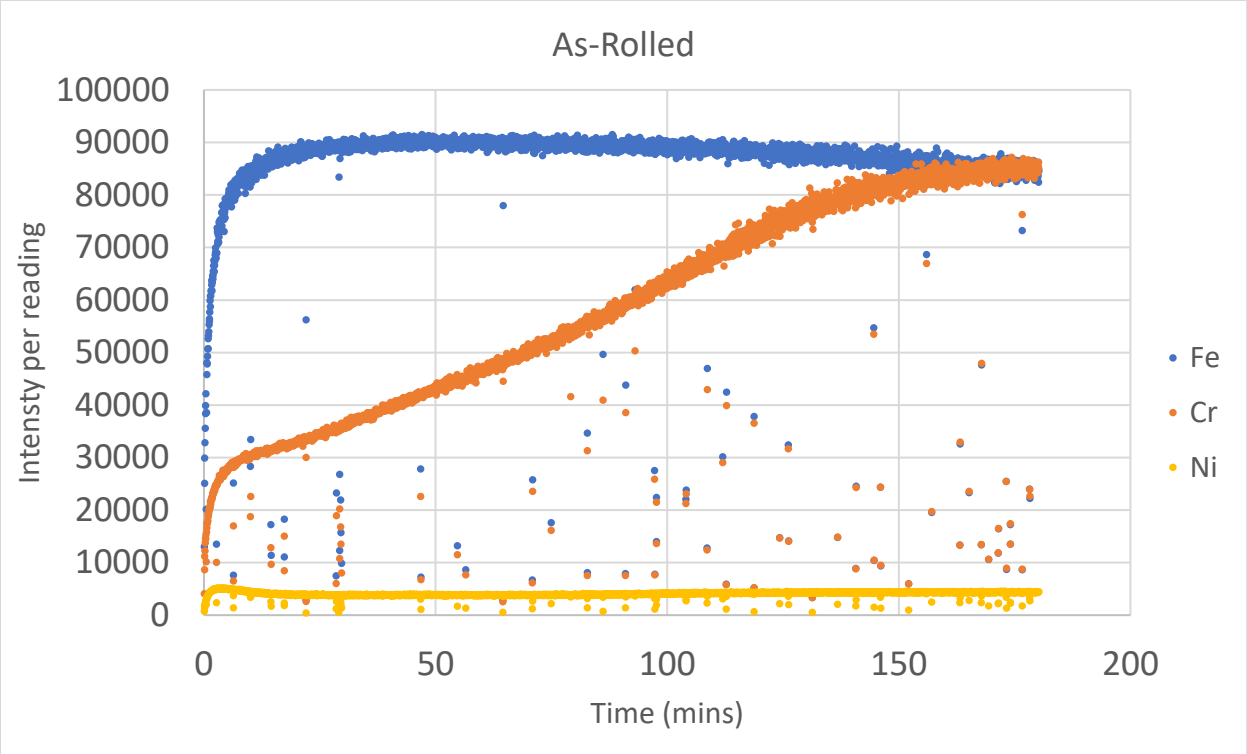

Figure 4-15: Amount of iron, chromium and nickel with increasing depth of as-rolled rebar

The analysis of the as-rolled surface reveals a high proportion of iron, Fe, as expected in a steel sample and reached the maximum limit of the detector after approximately 20 minutes of sputtering. The amount of chromium, Cr is much lower than Fe at the surface but gradually increases with increasing depth. Towards the end of the test, the amount of chromium appears to plateau at approximately the same level as the iron, reaching the limit of the detector. Meanwhile, the composition of nickel, Ni peaks at the surface and stabilizes at a lower level after approximately 15 minutes of sputtering.

The plateau observed for Fe and Cr is the upper limit at which ions could be distinguished by the detector. Hence, it is not possible to deduce the exact ratios of elements quantitatively once the limit is reached in this test. It is also not possible to determine the depth reached at the end of the test, as a profilometer of the required precision was not available.

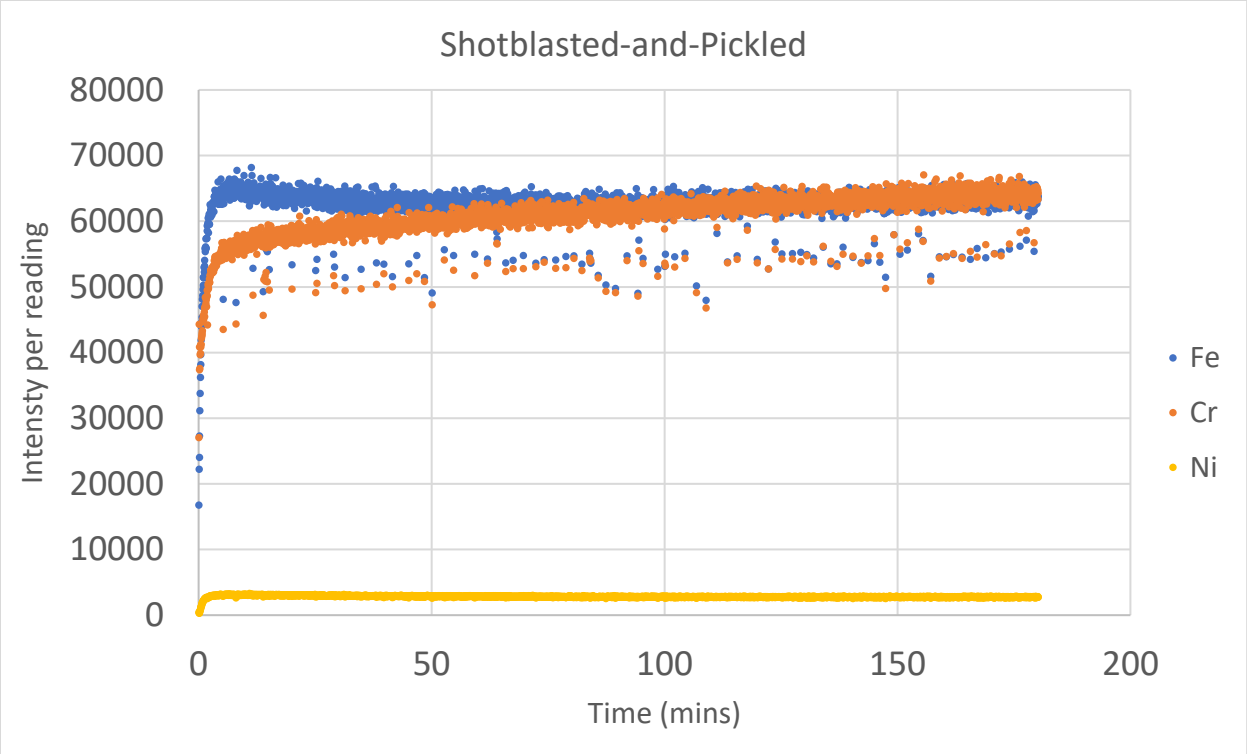

Figure 4-16: Amount of iron, chromium and nickel with increasing depth of shotblasted-and-pickled rebar

Meanwhile, the shotblasted-and-pickled specimen shows a much higher initial chromium content compared to the as-rolled specimen. There is a noticeable peak in iron at the start before decreasing slightly to a stable level. The intensity of chromium increases up to the 55,000 level, then increases more gradually up to the maximum detected intensity. Although the plateau shown by the iron and chromium did not reach the intensity limit observed in the as-rolled sample, it appears that the detection quality may have been distorted due to potential interference from magnetization of the iron on the surface.

The ratio of chromium to nickel observed from the graph is much higher compared to the 22:5 ratio expected in this alloy. This can be explained by the selective oxidation of chromium, which leads to more chromium being found in the passive film. Furthermore, when contrasting between the as-rolled and shotblasted-and-pickled samples, there is a clear lack of chromium in the outer layer of the mill scale. This result is in agreement with studies of passive film on

stainless steel, which describes the film as a bilayer structure: the outer layers are mainly made up of iron oxides and another inner layer richer in chromium made up of Fe-Cr spinel [64]–[67].

4.2 Rapid screening test

Three rounds of Rapid Screening Test were conducted with two replicates of each bar surface finish in each round. The plots of open circuit potential (OCP) over the first 24 hours and the corrosion current density, i_0 over the subsequent four days for all specimens are shown in the following Figure 4-17 to Figure 4-21.

From the plots of open circuit potential, in general the specimens showed a gradual decrease in potential over the first 24 hours. However, some specimens showed different behaviours. PKSB-04 had inconsistent potential readings between 4 and 24 hours after the test was initiated. Meanwhile, SBO-04 and SBO-06 also displayed unstable potential readings throughout the 24-hour period.

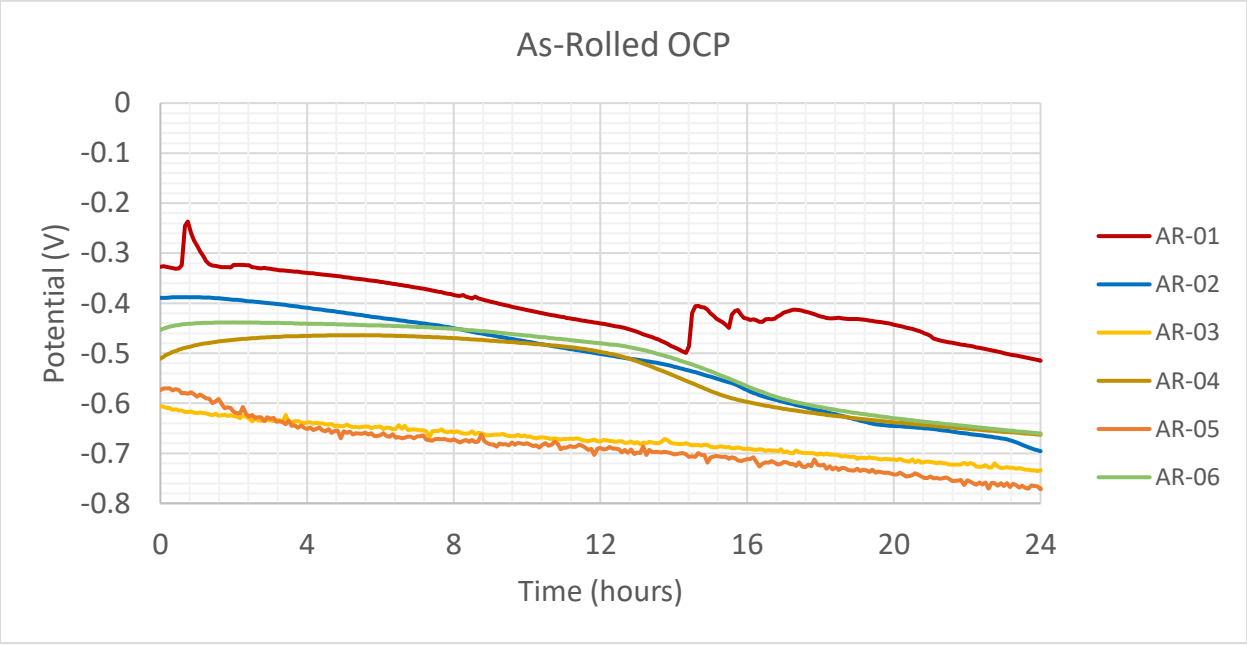

Figure 4-17: Plot of open circuit potential for as-rolled rebar

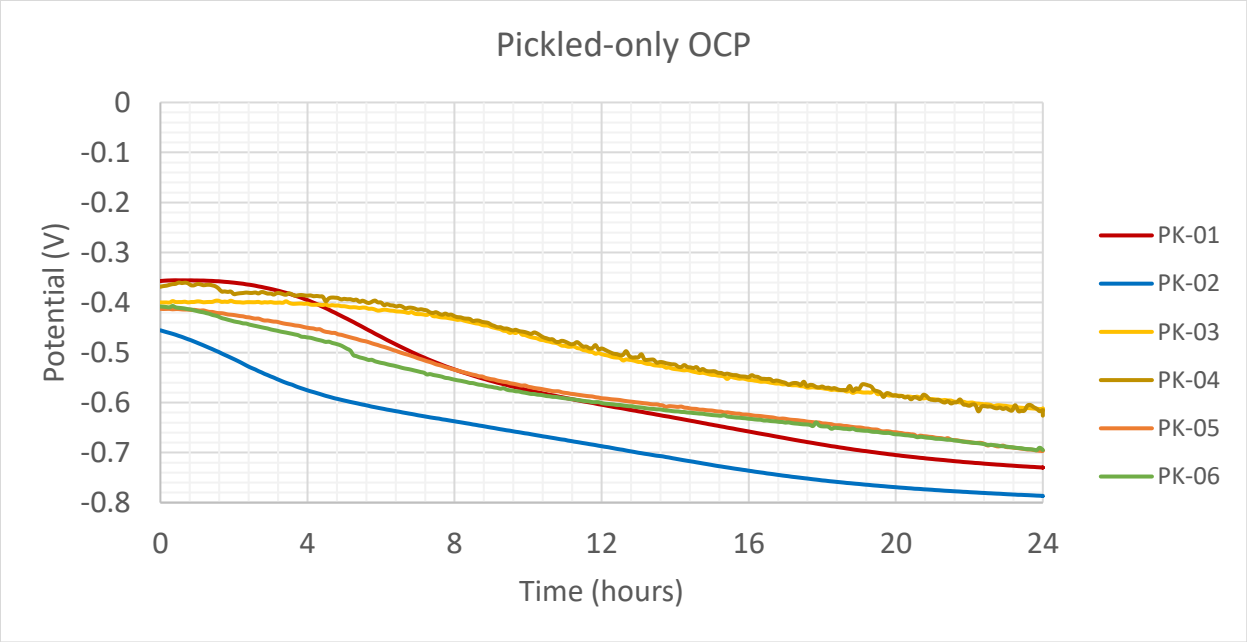

Figure 4-18: Plot of open circuit potential for pickled-only rebar

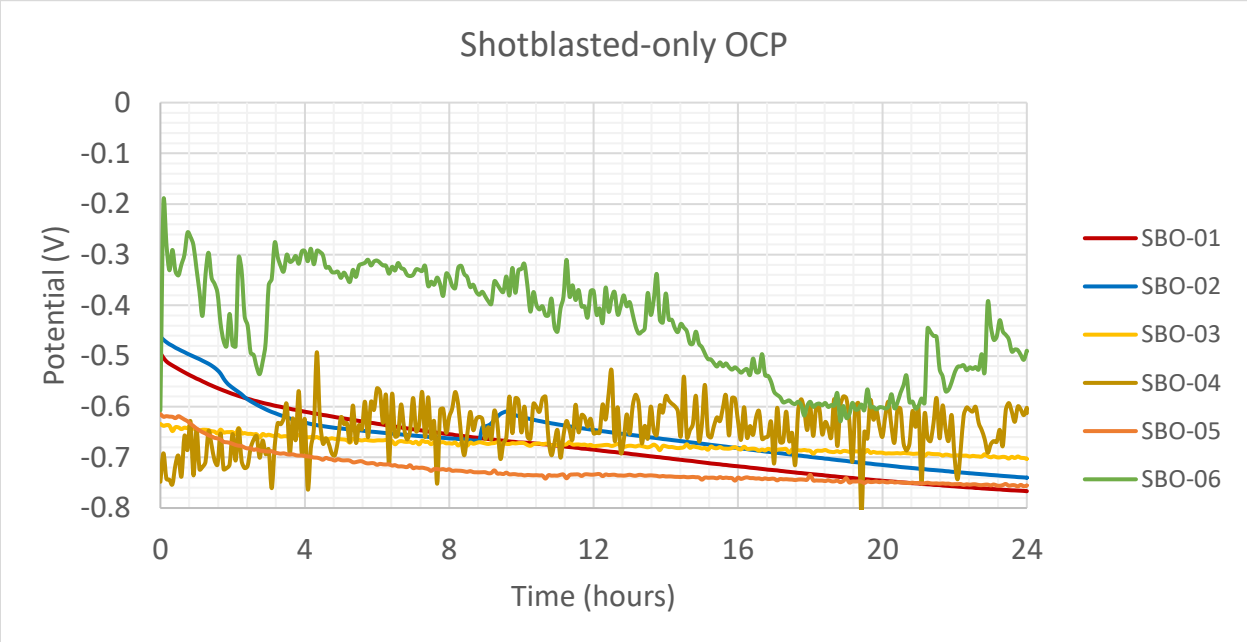

Figure 4-19: Plot of open circuit potential for shotblasted-only rebar

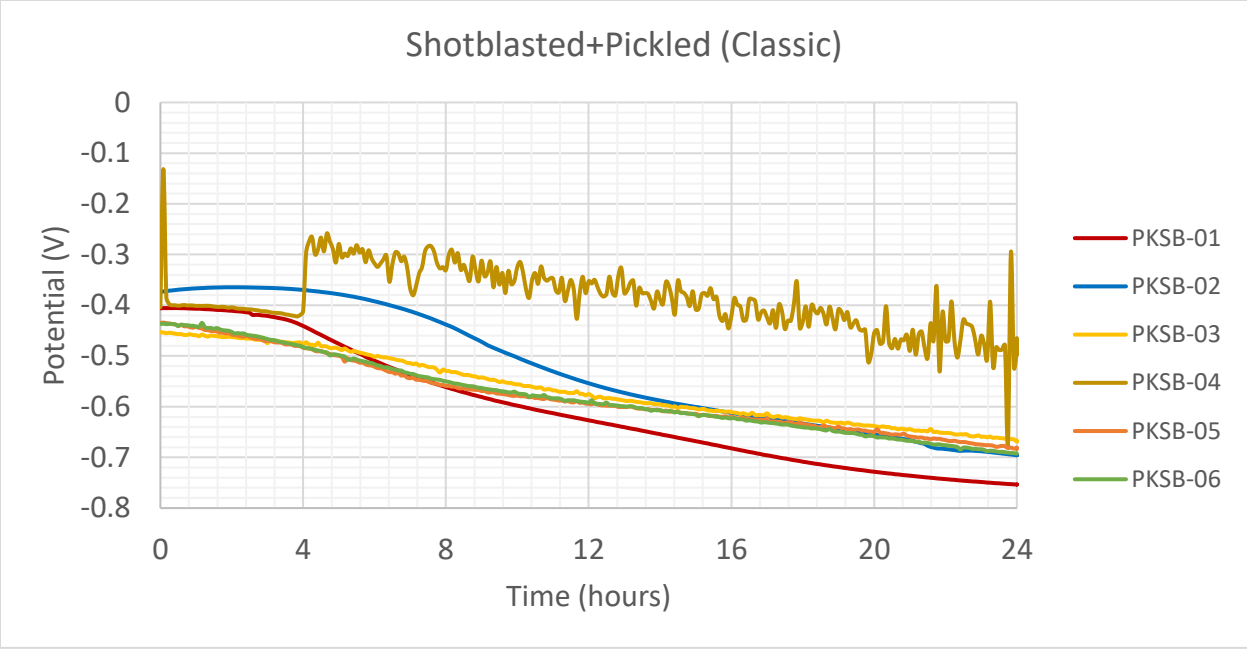

Figure 4-20: Plot of open circuit potential for shotblasted-and-pickled rebar with classic lug

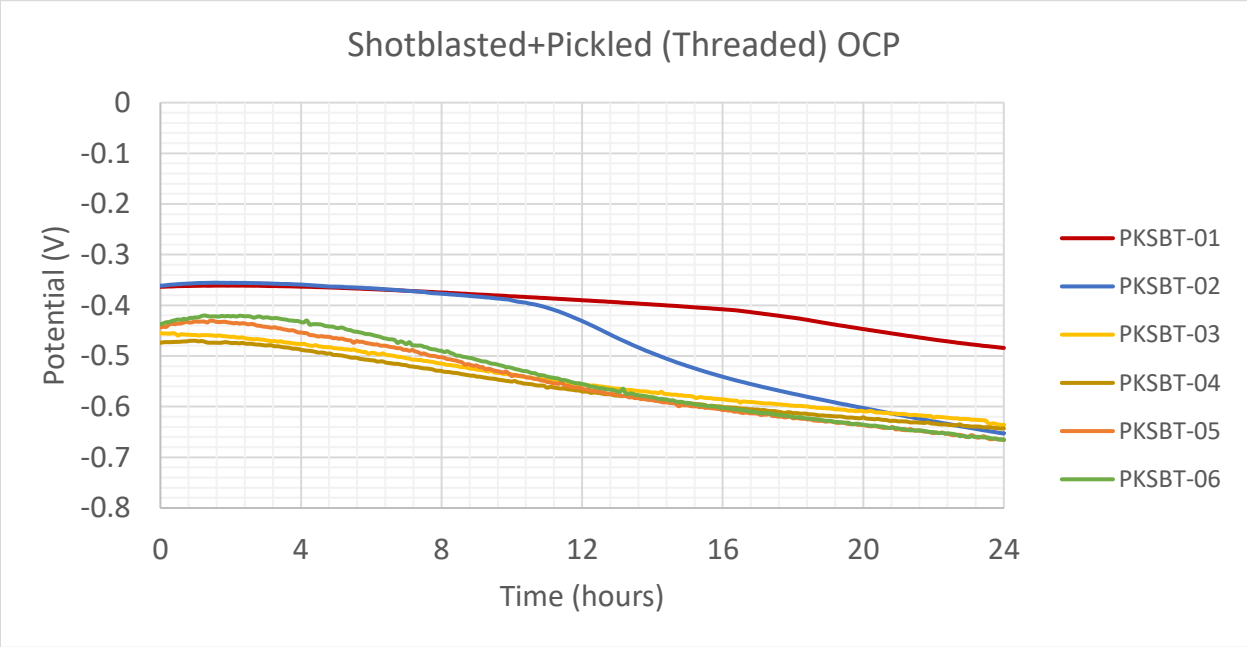

Figure 4-21: Plot of open circuit potential for shotblasted-and-pickled rebar with threaded lug

After polarization for 96 hours, no active corrosion was observed on any of the as-received specimens or those which had been shotblasted-and-pickled. In contrast, two the six shotblasted-only specimens had indications of active corrosion, as shown in Figure 4-26. Active corrosion is indicated by a consistent corrosion current density several orders of magnitude higher than the passive current density, as demonstrated on the plot. Generally, 1 mA/m^2 is equivalent to material loss of 1 µm/year.

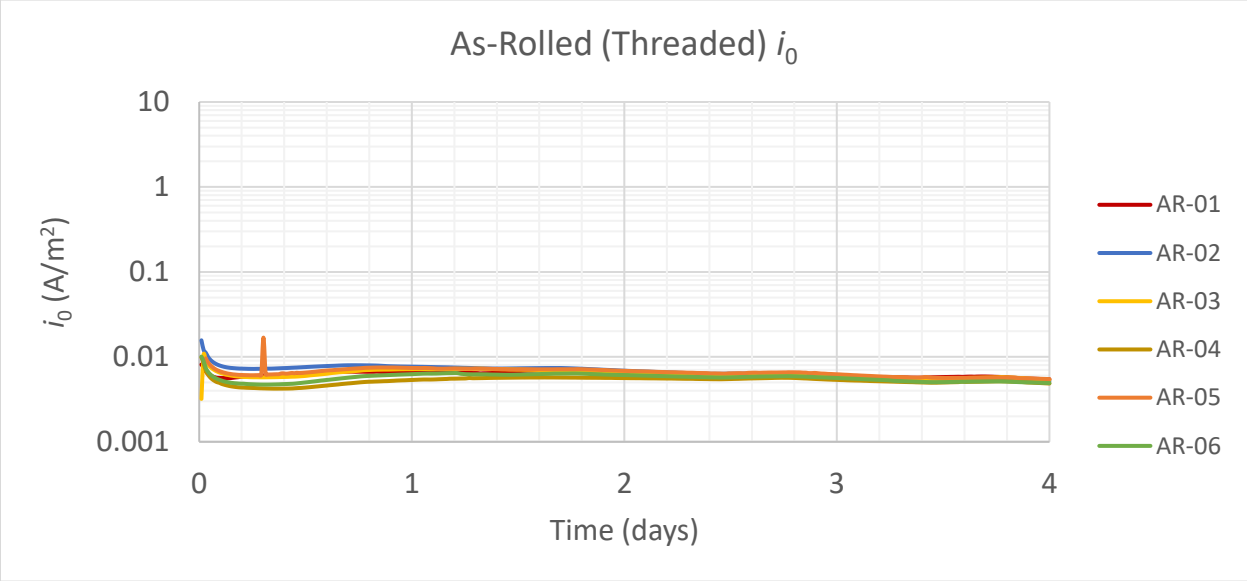

Figure 4-22: Plot of corrosion current density for as-rolled rebar

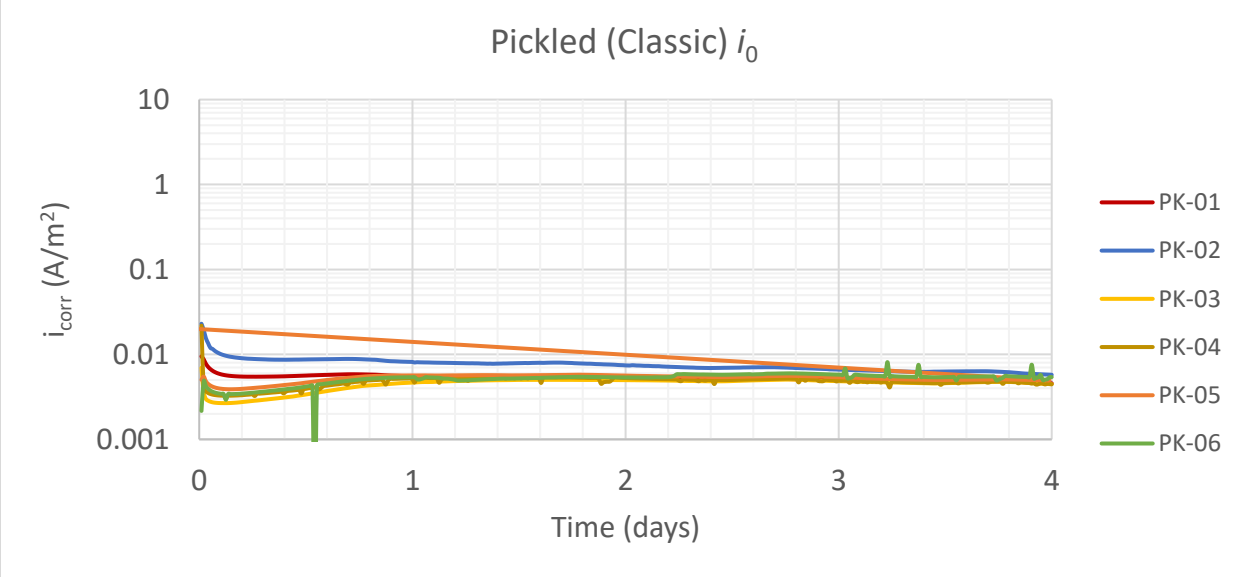

Figure 4-23: Plot of corrosion current density for pickled-only rebar

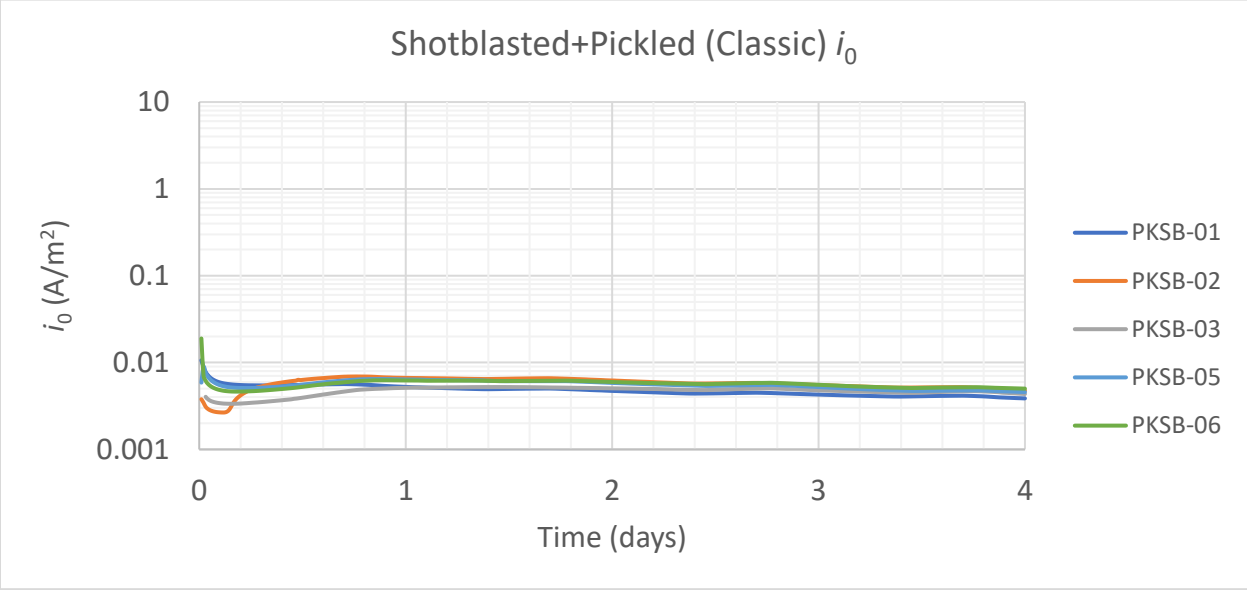

Figure 4-24: Plot of corrosion current density for shotblasted-and-pickled rebar with classic lug

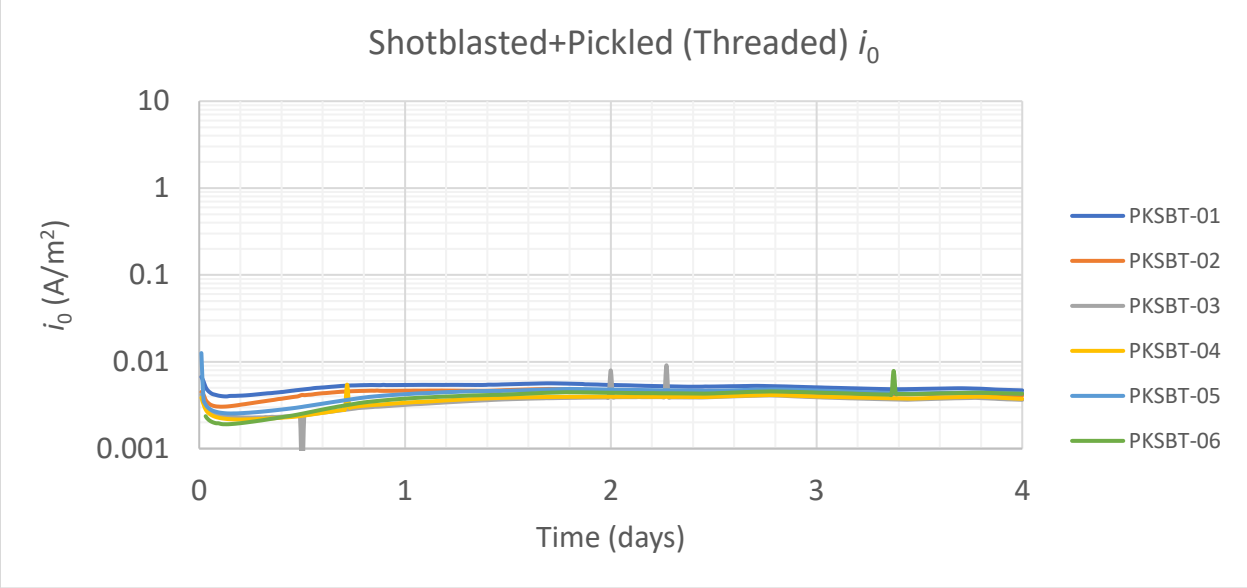

Figure 4-25: Plot of corrosion current density for shotblasted-and-pickled rebar with threaded lug

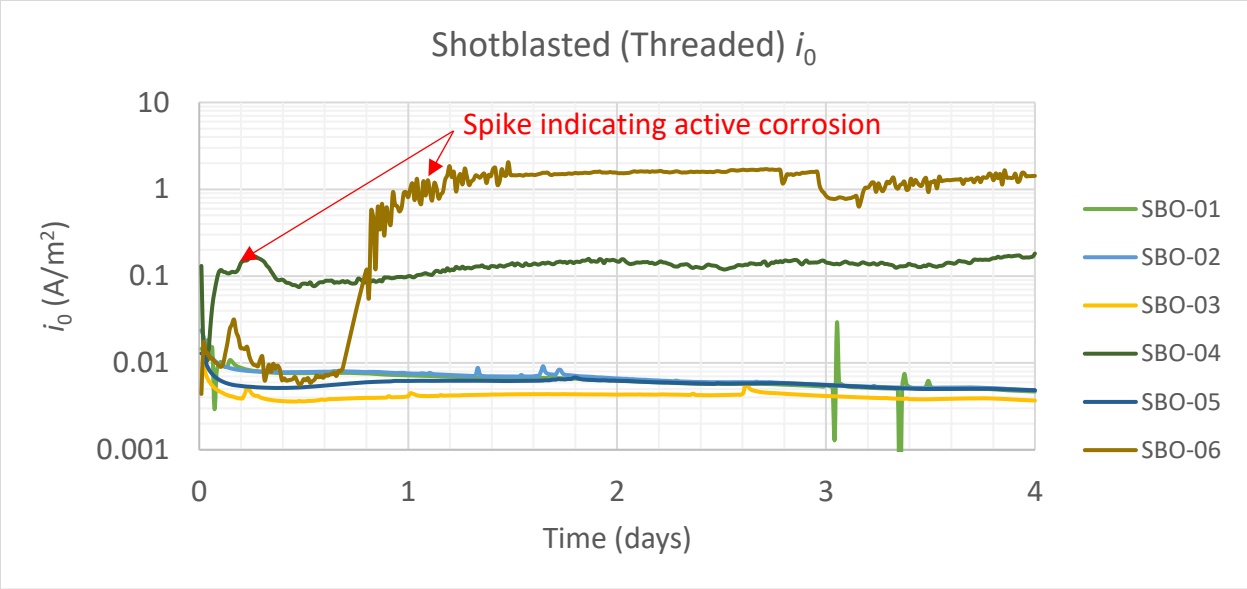

Figure 4-26: Plot of corrosion current density for shotblasted-only rebar

When comparing the plots of OCP and i_0, the specimens with inconsistent potential readings are also the same specimens with unstable i_0 measurements.

In the case of SBO-04 and SBO-06, the specimens curves exhibit a rapid increase in current densities after several hours of polarization followed by a fairly constant rate therafter. Post-test examination of the rebar revealed evidence of active corrosion on the bars, the difference between the measured rates being attributed to different areas of active corrosion, the data giving only an average over the whole bar. Figure 4-27 shows the condition of SBO-04. Minor crevice corrosion was found under the lacquer, but most of the corrosion product was found on the area exposed to concrete. Crevice corrosion occurred since the lacquer did not form a complete seal on the surface of the rebar which led to gaps between the lacquer and surface of the rebar. Such small spaces are favourable conditions for crevice corrosion. If corrosion occurred only under the lacquer and nowhere else, this would be a false positive and the specimen would not be considered to have corroded. In this case corrosion product was observed on the exposed surface, so the specimen was counted as a corroded specimen.

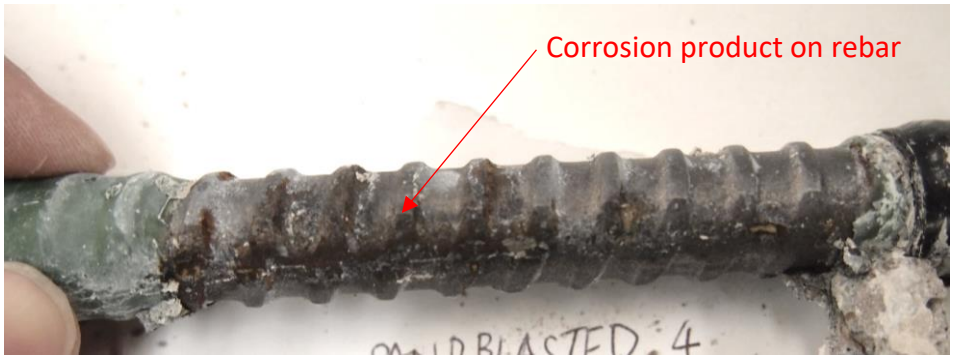

Figure 4-27: Specimen SBO-04 after test

Figure 4-28: Corrosion product found under lacquer at the end of rebar SBO-04

In addition, SBO-06 also had visible evidence of active corrosion. Cracks were observed on the surface of the concrete cylinder, with rust diffusing out to the surface, as seen in Figure 4-29. Again, post-test examination of the rebar shows extensive active corrosion. For this specimen, no corrosion was found under the lacquer, so the corrosion rate is attributed solely to the exposed area of the bar.

Figure 4-29: Cracked concrete cylinder containing SB06 with rust on surface

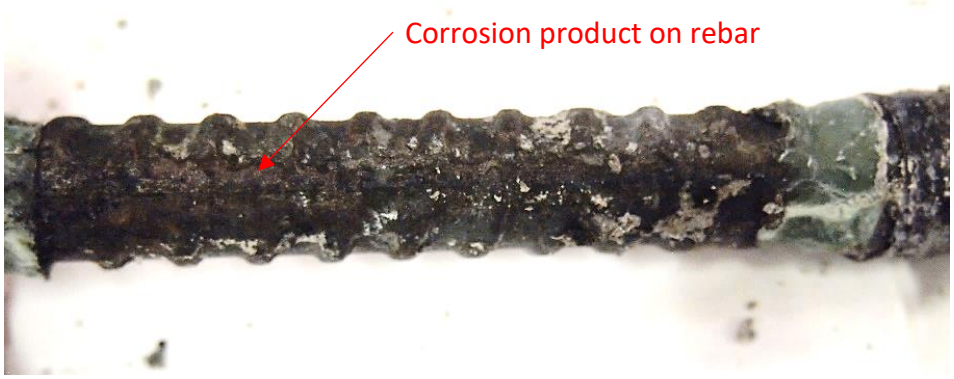

Figure 4-30: Specimen SBO-06 after test

Meanwhile, PKSB-04 had unstable potential and corrosion current density measurements throughout the duration of the test. The specimens were autopsied post-test, and no corrosion products were observed on the rebar for PKSB-04. Based on the magnitude of the current density observed in that specimen, there would have been severe corrosion on the rebar if the readings were genuine. Hence, the unstable reading observed is attributed to a loose or faulty connection with the potentiostat during the test.

Figure 4-31: PKSB-04 after test

4.3 Longer term exposure test

After the specimens were demoulded, the specimens were stored in the laboratory at ambient conditions. The temperature of the room varied from 23 to 27 degrees Celsius, with relative humidity varying between 12% and 57%. During this time, the macrocell potential, i.e., the potential drop across the standard resistor joining the top and bottom bars, was monitored while the bars were allowed to passivate.

The ponding wells were filled with saturated calcium hydroxide to maintain the high pH environment and prevent calcium hydroxide in the pore solution from leaching out. The ponding well was kept covered to minimize evaporation of the solution. However, it was observed that the solution permeated through the specimen and flowed out of the bottom and side surfaces of the specimen. The solution in the ponding well drained within a day, and over time the solution accumulated in the containers which held the specimens. This resulted in specimens being immersed in solution and reducing oxygen supply to the two bottom rebar cathodes, which could hinder the reduction reaction. Hence the specimens were placed on plywood pedestals above the drained solution to allow the bottom surface to be exposed to air and not immersed in solution.

Figure 4-32: Mortar specimen with sodium chloride crystals on surface

200 days after the mortar specimens were cast, sodium chloride was added to the ponding well. After two weeks, sodium chloride was crystallizing on the surface of the mortar specimen. This phenomenon is caused by the hygroscopic property of sodium chloride. The critical relative humidity of sodium chloride at 20°C is 74% [68]. If the relative humidity of the surrounding is greater than that, then moisture from the atmosphere would be absorbed by the salt. However, if the relative humidity of the surrounding is less than 74%, then water evaporates, leading to crystallization of the salt. The ponding well was monitored closely and kept filled daily to ensure a supply of chlorides to the rebar.

4.3.1 Macrocell potential and current measurements

Using Ohm's Law, the macrocell potential measurements were converted to current using Equation 3-1. Then, it is converted into current density by dividing with the exposed area of the top bar. The following plots show the corrosion current density, i_0 over time. In these plots, positive values indicate oxidation of the top bar, the working electrode, while negative values indicate oxidation of the bottom bars, the counter electrodes. A corrosion current density of 0.001 A/m^2 is approximately equal to a loss of material of 1 µm annually. Note that the vertical

axis for the following graphs is on a linear scale, whereas the i_0 plots for the rapid screening test in Section 4.2 covered a larger range of current densities and were on a log scale.

Sodium chloride was added to the specimens 200 days after casting. This is illustrated on the graphs with a dashed line.

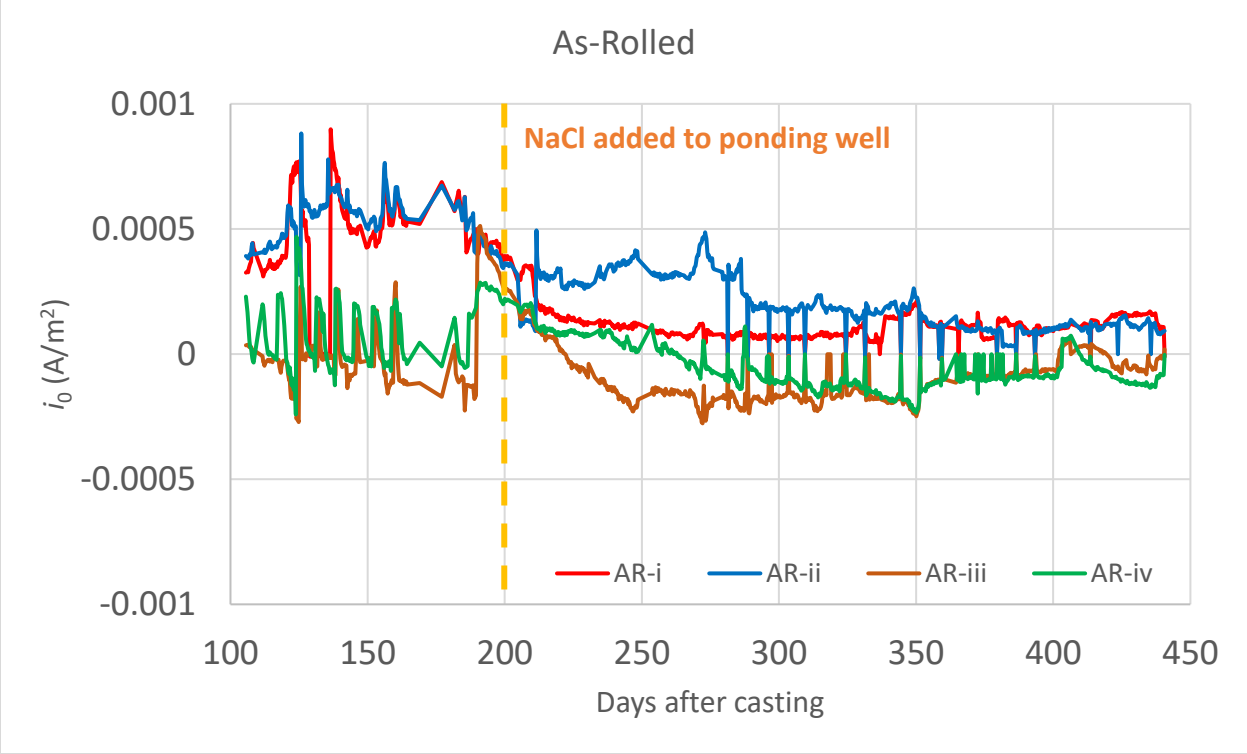

Figure 4-33: Plot of corrosion current density, i_0 over time for as-rolled rebar

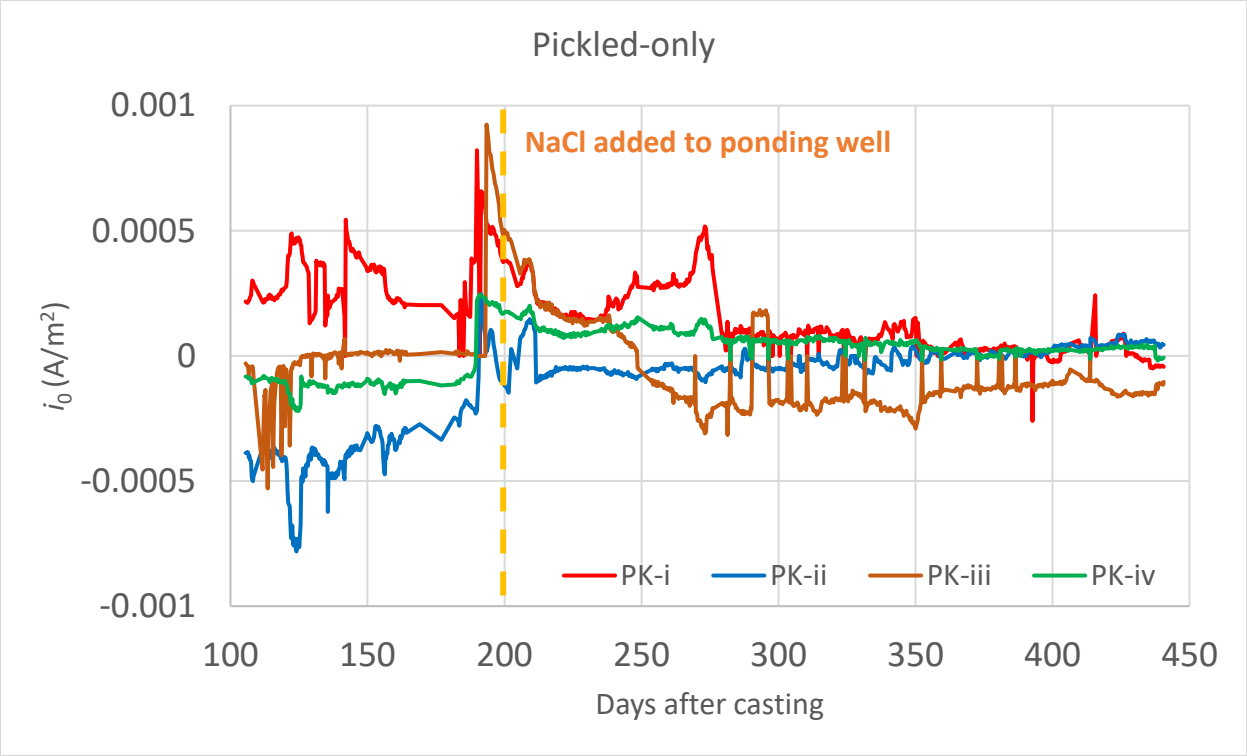

Figure 4-34: Plot of corrosion current density, i_0 over time for pickled-only rebar

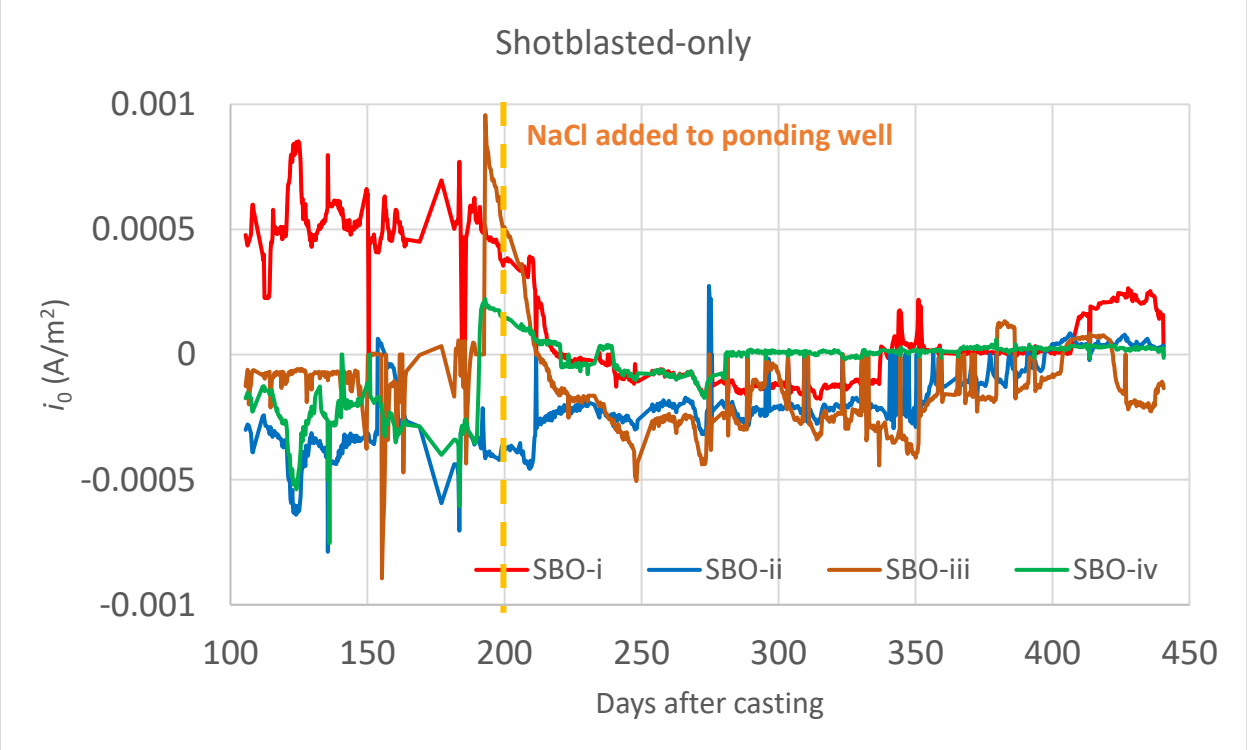

Figure 4-35: Plot of corrosion current density, i_0 over time for shotblasted-only rebar

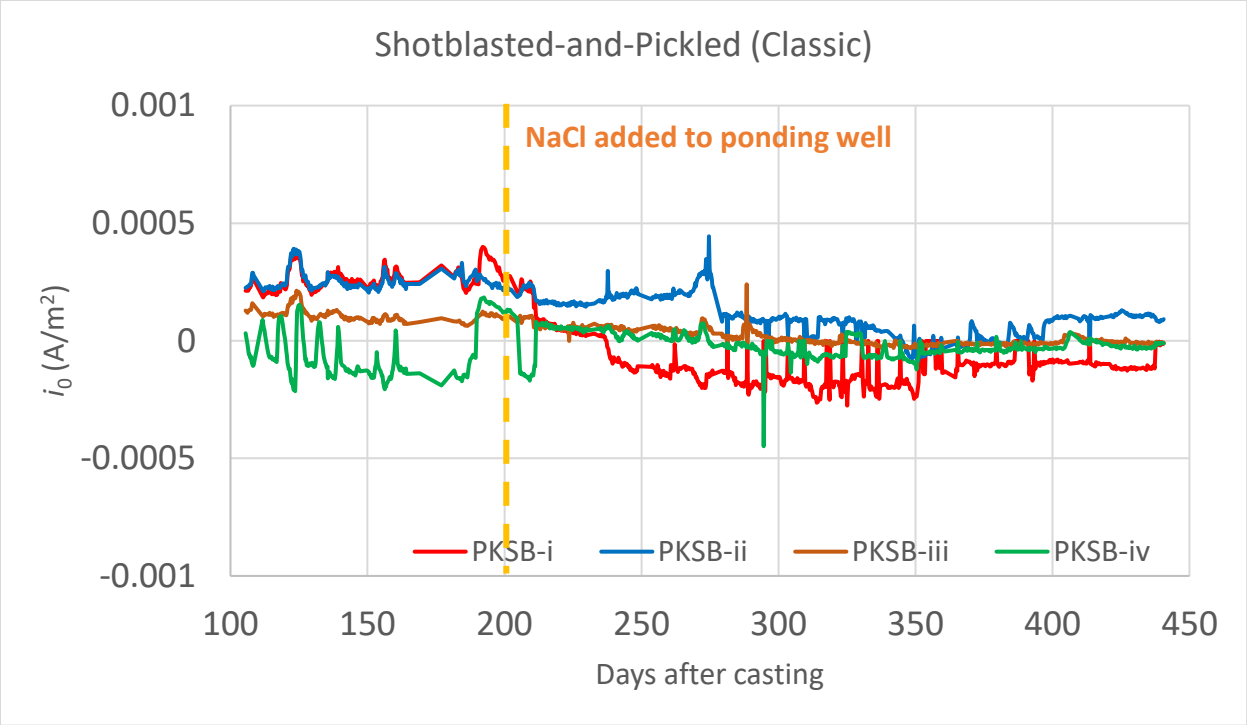

Figure 4-36: Plot of corrosion current density, i_0 over time for shotblasted-and-pickled rebar with classic lug

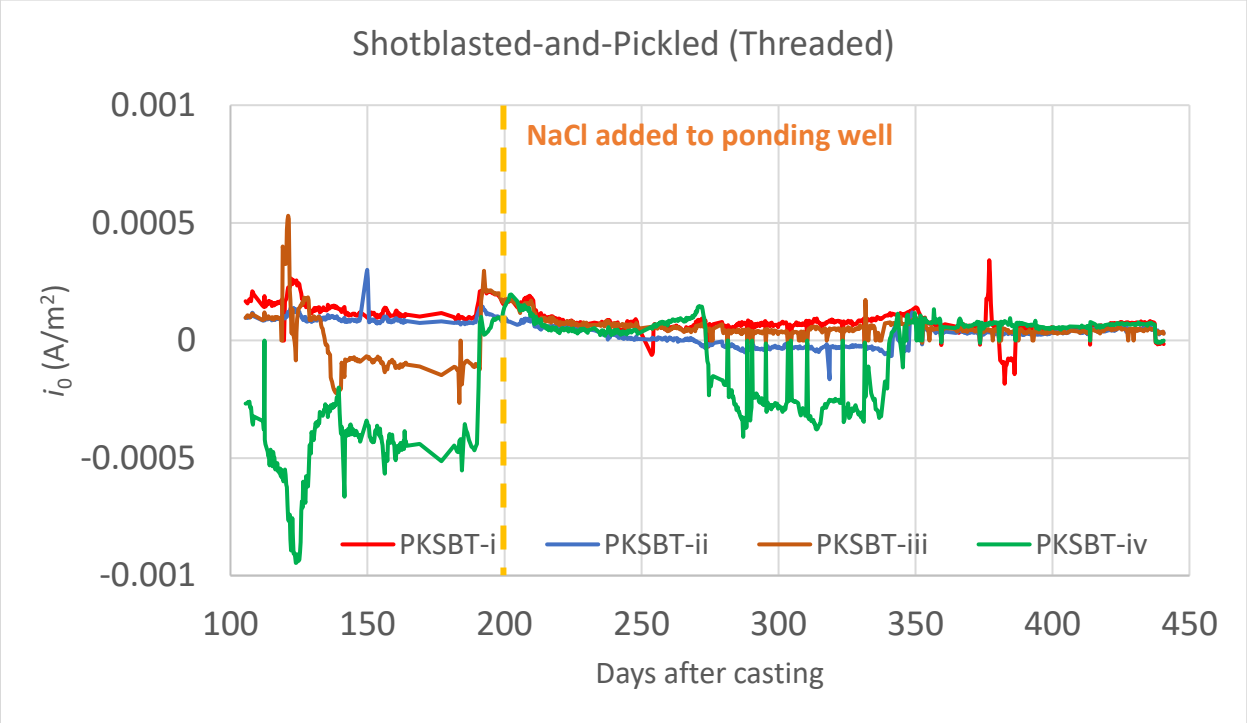

Figure 4-37: Plot of corrosion current density, i_0 over time for shotblasted-and-pickled rebar with threaded lug

When considering the figures above, active corrosion would have been represented by positive values of i_0 several orders of magnitude higher than the "steady state" value over a sustained period of time. None of the specimens displayed indications of continuous active corrosion. However, it was observed that all specimens experience periodic jumps in i_0. This is normal behaviour as the steel begins oxidizing and then repassivates, causing periodic sharp increases in current density but were not sustained over time.

The specimens showed more fluctuation in i_0 during the period before sodium chloride was added to the well. After sodium chloride started being added on the 200-day mark, the i_0 of the specimens showed less variability. This can be explained by the chlorides creating a driving force in order to initiate pitting. Before chlorides were present, the oxidation process was more stochastic and random, hence more variability would be expected. When the supply of chlorides was started and maintained, oxidation became more likely where chlorides were present.

Out of the four replicates for each type of surface condition, one specimen of each (labelled no. (ii) for each type), was not exposed to chlorides. The interesting observation from the plots above are that specimen (ii) for all surface conditions did not show significantly different behaviour compared to the other three replicates. In some cases, for example PKSBT-ii, the specimen displayed very similar behaviour to the other three replicates. This implies that the measured potentials are within the passive region for all specimens.

From the plots, negative i_0 was measured on at least one replicate out of three which were exposed to chlorides for all surface conditions. When considering the as-rolled, shotblasted-only, and pickled-only specimens, it is interesting that the counter electrodes were oxidizing more than the top bars. This is despite the fact that all bottom bars had undergone the conventional shotblasting and pickling processes after hot-rolling, which should be more resistant to corrosion when compared to an untreated or partially treated rebar.

At several times such as at 125 and 184 days, at least one specimen from each bar type experienced a large sudden increase in i_0. Most of them gradually decreased again over time

with the exception of PKSBT-iv. These spikes are probably a result of local electrical interference since it is sudden and occurs across several specimens at the same time.

4.3.2 Open circuit potential measurements

The following graphs show the open circuit potential (OCP) of the top bars over time since casting for each specimen. Data shown in the figure begin 128 days after casting. This is because data collected prior to that point were measured using a single reference electrode. This was changed to using four separate reference electrodes, one for each replicate. This reduces systematic error if the reference electrode had a drift in potential. This also still allows for comparison between rebar with different surface conditions if needed. However, data collected up to that point are not shown since it would not be possible to compare them to each other between periods.

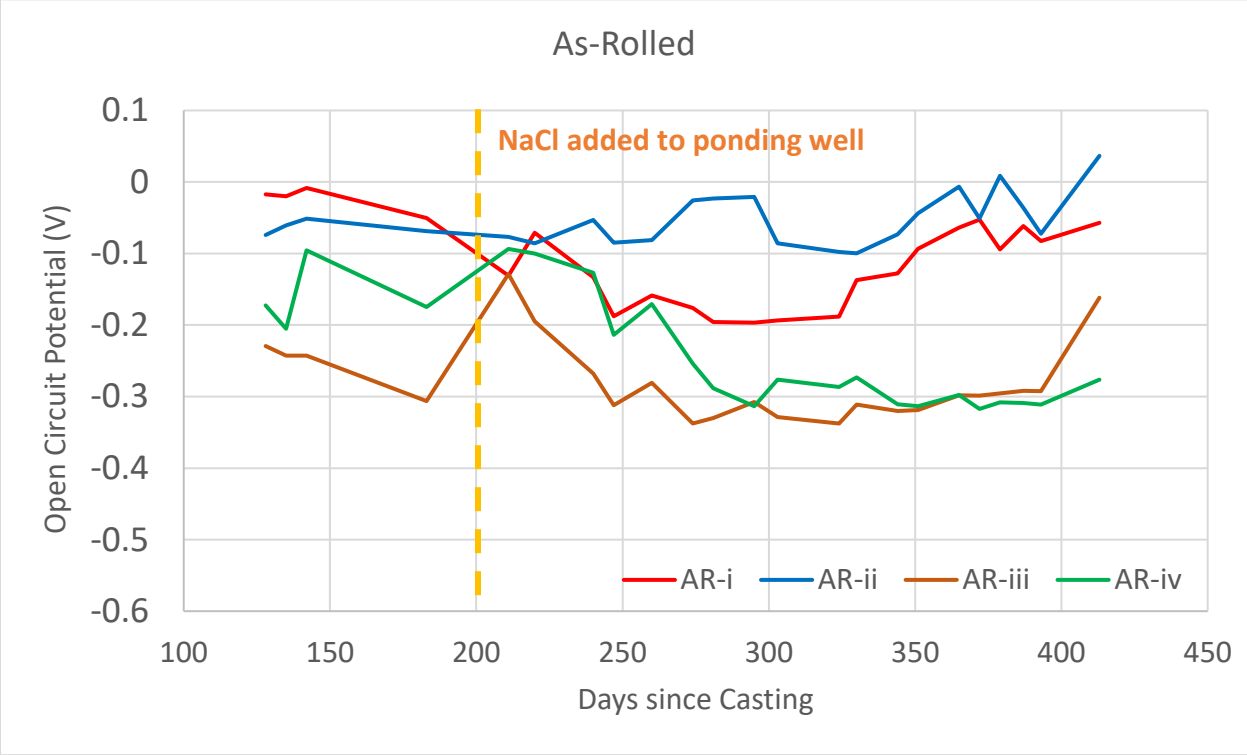

Figure 4-38: Open circuit potential of as-rolled rebar over time

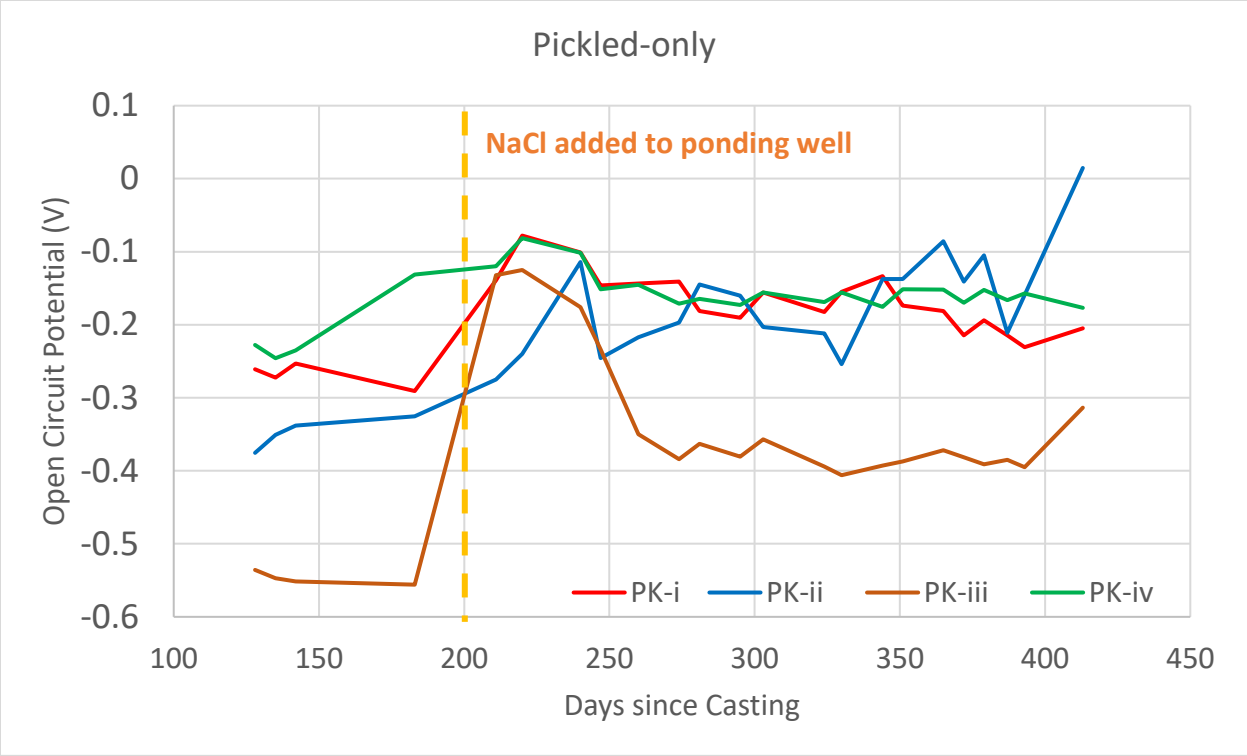

Figure 4-39: Open circuit potential of pickled-only rebar over time

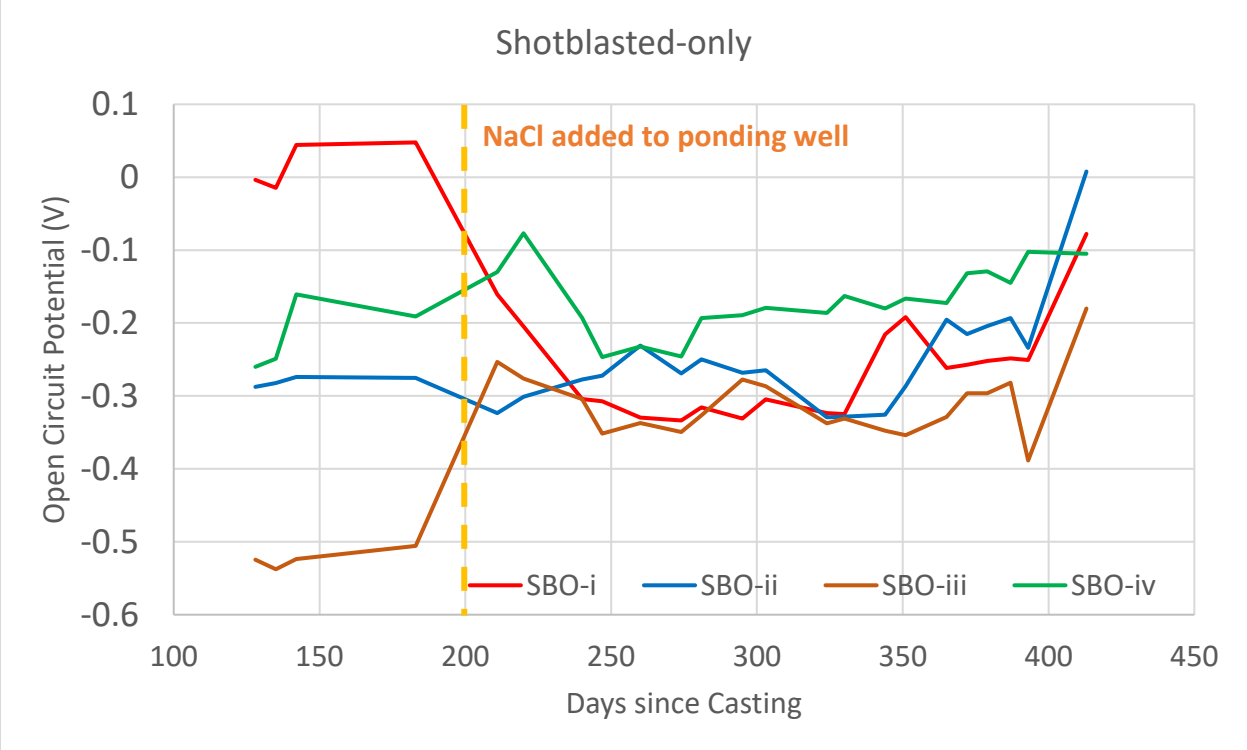

Figure 4-40: Open circuit potential of shotblasted-only rebar over time

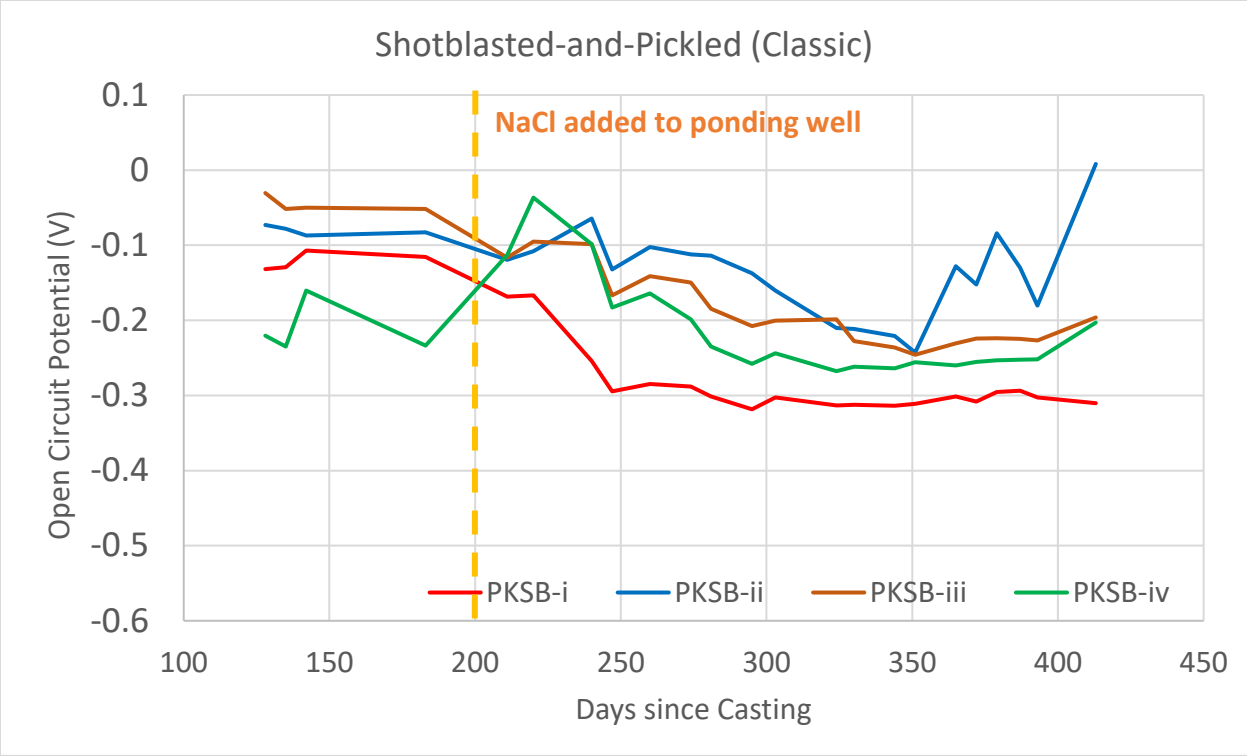

Figure 4-41: Open circuit potential of shotblasted-and-pickled rebar (classic lug) over time

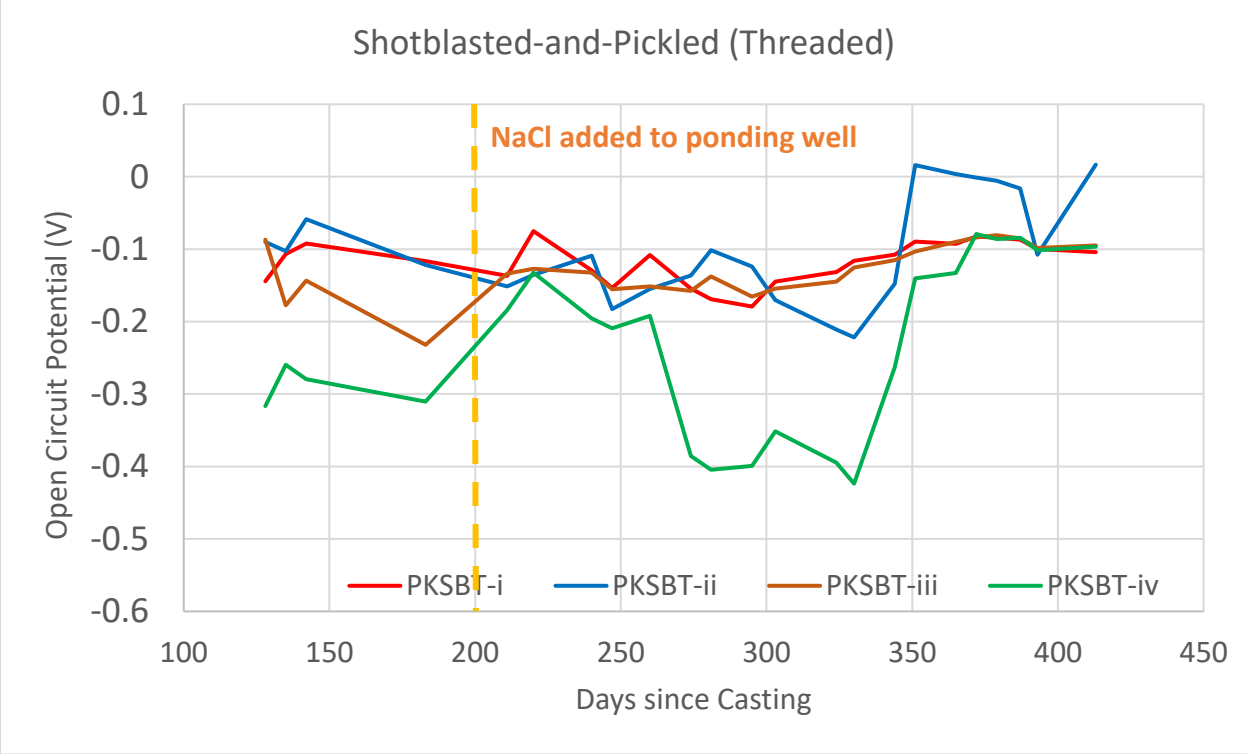

Figure 4-42: Open circuit potential of shotblasted-and-pickled rebar (threaded lug) over time

The behaviour of specimens can be divided into two stages, before and after chlorides were added. Before chlorides were added, the OCP for all surface conditions except the as-rolled remained stable. The as-rolled trended in the negative direction, suggesting a more active corrosion behaviour even before chlorides were added. However, most specimens showed a jump in OCP values at the 183-day point. At this time, the specimens were allowed to dry and no solution was added to the ponding well. This led to decreased conductivity, hence a more positive or passive OCP value was observed here. Not all specimens experienced this jump, as these specimens dried out more slowly. This observation was also repeated at the 390-day mark, where specimens dried out as the ponding well was not filled over Christmas break since the laboratory was closed.

When chlorides were added, all specimens started showing a more negative value of OCP. The drop in OCP for all specimens varied between 100 to 300 mV for specimens with chlorides, after which it remained stable up to the end, except for PKSBT-iv which experienced a large increase This was unusual behaviour which suggested possible repassivating behaviour, especially when considering it also experienced a significantly larger drop in OCP compared to the other PKSBT specimens. In addition, the macrocell i_0 was in the negative range in this period (300-350 days) seen in Figure 4-37, further emphasizing this behaviour.

Meanwhile, specimens with chloride-free solution in the ponding well (all blue curves in the figures) tended to fluctuate but generally exhibited more positive OCP values compared to corresponding specimens with chlorides. In all cases, these specimens had the most positive OCP value prior to autopsy, with the exception of AR-ii which had the second highest.

4.3.3 Microcell corrosion rate measurements

The following figures show the corrosion current density for each specimen obtained from the linear polarization resistance (LPR) test and the galvanostatic potential (GP) test. The method for calculating i_0 was detailed in Section 3.2.4.

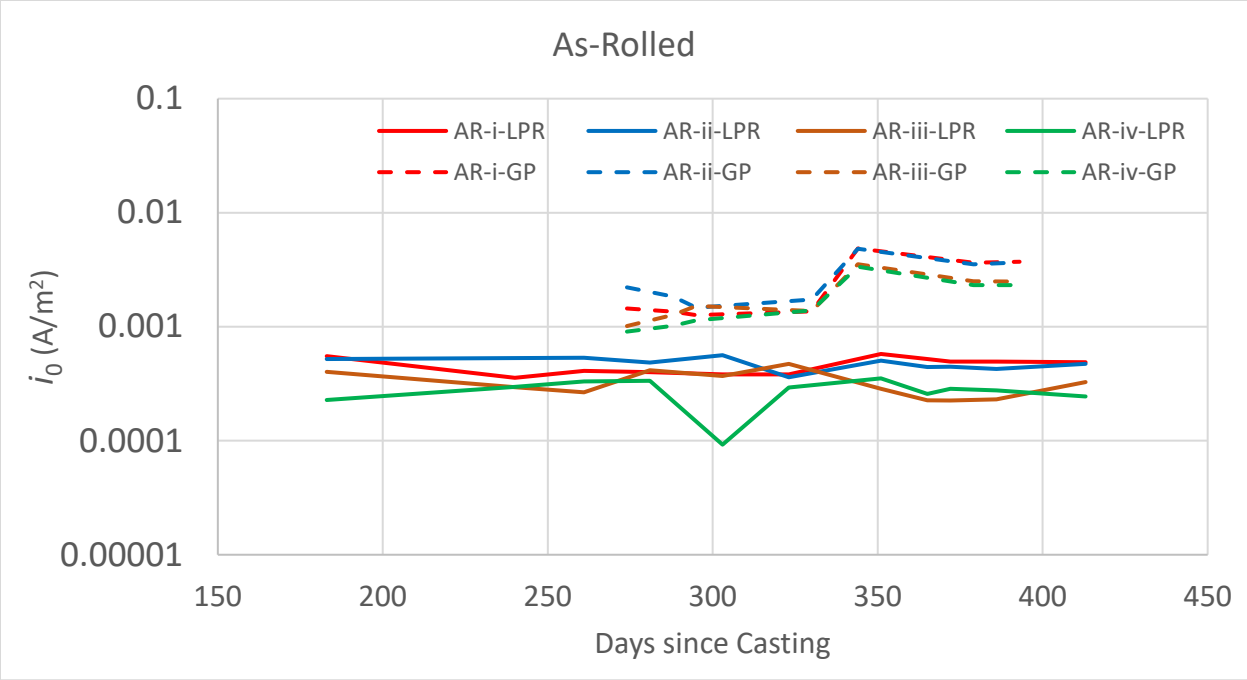

Figure 4-43: Plot of corrosion current density, i_0 over time from LPR and GP tests for as-rolled rebar

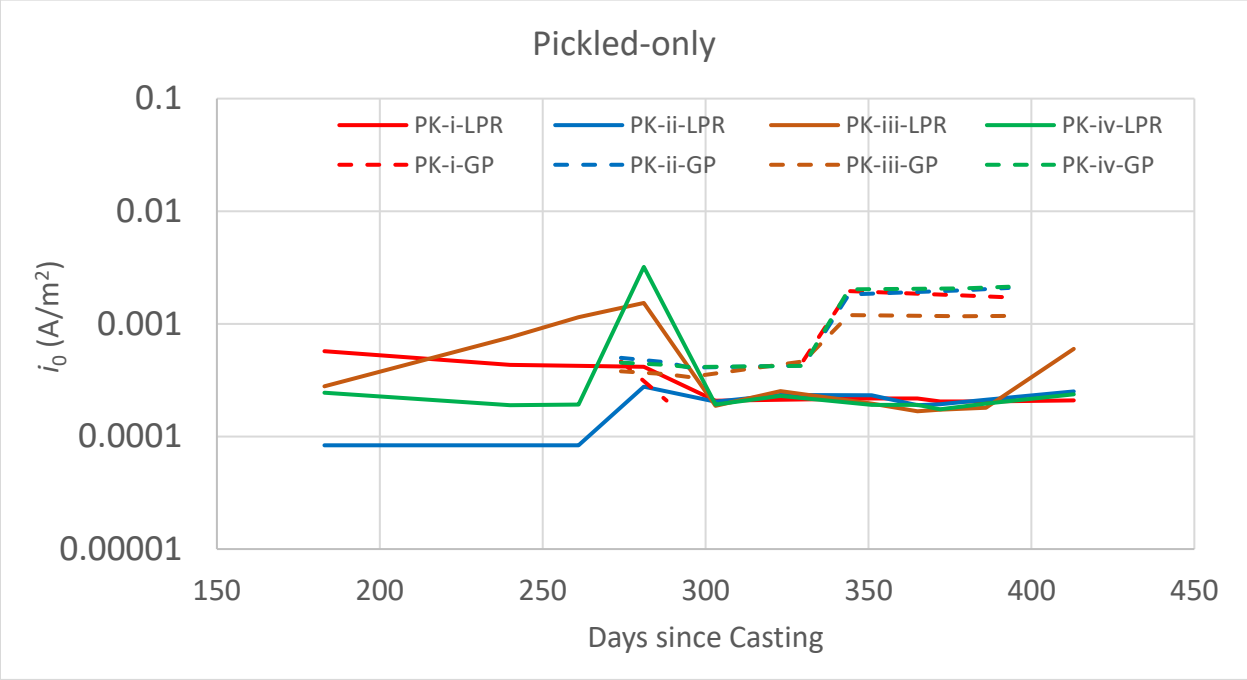

Figure 4-44: Plot of corrosion current density, i_0 over time from LPR and GP tests for pickled-only rebar

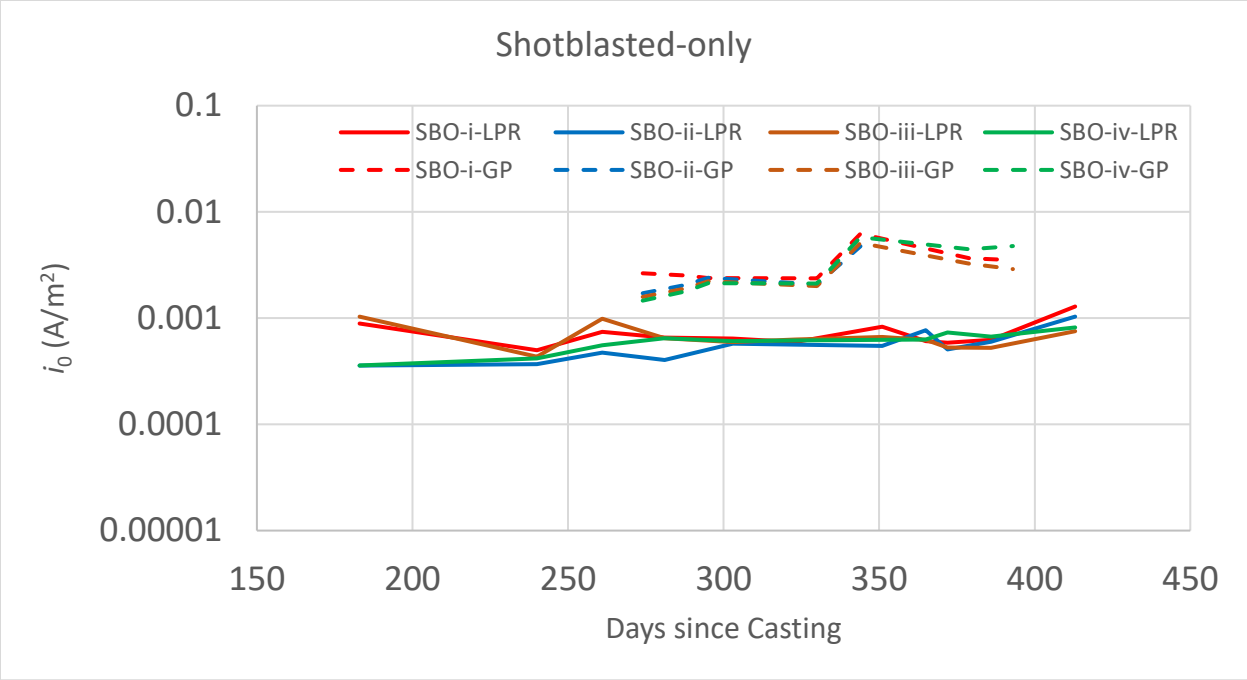

Figure 4-45: Plot of corrosion current density, i_0 over time from LPR and GP tests for shotblasted-only rebar

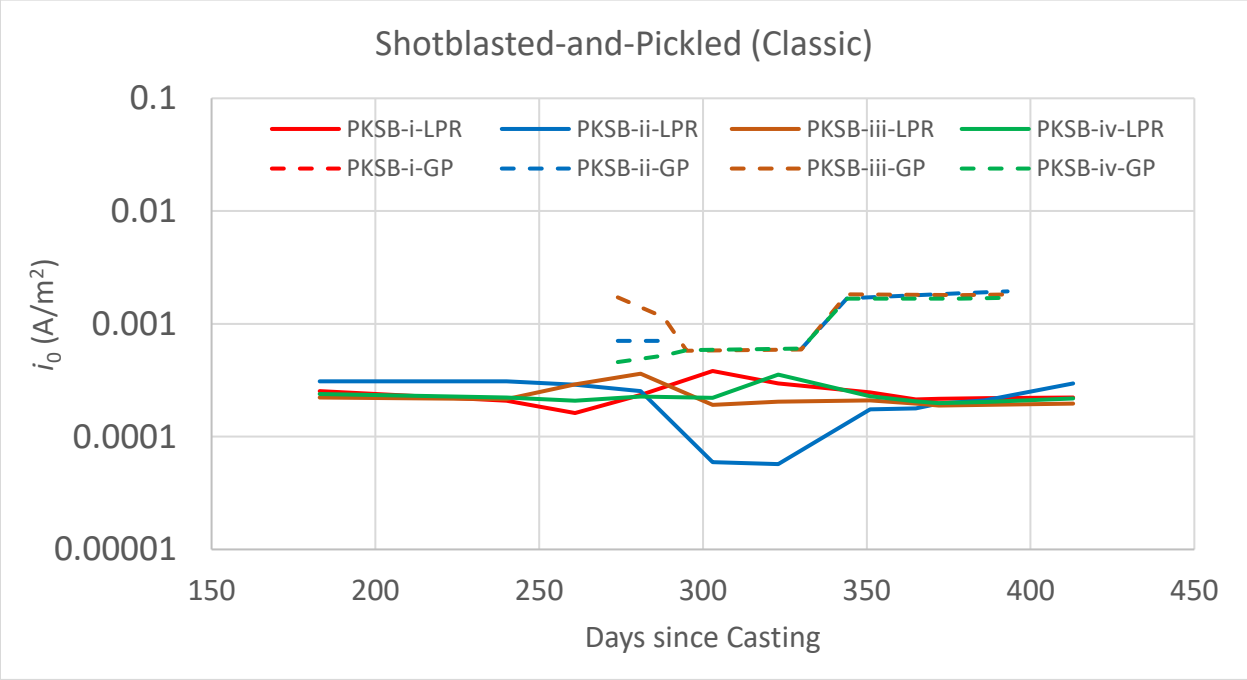

Figure 4-46: Plot of corrosion current density, i_0 over time from LPR and GP tests for shotblasted-and pickled rebar with classic lug

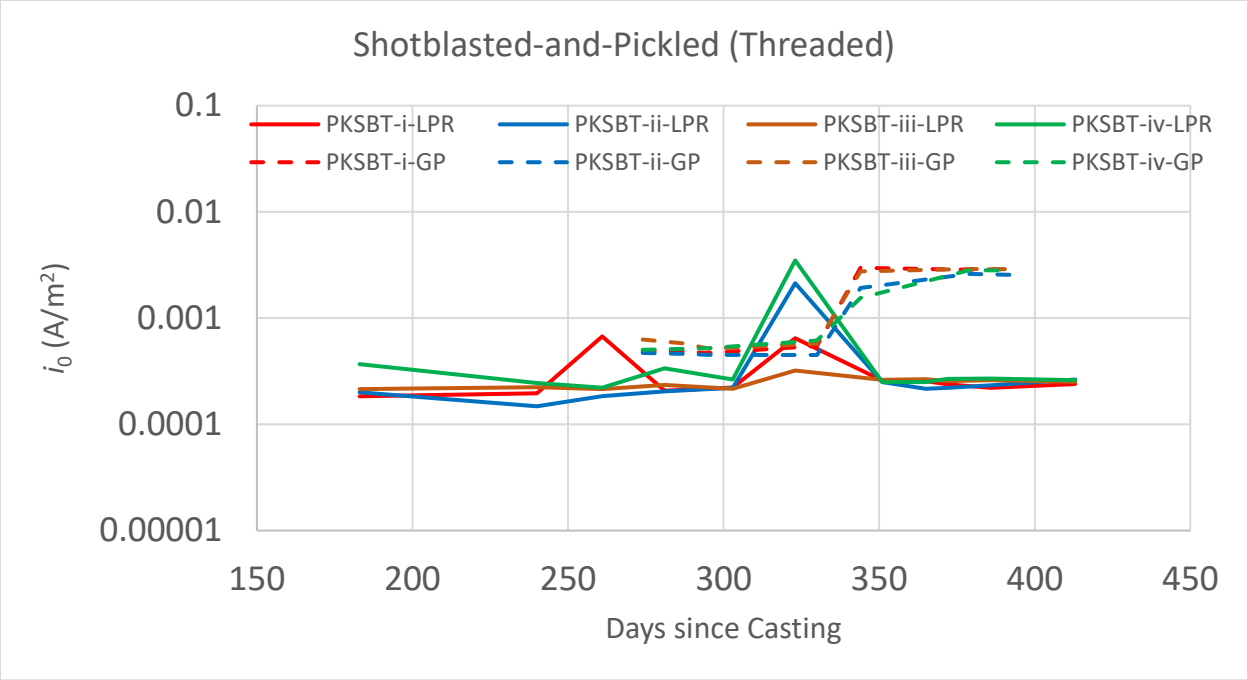

Figure 4-47: Plot of corrosion current density, i_0 over time from LPR and GP tests for shotblasted-and pickled rebar with threaded lug

The i_0 values obtained from LPR are generally stable for all specimens. In most cases, the values are under $1 \times 10^{-3}\ A/m^2$, except for the shotblasted-only specimens after 400 days which just exceed that threshold. There are periodic regions where several specimens show a temporary increase in i_0, such as those seen in pickled-only specimens at 281-days or PKSBT specimens at 323-days. Since this increase only occurred in several specimens tested together on the same day, it was deemed to be experimental noise due to equipment issues such as loose wiring or a temporary electrical disturbance.

Meanwhile, the i_0 values obtained from GP are much higher compared to LPR values. This is due to incomplete stabilization of potential from the specimens during the test, as described in Chapter 3. This meant that the polarization resistance, R_p was undercounted, leading to a greater i_0 since i_0 is inversely proportional to of R_p. Furthermore, these i_0 values account for the drop in potential due to resistance from the mortar. Hence, the corresponding polarization resistance, R_p would also be lower leading to a greater i_0.

As described in Section 3.2.4, the polarization current was increased from 10 µA to 150 µA on all specimens for the GP test. This accounted for the sharp increase in i_0 which can be observed after 334-days. However, for the as-rolled and shotblasted-only specimens, this increased failed to generate the expected plateau in potential. Even after increasing the polarization to 300 µA, complete measurements were not possible in these specimens.

4.3.4 Autopsy of specimens

After 440 days, two replicates from each type of rebar were cut open to expose the rebar for inspection. Both replicates had been exposed to chlorides. As described in Section 3.2.3, a wet cut method is used for cutting. However, in some specimens, it was observed that some water may have infiltrated to the rebar level.

During the autopsy, cracking was observed at the bottom of the ponding well on specimens PK-iv and PKSB-iv. The cracks appear to be running parallel over the rebar in the mortar. This was attributed to cracking created from the uneven surface on the formwork. Cling film had been used to wrap the extruded polystyrene used to create a ponding well in the formwork. The small creases from the cling film created an uneven surface which led to more force needed during demoulding from the formwork. Moreover, the cracking may have been exacerbated by the precipitation of calcium hydroxide and sodium chloride crystals in the pores of the mortar when the specimen dried out.

Figure 4-48: Specimen PK-iv with cracks at the bottom of the ponding well. Walls of the well had been removed

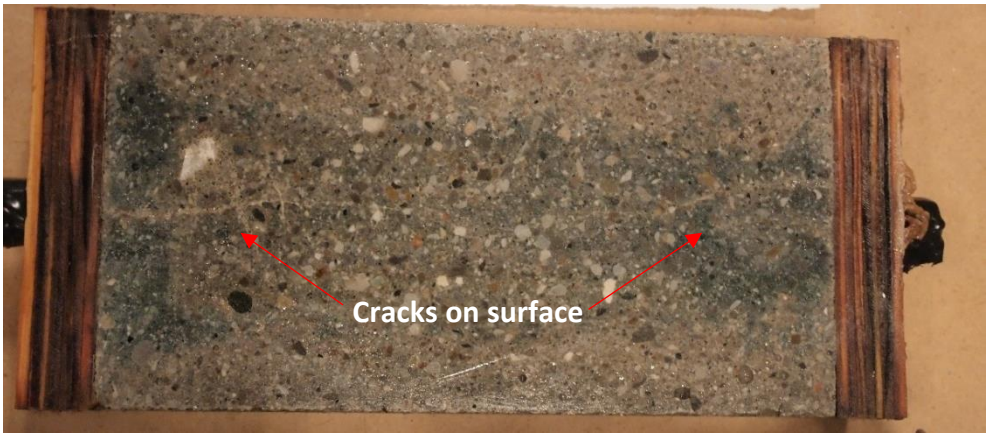

Figure 4-49: Specimen PKSB-iv with cracks at the bottom of the ponding well. Walls of the well had been removed

All ten rebar specimens which were removed from the mortar did not show any signs of active corrosion. This agrees with electrochemical testing results described in the previous section. Figure 4-50 shows one bar from each type of surface condition on the rebar removed from the mortar.

Figure 4-50: Autopsied rebar from mortar specimens. From top: as-rolled, pickled-only, shotblasted-only, shotblasted-and-pickled (classic), shotblasted-and-pickled (threaded)

4.3.5 X-ray fluorescence (XRF) analysis of mortar prism

When the longer-term specimens were autopsied, the mortar prisms were cut such that the top bar was separated from the bottom bars. The mortar prism with the top bar was carefully split in half to preserve the rebar impression in the mortar which had been in contact with the rebar. One half of the cut prism is shown in Figure 4-51.

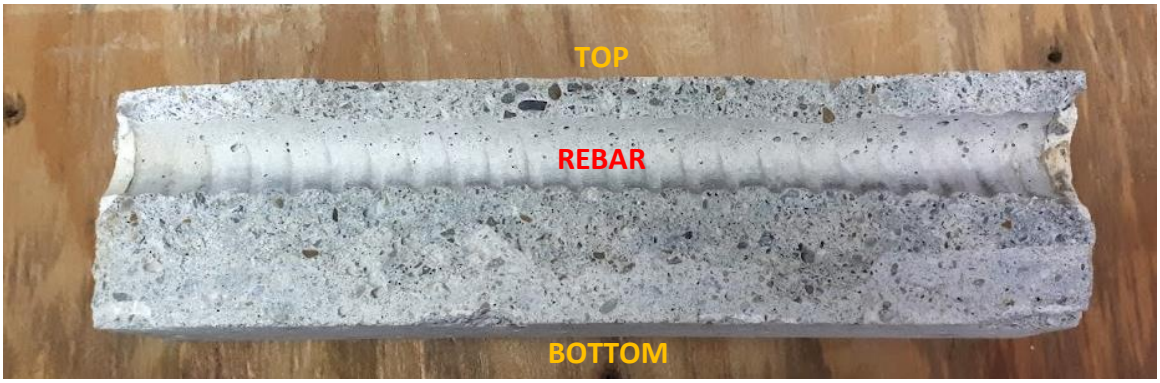

Figure 4-51: Split mortar prism from longer-term corrosion test

XRF measurements were taken along the rebar impression, as well as along the top and bottom surfaces in order to measure the amount of chloride present in the mortar. Table 4-1 shows the average mass percent of chlorides from five readings taken in these locations. The amounts measured by XRF have been calibrated such that they represent mass percent of cementitious material as generally reported in literature, since any scanned area of the prism is only made up of 22.2% cementitious material, based on the mix design of the specimen.

Table 4-1: Mass percentage of chloride ions on specimen by mass of cementitious material

	% Cl^- (by mass of cementitious material)
Top	1.82
Rebar level	1.15
Bottom	0.30

It was observed that the surface of the mortar around the rebar was made up of primarily cement paste, due to the initial formation of paste at the rebar surface, However, this layer of

cementitious paste is generally only 1-2 mm thick and the depth of penetration from X-rays exceeds this layer of cement paste. Hence the measurements collected are interpreted as percentages from the entire mortar instead of only the cementitious paste.

5 Discussion

5.1 Impact of post-rolling surface treatments on rebar corrosion behaviour

The rapid screening test and electrochemical tests on longer term test specimens all show that the specimens are still in passive condition at the end of each test respectively. This was confirmed with observations from the autopsied mortar specimens, which did not reveal any evidence of corrosion on the rebar. As expected, the shotblasted-and-pickled specimens did not show any evidence of corrosion with a corrosion current density, i_0 of 1×10^{-4} A/m^2.

More importantly, in the longer-term exposure specimens, the behaviour of the as-rolled rebar did not significantly differ from that of the conventional shotblasted-and-pickled rebar. This is despite cracks being found in the mill scale and a more permeable than expected mortar which provided ample amounts of chlorides to the top bar.

Images from microscopy revealed that the mill scale on as-rolled rebar contained cracks and defects on the surface. This is unsurprising since the mill scale is inherently brittle and would be susceptible to damage from handling or cracking due to temperature change as the rebar cools after rolling. Meanwhile, the SIMS analysis shows the composition of the mill scale to be similar to that of passive layers. In addition, the structure of the mill scale also resembles a passive film on stainless steel described in various work [32], [35], [38], except that a mill scale is orders of magnitude thicker compared to a passive film. This was qualitatively confirmed using EDS described in Section 4.1.2, where two distinct layers of oxides can be observed on cross-section SEM micrographs. The outer layer was predominantly iron oxides, while the inner layer of oxide contained iron and elevated levels of chromium. Neither SIMS nor EDS allows for determination of the molecular makeup in the oxides. It was also unclear whether the inner layer is as brittle as the outer layer, or if it is a more uniform layer with fewer defects.

When the rebar in the longer-term test was autopsied, no differences were observed on the rebar surface after over 400 days in a high pH environment. It did not appear that there had been any change to the mill scale, but a more detailed examination would be needed to

confirm this. For instance, the composition could be determined using EDS to see if the mill scale had changed over time.

It is important to note that these observations only apply for stainless steel used in a high pH environment. This is because in a high pH environment, iron and chromium are naturally passive [7]. Haematite (Fe_2O_3) and magnetite (Fe_3O_4) or a metastable chromium oxide (Cr_2O_3) tends to form and creates a protective barrier in the absence of chlorides. Cr_2O_3 breaks down when an anodic current is applied on the system, as shown in Figure 5-1. Incidentally, these oxides are the same compounds present in the mill scale [31], so it is likely that these compounds in the mill scale would remain stable in concrete if no chlorides are present.

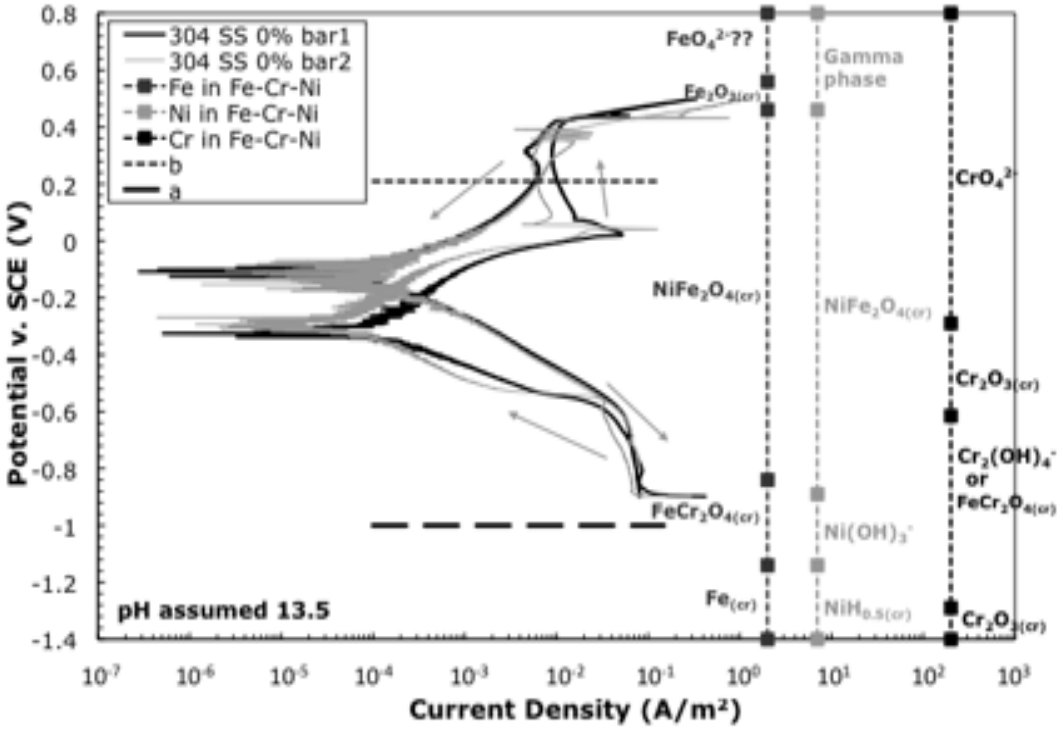

Figure 5-1: Equilibrium species of iron, chromium, and nickel at different potentials at pH 13.5 *[courtesy of C.M. Hansson]*

The two rebar conditions with partially removed mill scale are the shotblasted-only and pickled-only rebar. From the rapid screening test, two of the six shotblasted-only specimens were the only bars displaying signs of active corrosion. Both optical and scanning electron micrographs show that the shotblasted-only specimen had a much less uniform layer of mill scale around the

rebar compared to the as-rolled rebar. This leads to at least three possible causes for the active corrosion.

Firstly, according to the manufacturer, the shotblasting process was conducted using cast steel grit as the shotblasting medium [69]. This is unusual since the medium used by other stainless steel rebar manufacturers is generally non-metallic (such as silica) or stainless steel chips. Carbon steel corrodes more easily than stainless steel, so it is unclear why this medium was selected for shotblasting. The impact from the shotblasting process could lead to steel chips being embedded in the rebar and preferentially corroded, which could be a reason why active corrosion was observed in the rapid screening test.

Next, shotblasting is intended to remove the mill scale, but the present study indicates that removal is not complete. This can lead to galvanic corrosion on the rebar since the mill scale and exposed steel can form a galvanic couple. This could initiate or aggravate corrosion on the rebar. Furthermore, it is generally believed that the pickling process to remove the outer layer of steel, which is partially chromium depleted, is necessary to provide full corrosion protection. This outer layer of steel would be exposed from the shotblasting, which lowers the resistance of the rebar to corrosion.

However, in the rapid screening test, the other four shotblasted-only and all six of the pickled-only rebar showed similar corrosion resistance to the conventional shotblasted-and-pickled rebar. Although the surface of the pickled-only bars had less mill scale remaining on the bar compared to shotblasted-only bars, there are significant areas where mill scale was found inside micropits in the rebar. If the mill scale is tightly packed without flaws then it may be fine; however, if the mill scale is loose then these pits are essentially locations for crevice corrosion to occur. Given the widespread presence of such pits, it is certain that some may be weaker and would form weak spots for corrosion to initiate.

In the longer-term exposure test, 15% sodium chloride solution was added to the ponding well in order to attempt to initiate corrosion on the rebar, as recommended by ASTM A955. From the results of this test, it is clear that this concentration of chlorides is insufficient to initiate

corrosion after exposure for 240 days. This is despite the rebar being cast in poor quality mortar with unusually high permeability allowing chlorides to reach the rebar quickly, as well as cracked mill scale in some specimens which present a higher likelihood of crevice corrosion in the mill scale. As a comparison, the equivalent concentration of sodium chloride solution used in the rapid screening test is 24%, and even with an aggressive anodic polarization applied, only two out of a total of 30 specimens tested corroded. This demonstrates the effectiveness of UNS 32205 stainless steel in resisting corrosion in very harsh environments.

5.2 Impact of rib pattern on corrosion behaviour

Rebar of two rib patterns were tested in this project. One is the classic diagonal lug with a prominent rectangular longitudinal rib, while the other is a rectangular threaded lug with rounded edges and without the longitudinal rib. Images of both are shown in Figure 3-2. Both rebar were shotblasted-and-pickled to allow comparison without considering full or partial mill scale covering. No distinct differences were observed in corrosion behaviour any of the tests.

The longitudinal rib has often been mentioned as a location for corrosion initiation, since the edges of the rectangular rib form a crevice. Corrosion on this rib often leads to delamination and degradation of bond between concrete and reinforcement [70]. For this reason, the threaded lug pattern does not have a longitudinal rib present. However, since both specimens did not experience corrosion, it is not possible to comment whether the absence of the longitudinal rib helps to eliminate this issue.

5.3 Application of galvanostatic pulse technique for specimens with mill scale

When the galvanostatic pulse (GP) test was carried out on the longer-term exposure specimens, specimens were not able to achieve a plateau in potential in the typical test period of 180 seconds, when polarized with a 10 μA current. As described in Section 3.2.4, the polarization current was increased to 150 μA. This was effective for specimens with very little or without mill scale, i.e. shotblasted-and-pickled and pickled-only; however, for specimens with some mill scale remaining, the test could not be completed even when polarization current was increased to 300 μA and the pulse period increased to 600 seconds.

The GP test functions based on considering the specimen as an electrical circuit, specifically a Randle's circuit as described in Section 3.2.4. Work from literature has described passive layers on stainless steel as behaving similar to a semiconductor, specifically a capacitor. When the specimen is polarized, the capacitor is being charged, hence an increase in potential is observed. However, when the capacitor is fully charged, the potential reaches a plateau.

Since a passive layer could be described as a semiconductor, it is expected that a mill scale would behave in a similar manner. However, the irregularities of the mill scale such as thickness and cohesiveness would affect its capacitance on a local level. One example is shown in Figure 5-2, for an as-rolled bar AR-(ii), exposed only to chloride-free mortar.

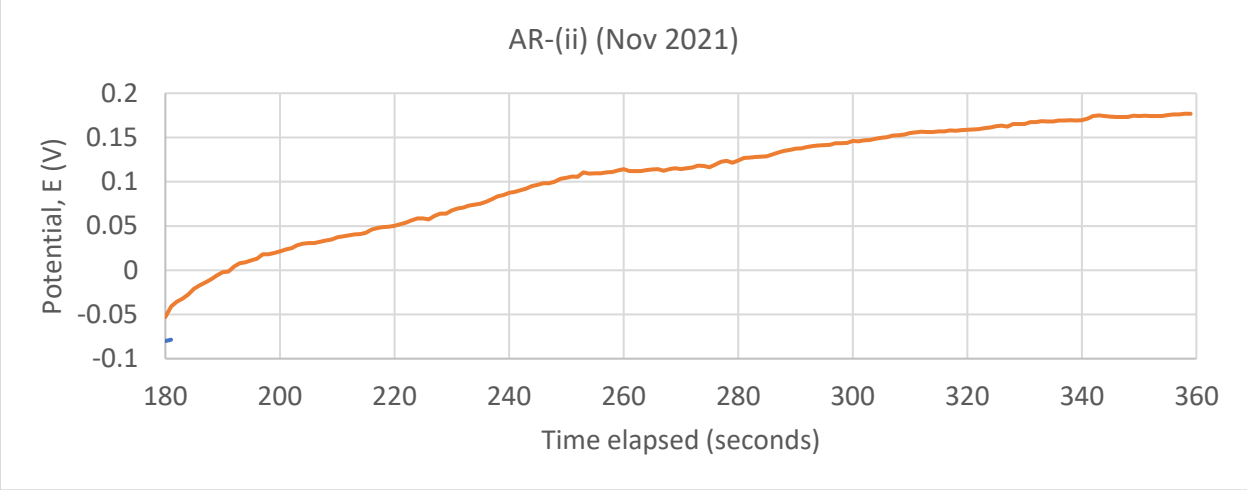

Figure 5-2: Plot of potential measurement in specimen AR-(ii) during a galvanostatic potential test

Local maxima or change in gradient of the curve could be observed at specific points such at time 230 seconds and 260 seconds but these were not maintained. One reason which could explain such behaviour is the variability in the mill scale leading to local variations in capacitance. It has been shown that cracks in the mill scale can lead to local areas of crevice corrosion under the mill scale and this phenomenon would also lead to local variations in potential [40]. The plot in Figure 5-2 should be contrasted with that in Figure 5-3, of a shotblasted-and-pickled bar, which shows the expected behaviour of a specimen in this test.

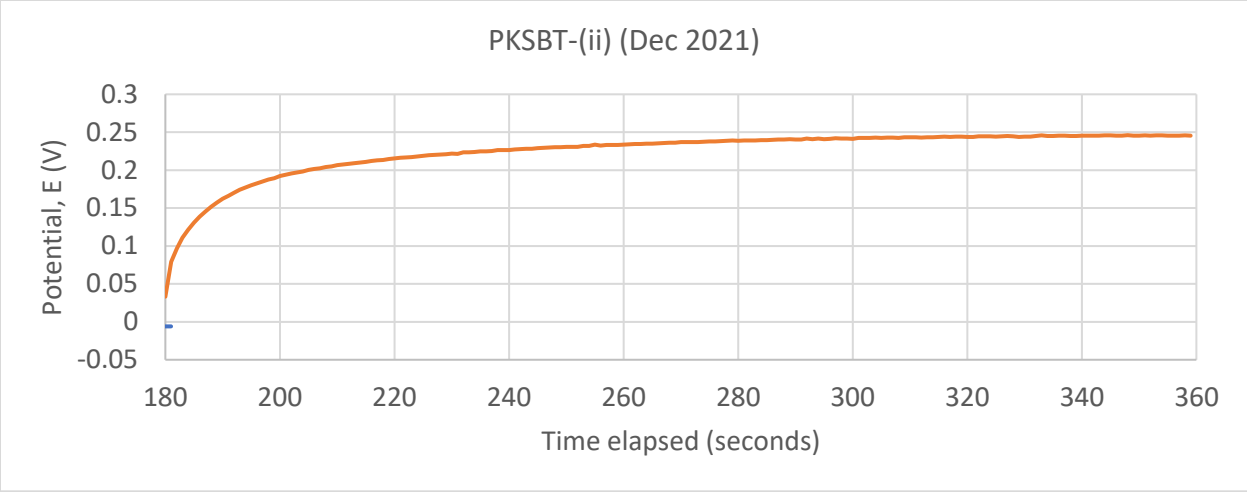

Figure 5-3: Plot of potential measurement in specimen PKSBT-(ii) during a galvanostatic potential test

This inability to plateau in potential was also found in shotblasted-only rebar since it has a less uniform mill scale layer compared to the as-rolled rebar, but not in the pickled-only rebar which had less mill scale remaining on the bar. Figure 5-4 shows the potential response from a GP test on a shotblasted-only rebar.

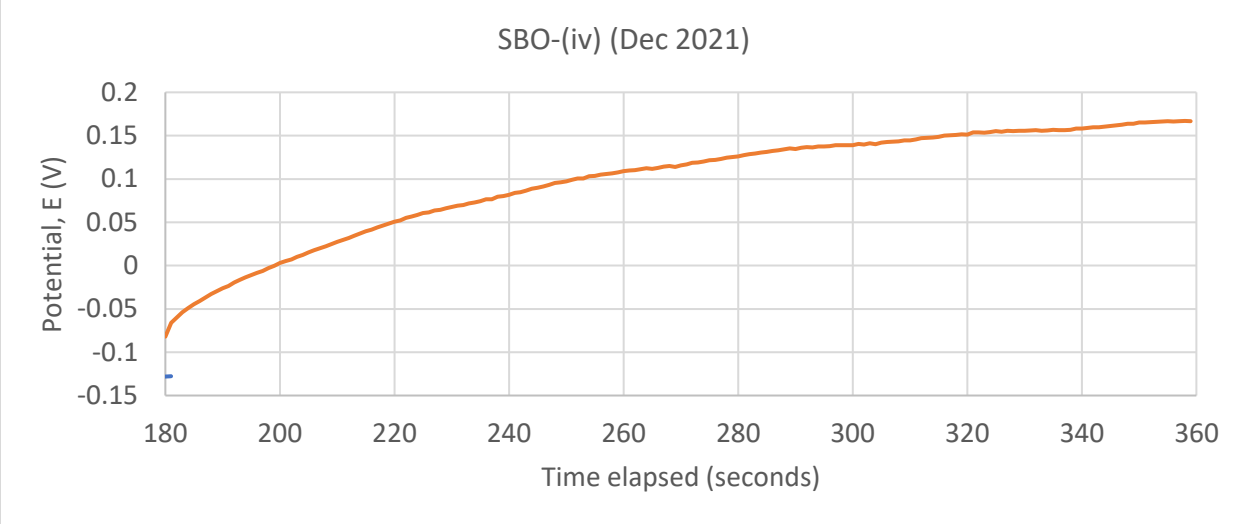

Figure 5-4: Plot of potential measurement in specimen SBO-(iv) during a galvanostatic potential test

Given the observations, it is clear that GP may not be as effective of a test for samples with mill scale present on stainless steel. Although an increased polarization current solved the issue for

samples with less or no mill scale, a polarization current which is too high could risk inducing corrosion in the specimen which would alter overall results.

Furthermore, the movement of ions and electrons through the mill scale is important since this would affect the oxidation reaction of the steel, whether this is at the steel – mill scale interface or at the mill scale – concrete interface. Hence, a better understanding of the electronic properties of mill scale in high pH environments is required to optimise the GP test.

5.4 Considerations for interpreting results from rapid screening test

There are several points that should be considered along with results from the rapid screening test. Firstly, it can be observed that most of the corrosion current density, i_0 for specimens in the rapid screening test are in a range between 5×10^{-3} to 1×10^{-2} A/m^2 range. These values are at least an order of magnitude higher than the values measured from the longer-term exposure test. This is because i_0 values from the rapid screening test are obtained from samples which had a +300 mV anodic polarization applied on the bars for 96 hours. In contrast, the long-term exposure specimens only received a +30 mV polarization during the LPR test and only for 6 minutes. Hence, the i_0 values from the rapid screening test and longer-term exposure test should not be used for comparison directly.

The rapid screening test specimens exemplify an exceedingly aggressive environment with days-old concrete and a high concentration of chloride ions. Chlorides were added to the mix at a rate of 7.5% by mass of cementitious. Work by van Niejenhuis et al [54] showed that this is the approximate solubility limit of chlorides in pore solution of this concrete mix. In an actual structure, it is highly improbable that the concentration of chlorides in the concrete would reach this level for several decades, if at all. This is because de-icing salts are applied only intermittently and during the winter months when low temperatures severely limit the diffusion rate of chlorides into the concrete.

Next, the magnitude of potential applied on the steel is very high. It is unlikely that a structure would experience this consistently in the field except in very specific situations, for example, where stray currents are present. Meanwhile, the short-term nature of the test means that the

concrete is still very fresh when the test begins. At this stage, the concrete would still be highly conductive to electron flow which increases electrochemical activity. The short time since casting also meant that there is little time for the passive film around a stainless steel rebar to stabilize before encountering chlorides.

Despite the comments above, the Rapid Screening Test is still a useful method to qualitatively compare corrosion performance between specimens tested under the same conditions in a short period of time.

5.5 Permeability of mortar specimens

As the project progressed, it was clear that the longer-term mortar specimens experienced higher than expected permeability. The solution in the ponding well drained within 24 hours which much higher than previous experiences with concrete, even though mortar is expected to have a higher permeability than concrete. The higher permeability is blamed on over-consolidation from vibration used during the casting process. Air voids in the specimen may have been induced in the specimen which, along with the shrinkage cracking in the ponding well, contributed to high flow of solution from the ponding well. This phenomenon appeared to slow down after chlorides were added to the ponding well. This may have been caused by crystallization of sodium chloride in the voids due to low relative humidity.

The impact of this issue could be attributed as the reason negative corrosion current density, i_0 was observed in the macrocell measurements. As discussed in Section 4.3.1, a negative measurement indicates that the cathodes or counter electrode rebars were oxidizing more quickly than the anode which is being tested. The counter electrodes used in the longer-term exposure specimens were conventional stainless steel rebar with the usual surface treatments, of the same alloy as the rebar of interest though made by a different manufacturer. Chlorides likely reached the level of the counter electrodes which would attack the passive layer on the counter electrodes. When all the electrodes were examined during the autopsy, no visible corrosion was found.

It is intriguing that negative measurements were obtained from specimens which contained rebar with some or no mill scale removed. In other words, the typical stainless steel rebar as counter electrodes were oxidizing more than those with mill scale present. This would further emphasize that stainless steel rebar with mill scale could perform effectively in the presence of chlorides as postulated earlier.

6 Conclusions and Recommendations

6.1 Conclusions

The conclusions from this study are limited to UNS 32205 duplex stainless steel rebar obtained from one manufacturer. It is not possible to extend these conclusions to other stainless steel grades or rebars from different manufacturers without further study.

1. When cast in concrete, the as-rolled rebar, with the mill scale left intact, shows the same corrosion resistance as rebar with all the conventional post-rolling treatments, i.e., shotblasting and then acid pickling. Neither surface showed any signs of active corrosion, despite the presence of cracks and flaws in the mill scale, as well as testing in the aggressive conditions in a rapid screening test, and in the case of the longer-term exposure test, being cast in poor quality mortar.

2. From the rapid screening test results, partial removal of mill scale by only shotblasting can have a detrimental effect on the corrosion performance of the rebar. This observation could be attributed to three different mechanisms. Firstly, the carbon steel grit used from the shotblasting process may have become embedded in the rebar surface, which would corrode preferentially. Secondly, observations of the shotblasted-only cross section revealed that the mill scale is not uniformly removed as there are areas with mill scale remaining and others almost completely removed. This could lead to galvanic corrosion between the exposed steel and the mill scale or even crevice corrosion under the remaining mill scale. Finally, any exposed surface would have a chromium depleted layer, which is more susceptible to corrosion.

3. None of the specimens in any of the surface conditions exhibited evidence of active corrosion from the electrochemical measurements after being cast in mortar for 440 days and exposed to a 15% by weight sodium chloride solution for the final 240 days. When selected bars were autopsied and examined after this period, no changes on the surface were observed visually. It was concluded that this concentration of sodium chloride

solution is inadequate to cause breakdown of the passive film on UNS 32205 stainless steel in this study after continuous exposure for 240 days, despite the rebar being cast in poor quality mortar, which allowed for faster diffusion of chlorides to the surface of the rebar. Furthermore, even when tested in an aggressive environment in a rapid screening test, only two out of the 30 specimens tested displayed active corrosion. This demonstrates the effectiveness of this grade of stainless steel rebar in resisting corrosion in high chloride environments.

4. Observations from microscopy revealed that the mill scale on stainless steel had bilayer structure with a “outer layer” of predominantly iron oxides and an “inner layer” of oxides containing iron and elevated levels of chromium, followed by a chromium depleted region in the steel alloy under the mill scale. This resembles the structure of a passive film on stainless steel with conventional post-rolling treatments, except that the mill scale is tens of micrometres thick while the thickness of the passive film is only a few nanometres.

5. The corrosion performance of the rebar is not affected when a threaded lug with rounded edges and no longitudinal rib on the rebar is used instead of the conventional diagonal lug with a sharp rectangular longitudinal rib. When comparing the specimens of both lug types, neither displayed active corrosion from a rapid screening test or from a longer-term exposure test.

6. The pickling or shotblasting processes alone performed on the rebar did not completely remove mill scale. When only shotblasting is used, large areas of the rebar surface still had significant mill scale remaining and exposed steel in some areas. Only pickling the rebar removes more mill scale compared to only shotblasting; however, there are significant regions on the rebar where the mill scale has become embedded in the alloy and the pickling process also produced some micropits.

7. The galvanostatic pulse test is not a suitable test for a stainless steel rebar with mill scale remaining on the bar. This is because the mill scale produces local variations in potential, which prevents the characteristic potential plateau developing when a current is applied. This issue may be minimized by increasing the polarization current; however, if a current is applied too high, then this may induce corrosion in the rebar, which affects the result of the test.

6.2 Recommendations

Based on the work done in this project, there are some recommendations for the application of the results and further work:

Due to lockdown and restricted laboratory activity at the onset and during the COVID-19 pandemic, the length of the longer-term exposure test was limited. In this study, the rebar was kept in a passive environment for 200 days and then 3 specimens of each surface condition were exposed to chlorides for 240 days. In practice, stainless steel rebar is expected to withstand annual application of de-icing salts or anti-icing brines for at least seven decades. The intention is to keep the remaining intact specimens for further evaluation for as long as possible.

A more extensive surface characterization of the rebar beyond visual inspection, as well as an investigation of the composition of the mill scale after the autopsy of the specimens, is recommended. However, the cement paste component of concrete bonds very well to stainless steel rebar. Therefore, there will be a layer of cement paste remaining when the bar is removed from the concrete or mortar specimen. There will be a challenge in attempting to remove the cement paste without also removing the surface layer of the rebar which is of interest for this study.

As stated earlier, the work in this study was carried out using UNS 32205 duplex stainless steel rebar from a single manufacturer. This study should be repeated on other grades of stainless

steel rebar to see whether the same conclusions can be extended for as-rolled rebar of other grades from different manufacturers.

A concentration of 15% by weight of sodium chloride was found to be insufficient to induce corrosion in UNS 32205 over the duration of this study. The concentration of chlorides should be increased, such that they are more effective in initiating corrosion on stainless steel, as well as be better at simulating de-icing agents used on infrastructure. Thus, this would produce a more representative result for a corrosion test. For instance, a commercial de-icing brine contains above 20% of chloride by weight [71]. This is significantly higher than the concentration specified by ASTM A955.

The specific volume of corrosion products of stainless steel should be determined to allow modelling of the stresses exerted on the concrete. The impact of any active corrosion on the concrete – stainless steel bond strength should be studied.

The galvanostatic pulse test was found to be not effective for stainless steel specimens with significant mill scale remaining on the surface of the rebar. A study should be conducted to investigate the optimal polarization current to be used, or a modification to the test procedure. This will improve the effectiveness of this test for evaluating corrosion activity on a stainless steel rebar with mill scale remaining.

7 References

[1] J. Lehne and F. Preston, “Making Concrete Change Innovation in Low-carbon Cement and Concrete,” London, United Kingdom, 2018. [Online]. Available: https://www.chathamhouse.org/sites/default/files/publications/2018-06-13-making-concrete-change-cement-lehne-preston-final.pdf.

[2] Royal Canadian Mounted Police, “Just the Facts – Winter driving,” 2019. https://www.rcmp-grc.gc.ca/en/gazette/just-the-facts-winter-driving (accessed Sep. 12, 2021).

[3] SnowKing1, “TowPlow and trucks on a Missouri rural Interstate (Licensed under CC-SA-3.0),” 2008. https://commons.wikimedia.org/wiki/File:TowPLow_front_view2.JPG (accessed Dec. 07, 2021).

[4] Canadian Standards Association, “CSA S6:19 - Canadian Highway Bridge Design Code.” CSA Group, Toronto, ON, p. 1185, 2019.

[5] A. Hering, “Corroded concrete and rebar at the bridge of Queen Elizabeth Way crossing the Welland River in Niagara Falls, Ontario, Canada (Licensed under CC-SA-3.0),” 2015. https://commons.wikimedia.org/wiki/File:Qew_bruecke_nf_beton_kaputt_33_von_46.jpg (accessed Dec. 07, 2021).

[6] D. A. Jones, *Principles and Prevention of Corrosion*, 2nd Editio. Upper Saddle River, NJ: Prentice-Hall, 1992.

[7] M. Pourbaix, *Atlas of Electrochemical Quilibria in Aqueous Solutions*, 2nd Englis. Houston, TX: National Association of Corrosion Engineers, 1974.

[8] C. M. Hansson, “Comments on electrochemical measurements of the rate of corrosion of steel in concrete,” *Cem. Concr. Res.*, vol. 14, no. 4, pp. 574–584, 1984, doi: 10.1016/0008-8846(84)90135-2.

[9] A. Poursaee and C. M. Hansson, “Potential pitfalls in assessing chloride-induced corrosion of steel in concrete,” *Cem. Concr. Res.*, vol. 39, no. 5, pp. 391–400, 2009, doi: 10.1016/j.cemconres.2009.01.015.

[10] J. P. Broomfield, *Corrosion of Steel in Concrete*, 2nd Editio. New York, NY: Taylor & Francis, 2007.

[11] P. Marcus, V. Maurice, and H. H. Strehblow, “Localized corrosion (pitting): A model of passivity breakdown including the role of the oxide layer nanostructure,” *Corros. Sci.*, vol. 50, no. 9, pp. 2698–2704, 2008, doi: 10.1016/j.corsci.2008.06.047.

[12] J. R. Davis, *ASM Specialty Handbook - Stainless Steels*. Materials Park, OH: ASM International, 1994.

[13] H. M. Cobb, *The History of Stainless Steel*. Materials Park, OH: ASM International, 2010.

[14] J. T. Pérez-Quiroz, J. Terán, M. J. Herrera, M. Martínez, and J. Genescá, “Assessment of stainless steel reinforcement for concrete structures rehabilitation,” *J. Constr. Steel Res.*, vol. 64, no. 11, pp. 1317–1324, 2008, doi: 10.1016/j.jcsr.2008.07.024.

[15] W. H. Hartt, “A Critical Review Of Corrosion Performance For Epoxy-Coated And Select Corrosion Resistant Reinforcements In Concrete Exposed To Chlorides,” 2012.

[16] A. Fahim, A. E. Dean, M. D. A. Thomas, and E. G. Moffatt, “Corrosion resistance of chromium-

steel and stainless steel reinforcement in concrete," *Mater. Corros.*, vol. 70, no. 2, pp. 328–344, 2019, doi: 10.1002/maco.201709942.

[17] C. M. Hansson, R. Haas, R. Green, R. C. Evers, O. K. Gepraegs, and R. Al Assar, "Corrosion Protection Strategies for Ministry Bridges: Final Report. MTO Consulting Assignment #9015-A-000034," Waterloo, ON., 2000.

[18] ASTM International and the Society of Automotive Engineers (SAE), *Metals and Alloys in the Unified Numbering System (UNS)*, 13th Editi. Warrendale, PA: SAE International, 2012.

[19] L. Bertolini, T. Pastore, F. Bolzoni, and P. Pedeferri, "Behaviour of stainless steel in simulated concrete pore solution," *Br. Corros. J.*, vol. 31, no. 3, pp. 218–222, 1996, doi: 10.1179/000705996798114572.

[20] J. H. Potgieter, P. A. Olubambi, L. Cornish, C. N. Machio, and E. S. M. Sherif, "Influence of nickel additions on the corrosion behaviour of low nitrogen 22% Cr series duplex stainless steels," *Corros. Sci.*, vol. 50, no. 9, pp. 2572–2579, 2008, doi: 10.1016/j.corsci.2008.05.023.

[21] M. C. Alonso, F. J. Luna, and M. Criado, "Corrosion behavior of duplex stainless steel reinforcement in ternary binder concrete exposed to natural chloride penetration," *Constr. Build. Mater.*, vol. 199, pp. 385–395, 2019, doi: 10.1016/j.conbuildmat.2018.12.036.

[22] C. B. Van Niejenhuis, S. Walbridge, and C. M. Hansson, "The performance of austenitic and duplex stainless steels in cracked concrete exposed to concentrated chloride brine," *J. Mater. Sci.*, vol. 51, no. 1, pp. 362–374, 2016, doi: 10.1007/s10853-015-9387-0.

[23] R. T. Loto, "Study of the corrosion behaviour of S32101 duplex and 410 martensitic stainless steel for application in oil refinery distillation systems," *J. Mater. Res. Technol.*, vol. 6, no. 3, pp. 203–212, 2017, doi: 10.1016/j.jmrt.2016.11.001.

[24] J. Ji, D. Darwin, and J. P. Browning, "Corrosion Resistance of Duplex Stainless Steels and MMFX Microcomposite Steel for Reinforced Concrete Bridge Decks," *Univ. Kansas Cent. Res. Inc*, no. 80, 2005.

[25] Y. Yu, S. Shironita, K. Souma, and M. Umeda, "Effect of chromium content on the corrosion resistance of ferritic stainless steels in sulfuric acid solution," *Heliyon*, vol. 4, no. 11, p. e00958, 2018, doi: 10.1016/j.heliyon.2018.e00958.

[26] A. Pardo, M. C. Merino, A. E. Coy, F. Viejo, R. Arrabal, and E. Matykina, "Pitting corrosion behaviour of austenitic stainless steels - combining effects of Mn and Mo additions," *Corros. Sci.*, vol. 50, no. 6, pp. 1796–1806, 2008, doi: 10.1016/j.corsci.2008.04.005.

[27] T. J. Mesquita, E. Chauveau, M. Mantel, N. Kinsman, V. Roche, and R. P. Nogueira, "Lean duplex stainless steels-The role of molybdenum in pitting corrosion of concrete reinforcement studied with industrial and laboratory castings," *Mater. Chem. Phys.*, vol. 132, no. 2–3, pp. 967–972, 2012, doi: 10.1016/j.matchemphys.2011.12.042.

[28] T. J. Mesquita, E. Chauveau, M. Mantel, N. Kinsman, and R. P. Nogueira, "Anomalous corrosion resistance behavior of Mo-containing SS in alkaline media: The role of microstructure," *Mater. Chem. Phys.*, vol. 126, no. 3, pp. 602–606, 2011, doi: 10.1016/j.matchemphys.2011.01.013.

[29] I. G. Ogunsanya and C. M. Hansson, "The Critical Chloride Concentration of Austenitic and Duplex Stainless Steel Reinforcing Bars," *Metall. Mater. Trans. A Phys. Metall. Mater. Sci.*, vol. 51, no. 9, pp. 4685–4694, 2020, doi: 10.1007/s11661-020-05874-2.

[30] P. Castro-Borges, O. T. De Rincón, E. I. Moreno, A. A. Torres-Acosta, M. Martínez-Madrid, and A.

Knudsen, “Performance of a 60-year-old concrete pier with stainless steel reinforcement,” *Mater. Perform.*, vol. 41, no. 10, pp. 50–55, 2002.

[31] S. Cho and J. Lee, “Metal recovery from stainless steel mill scale by microwave heating,” *Met. Mater. Int.*, vol. 14, no. 2, pp. 193–196, 2008, doi: 10.3365/met.mat.2008.04.193.

[32] M. F. Montemor, A. M. P. Simões, M. G. S. Ferreira, and M. Da Cunha Belo, “The role of Mo in the chemical composition and semiconductive behaviour of oxide films formed on stainless steels,” *Corros. Sci.*, vol. 41, no. 1, pp. 17–34, 1999, doi: 10.1016/S0010-938X(98)00126-7.

[33] L. F. Li, Z. H. Jiang, and Y. Riquier, “High-temperature oxidation of duplex stainless steels in air and mixed gas of air and CH4,” *Corros. Sci.*, vol. 47, no. 1, pp. 57–68, 2005, doi: 10.1016/j.corsci.2004.05.008.

[34] I. Saeki *et al.*, “Growth process of protective oxides formed on type 304 and 430 stainless steels at 1273 K,” *Corros. Sci.*, vol. 40, no. 8, pp. 1295–1305, 1998.

[35] L. Hamadou, A. Kadri, and N. Benbrahim, “Impedance investigation of thermally formed oxide films on AISI 304L stainless steel,” *Corros. Sci.*, vol. 52, no. 3, pp. 859–864, 2010, doi: 10.1016/j.corsci.2009.11.004.

[36] N. Sato, “An overview on the passivity of metals,” *Corros. Sci.*, vol. 31, no. C, pp. 1–19, 1990, doi: 10.1016/0010-938X(90)90086-K.

[37] M. G. S. Ferreira, N. E. Hakiki, G. Goodlet, S. Faty, A. M. P. Simões, and M. Da Cunha Belo, “Influence of the temperature of film formation on the electronic structure of oxide films formed on 304 stainless steel,” *Electrochim. Acta*, vol. 46, no. 24–25, pp. 3767–3776, 2001, doi: 10.1016/S0013-4686(01)00658-2.

[38] N. E. Hakiki, M. F. Montemor, M. G. S. Ferreira, and M. Da Cunha Belo, “Semiconducting properties of thermally grown oxide films on AISI 304 stainless steel,” *Corros. Sci.*, vol. 42, no. 4, pp. 687–702, 2000, doi: 10.1016/S0010-938X(99)00082-7.

[39] T. D. Marcotte and C. M. Hansson, “Corrosion products that form on steel within cement paste,” *Mater. Struct. Constr.*, vol. 40, no. 3, pp. 325–340, 2007, doi: 10.1617/s11527-006-9170-4.

[40] P. Ghods, O. B. Isgor, G. A. McRae, J. Li, and G. P. Gu, “Microscopic investigation of mill scale and its proposed effect on the variability of chloride-induced depassivation of carbon steel rebar,” *Corros. Sci.*, vol. 53, no. 3, pp. 946–954, 2011, doi: 10.1016/j.corsci.2010.11.025.

[41] R. G. Pillai and D. Trejo, “Surface Condition Effects on Critical Chloride Threshold of Steel Reinforcement,” *ACI Mater. J.*, pp. 103–109, 2005.

[42] M. F. Hurley and J. R. Scully, “Threshold chloride concentrations of selected corrosion resistant rebar materials compared to carbon steel,” *NACE - Int. Corros. Conf. Ser.*, vol. 2005-April, no. October, pp. 892–905, 2005.

[43] L. Ding and A. Poursaee, “The impact of sandblasting as a surface modification method on the corrosion behavior of steels in simulated concrete pore solution,” *Constr. Build. Mater.*, vol. 157, pp. 591–599, 2017, doi: 10.1016/j.conbuildmat.2017.09.140.

[44] L. F. Li and J. P. Celis, “Pickling of austenitic stainless steels (a review),” *Can. Metall. Q.*, vol. 42, no. 3, pp. 365–376, 2003, doi: 10.1179/cmq.2003.42.3.365.

[45] I. G. Ogunsanya and C. M. Hansson, “Reproducibility of the corrosion resistance of UNS S32205 and UNS S32304 stainless steel reinforcing bars,” *Corrosion*, vol. 76, no. 1, 2020, doi:

10.5006/3360.

[46] B. L. Gabriel, “Scanning Electron Microscopy,” in *ASM Handbook Volume 12: Fractography*, Materials Park, OH: ASM International, 1987, pp. 166–178.

[47] A. Benninghoven, “Chemical Analysis of Inorganic and Organic Surfaces and Thin Films by Static Time-of-Flight Secondary Ion Mass Spectrometry (TOF-SIMS),” *Angew. Chemie Int. Ed. English*, vol. 33, no. 10, pp. 1023–1043, 1994, doi: 10.1002/anie.199410231.

[48] D. W. Mogk, “Time-of-Flight Secondary Ion Mass Spectrometry (ToF-SIMS),” *Science Education Resource Center*. https://serc.carleton.edu/research_education/geochemsheets/techniques/ToFSIMS.html (accessed Dec. 16, 2021).

[49] M. Schönning, S. Randström, and M. Adair, “Chloride tolerance of stainless steel reinforcement using an accelerated in-concrete method,” 2011.

[50] P. G. H. Loudfoot, “The Adaptation of a Rapid Screening Test to Rank the Corrosion Behaviour of Stainless Steel Reinforcing Bars in Concrete,” University of Waterloo, 2018.

[51] C. B. Van Niejenhuis, T. W. Bandura, and C. M. Hansson, “Evaluation of the proposed European test procedure for ranking stainless steel rebar,” *Corrosion*, vol. 72, no. 6, pp. 834–842, 2016, doi: 10.5006/2000.

[52] Ontario Provincial Standards, “OPSS.PROV 1002: Material Specification for Aggregates - Concrete.” Ontario, Canada, 2018.

[53] Ontario Provincial Standards, “OPSS.PROV 1350: Material Specification for Concrete - Materials and Production.” Ontario, Canada, 2019.

[54] C. B. Van Niejenhuis, I. G. Ogunsanya, and C. M. Hansson, “Analysis of pore solution of different cements with and without admixed chlorides,” *ACI Mater. J.*, vol. 117, no. 3, pp. 21–28, 2020, doi: 10.14359/51724590.

[55] ASTM International, “ASTM A955-09: Standard Specification for Deformed and Plain Stainless Steel Bars for Concrete Reinforcement,” p. 11, 2009.

[56] A. Michel and B. J. Pease, “Moisture ingress in cracked cementitious materials,” *Cem. Concr. Res.*, vol. 113, no. August, pp. 154–168, 2018, doi: 10.1016/j.cemconres.2018.08.009.

[57] C. M. Hansson, A. Poursaee, and S. J. Jaffer, “Corrosion of Reinforcing Bars in Concrete,” 2012, doi: 10.3323/jcorr1954.18.3_110.

[58] ASTM International, “ASTM G59-97: Standard Test Method for Conducting Potentiodynamic Polarization Resistance Measurements.” ASTM International, West Conshohocken, PA., p. 4, 2014, doi: https://doi.org/10.1520/G0059-97R20.

[59] M. . Stern and A. L. Geary, “Electrochemical Polarization: I. A Theoretical Analysis of t h e Shape of Polarization Curves,” *J. Electrochem. Soc.*, vol. 104, no. 1, p. 751, 1957, doi: 10.1149/1.2428473.

[60] C. Andrade and J. A. Gonzalez, “Quantitative Measurements of Corrosion Rate of Reinforcing Steels Embedded in Concrete Using Polarization Resistance Measurements.,” *Werkstoffe und Korrosion*, vol. 29, no. 8, pp. 515–519, 1978, doi: 10.1002/maco.v29:8.

[61] C. J. Newton and J. M. Sykes, “A galvanostatic pulse technique for investigation of steel corrosion in concrete,” *Corros. Sci.*, vol. 28, no. 11, pp. 1051–1074, 1988, doi: 10.1016/0010-

938X(88)90101-1.

[62] M. J. Hunt, “Effects of De-icing and Anti-icing Chemicals on the Durability of Reinforcing Steel in Concrete,” University of Waterloo, 2013.

[63] I. G. Ogunsanya, “Evaluation of the Corrosion Behaviour of Continuously Galvanized Rebar,” University of Waterloo, 2016.

[64] E. Hamada *et al.*, “Direct imaging of native passive film on stainless steel by aberration corrected STEM,” *Corros. Sci.*, vol. 52, no. 12, pp. 3851–3854, 2010, doi: 10.1016/j.corsci.2010.08.025.

[65] Y. Gui, Z. J. Zheng, and Y. Gao, “The bi-layer structure and the higher compactness of a passive film on nanocrystalline 304 stainless steel,” *Thin Solid Films*, vol. 599, pp. 64–71, 2016, doi: 10.1016/j.tsf.2015.12.039.

[66] V. Maurice, W. P. Yang, and P. Marcus, “X-Ray Photoelectron Spectroscopy and Scanning Tunneling Microscopy Study of Passive Films Formed on (100) Fe-18Cr-13Ni Single-Crystal Surfaces,” *J. Electrochem. Soc.*, vol. 145, no. 3, pp. 909–920, 1998, doi: 10.1149/1.1838366.

[67] G. Lorang, M. Da Cunha Belo, A. M. P. Simões, and M. G. S. Ferreira, “Chemical Composition of Passive Films on AISI 304 Stainless Steel,” *J. Electrochem. Soc.*, vol. 141, no. 12, pp. 3347–3356, 1994, doi: 10.1149/1.2059338.

[68] B. B. S. Phull and R. M. Kain, “Corrosion and Protection of Structures in Marine Atmospheres,” *STRUCTURE magazine*, no. August, 2004.

[69] P. Som, “Personal Communications.” Hamilton ON., 2021.

[70] C. Fu, D. Fang, H. Ye, L. Huang, and J. Wang, “Bond degradation of non-uniformly corroded steel rebars in concrete,” *Eng. Struct.*, vol. 226, no. October 2020, p. 111392, 2021, doi: 10.1016/j.engstruct.2020.111392.

[71] C. B. Van Niejenhuis and C. M. Hansson, “Detrimental Effects of Anti-Icing Brines on Concrete Durability,” *Concr. Int.*, vol. 41, no. 11, pp. 30–34, 2019.

A. Appendix A: Construction Drawing of Longer-Term Exposure Test Specimen

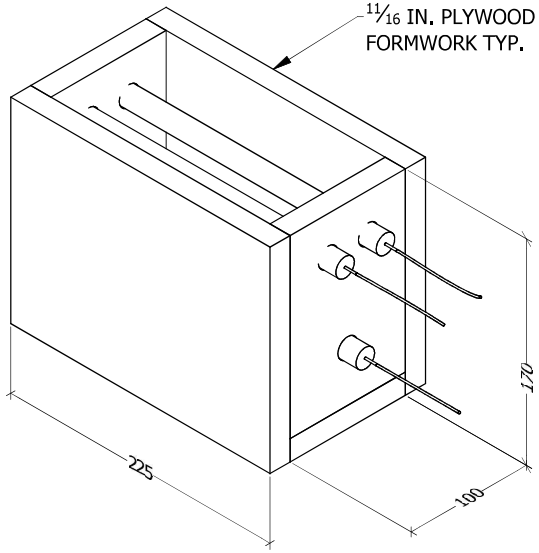

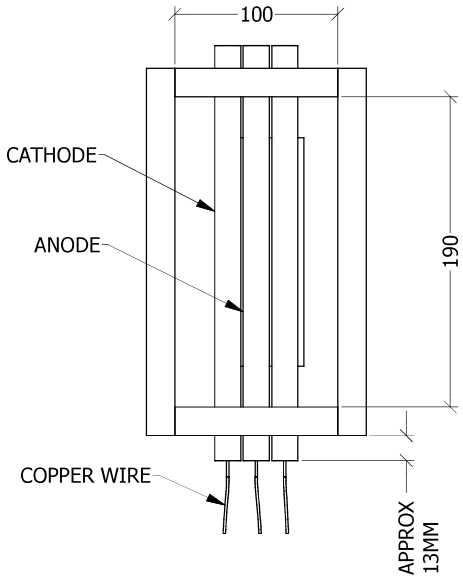

PLAN VIEW

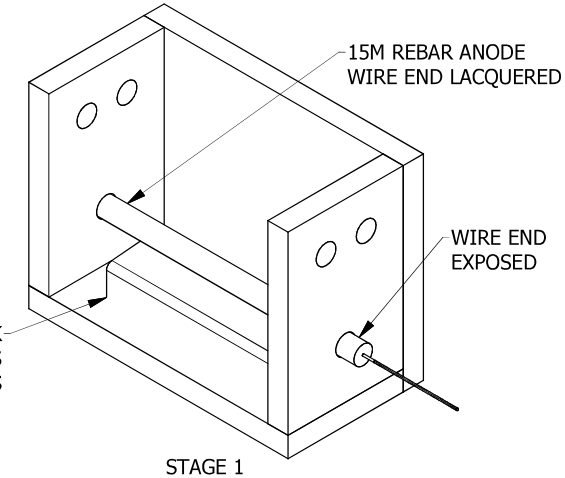

STAGE 1
ANODE AND EMBEDDED FOAM

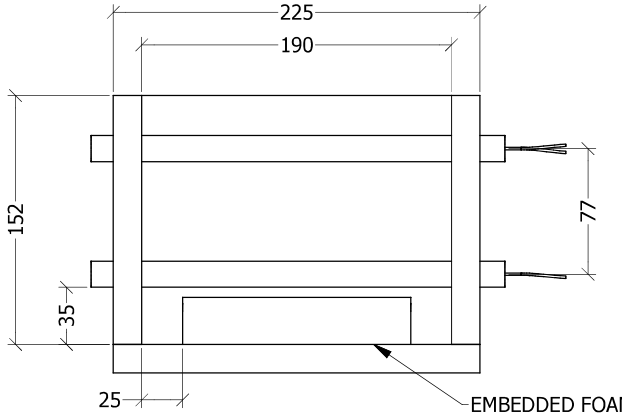

SIDE ELEVATION

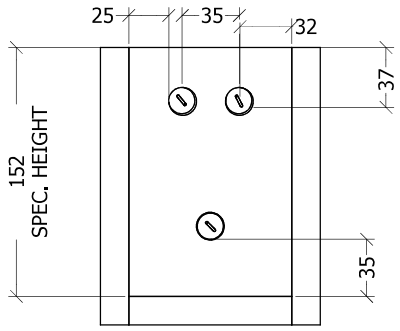

FRONT ELEV

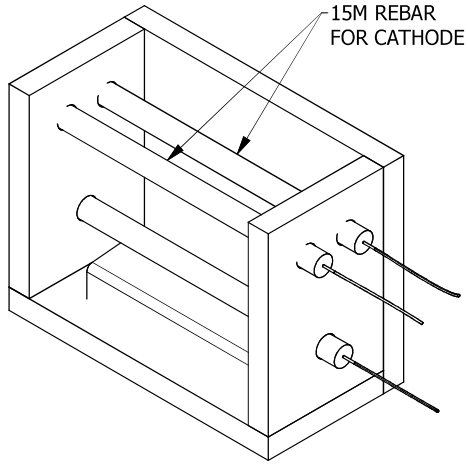

STAGE 2
CATHODE LAYOUT

DRAWN FY	24-JUN-2020		
CHECKED			
QA		TITLE	
MFG			
APPROVED			
		SIZE D	DWG NO Dwg_Specimen_small REV
		SCALE 1 : 1.5	SHEET 2 OF 4

B. Appendix B: Construction Drawing of Specimen Clamp Frame for Concrete Saw Cutting

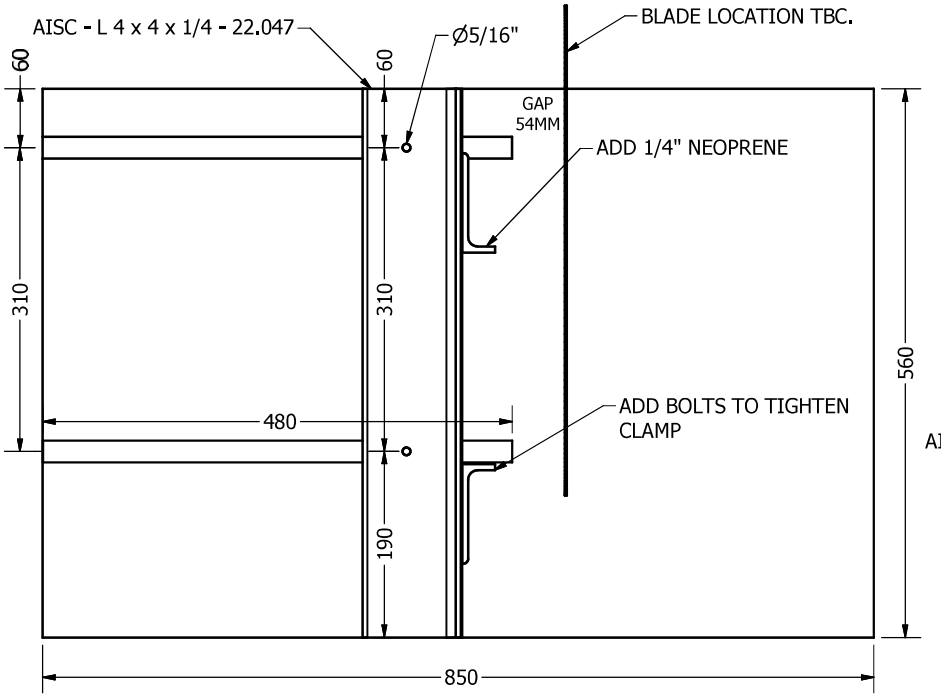

OVERALL PLAN VIEW

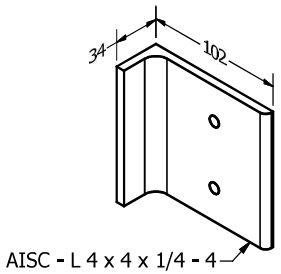

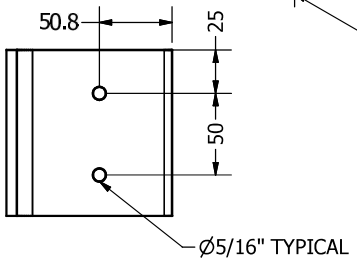

CLAMP

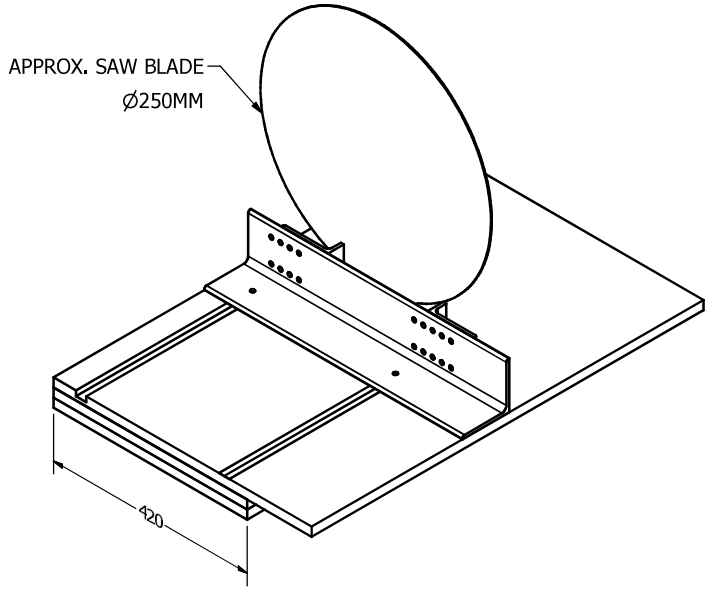

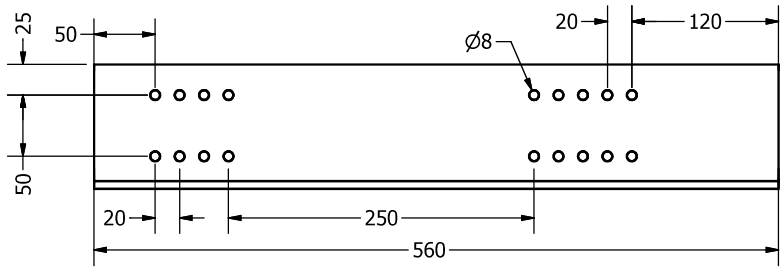

SIDE FENCE HOLE PROFILE

DRAWN fyyan	25-Nov-2021	
CHECKED		TITLE: SPECIMEN HOLDER FOR CONCRETE SAW
QA		
MFG		
APPROVED		
SIZE B		DWG NO Drawing_Clamp01 — REV 2.1
SCALE 1/5		SHEET 1 OF 1

C. Appendix C: Rebar Specimen Images Before and After Rapid Screening Test

The following images show the condition of the rebar specimens before being cast in concrete and immediately after removal from concrete when the rapid screening test had been completed.

Note: Images of specimens 01 and 02 for all surface conditions are not included in this section. This is because the images for those specimens were taken 24 hours after the specimens were autopsied instead of immediately after removal from the concrete. Corrosion product is seen on the bars in those photographs even though none were present when inspected immediately after cutting open the concrete. These bars had oxidized in atmosphere and displayed corrosion product which was not a direct result of the rapid screening test, so they are no longer representative of the condition of the bars after testing.

AR-03

Figure C-1: Specimen AR-03 before testing (top) and after testing (bottom)

AR-04

\

Figure C-2: Specimen AR-04 before testing (top) and after testing (bottom)

AR-05

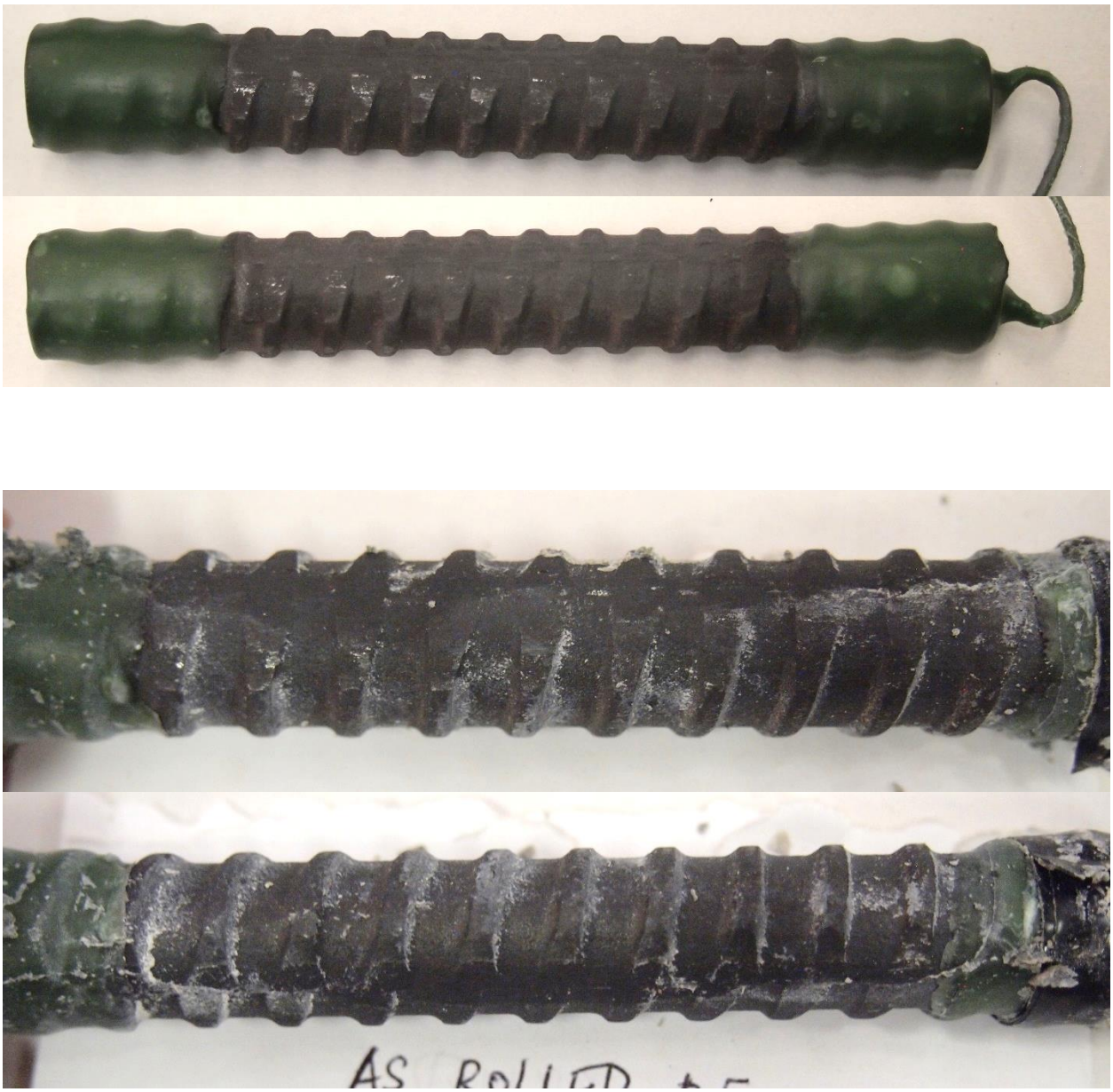

Figure C-3: Specimen AR-05 before testing (top) and after testing (bottom)

AR-06

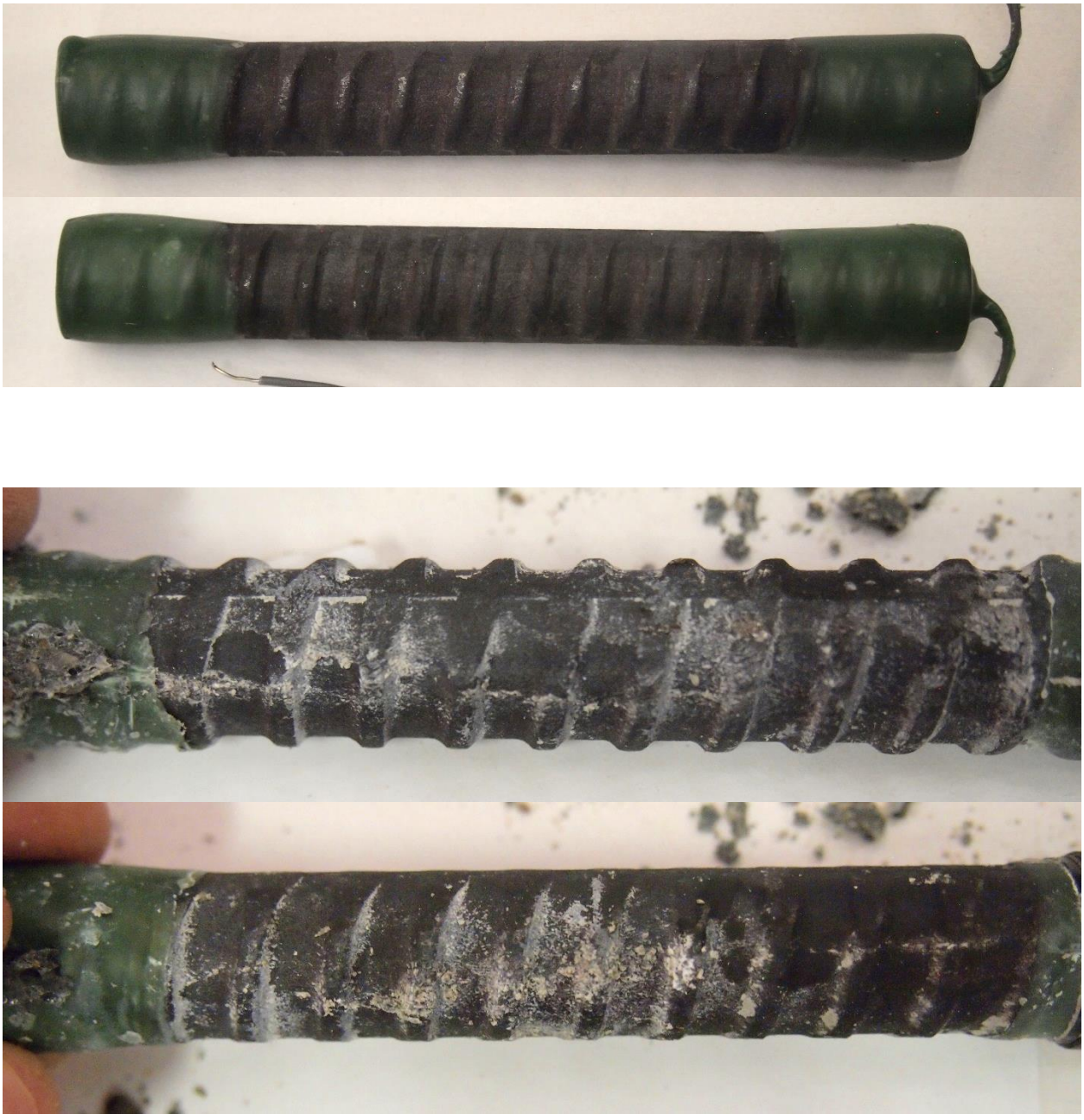

Figure C-4: Specimen AR-06 before testing (top) and after testing (bottom)

PK-03

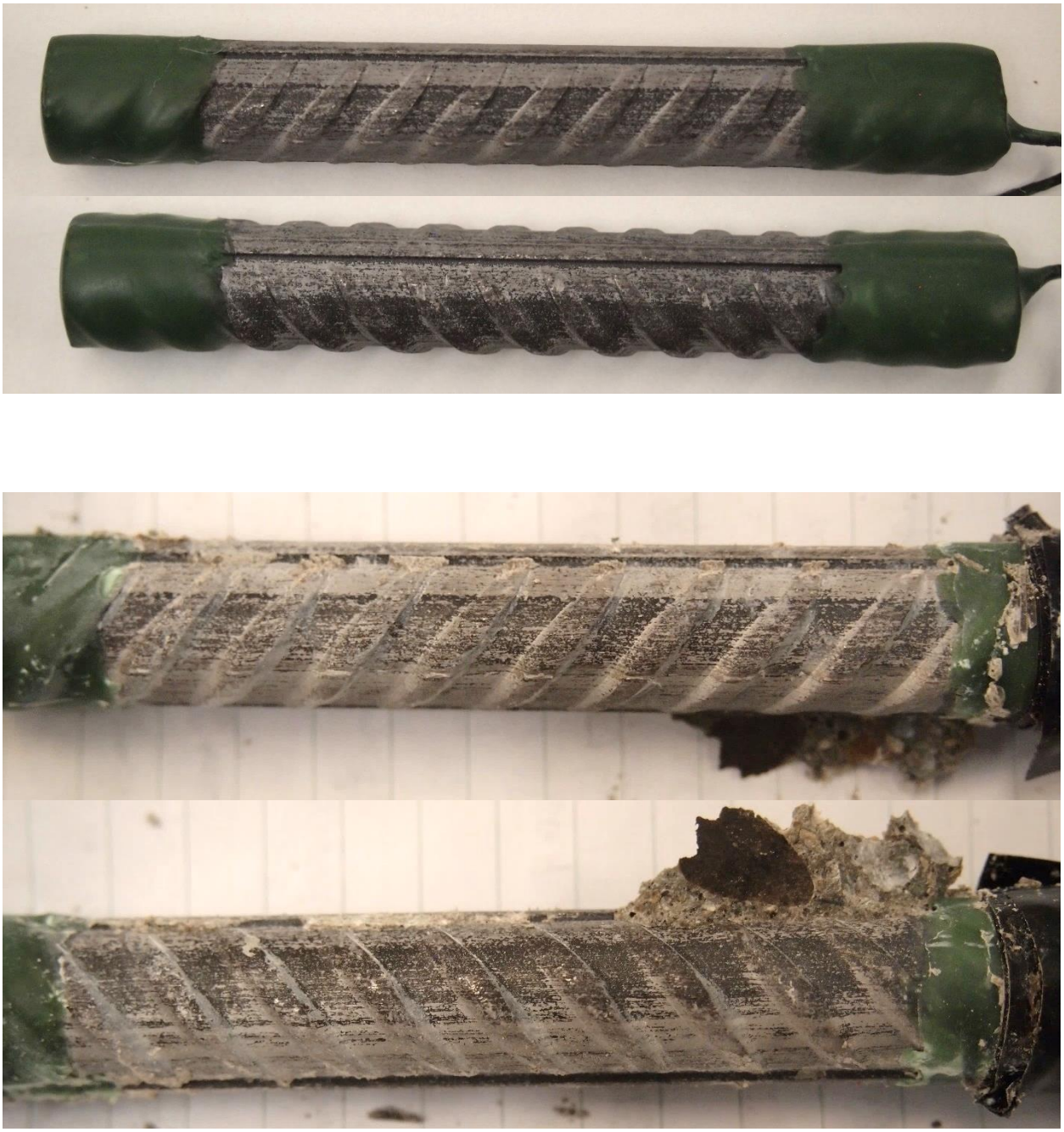

Figure C-5: Specimen PK-03 before testing (top) and after testing (bottom)

PK-04

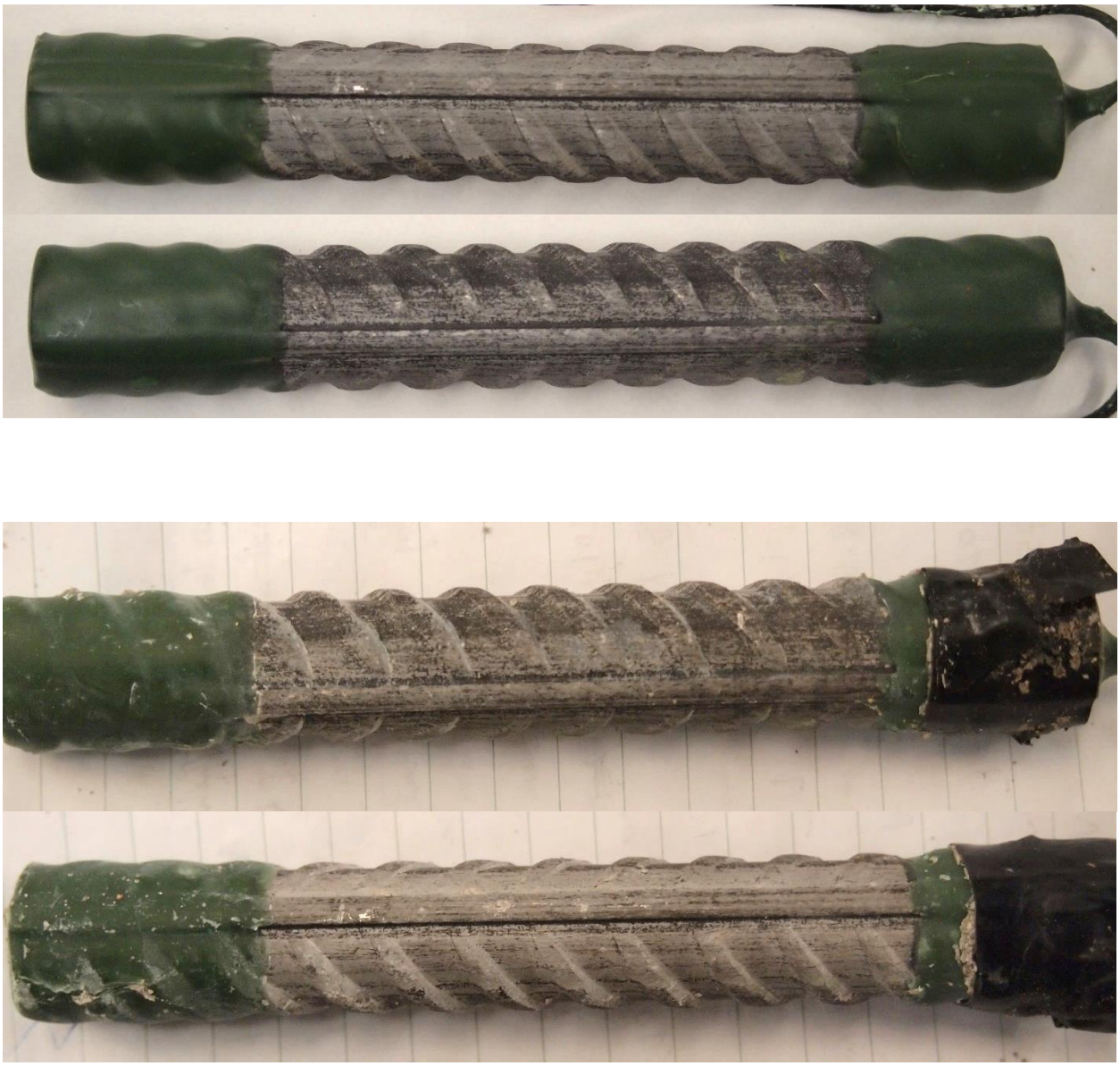

Figure C-6: Specimen PK-04 before testing (top) and after testing (bottom)

PK-05

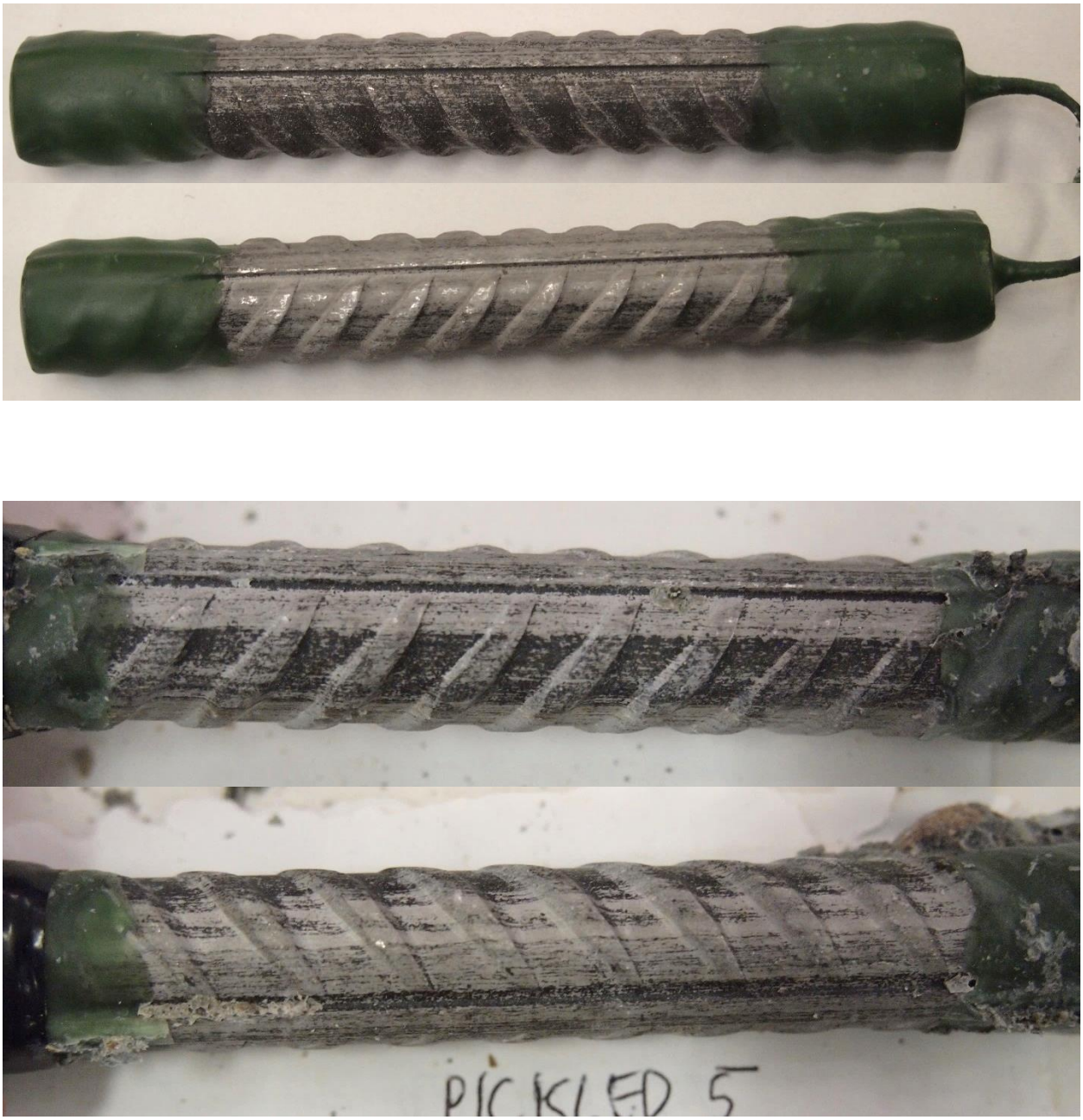

Figure C-7: Specimen PK-05 before testing (top) and after testing (bottom)

PK-06

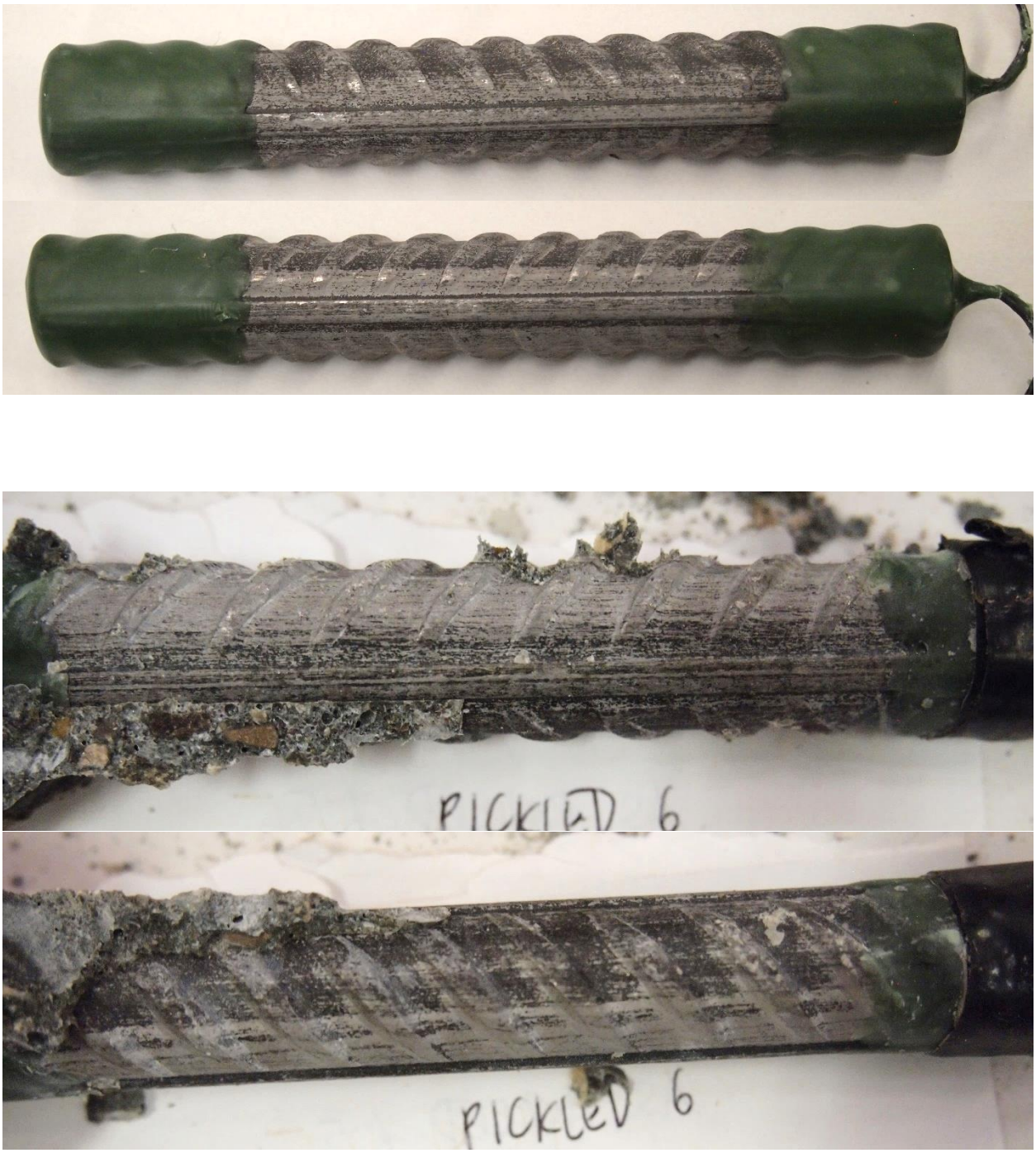

Figure C-8: Specimen PK-06 before testing (top) and after testing (bottom)

PKSB-03

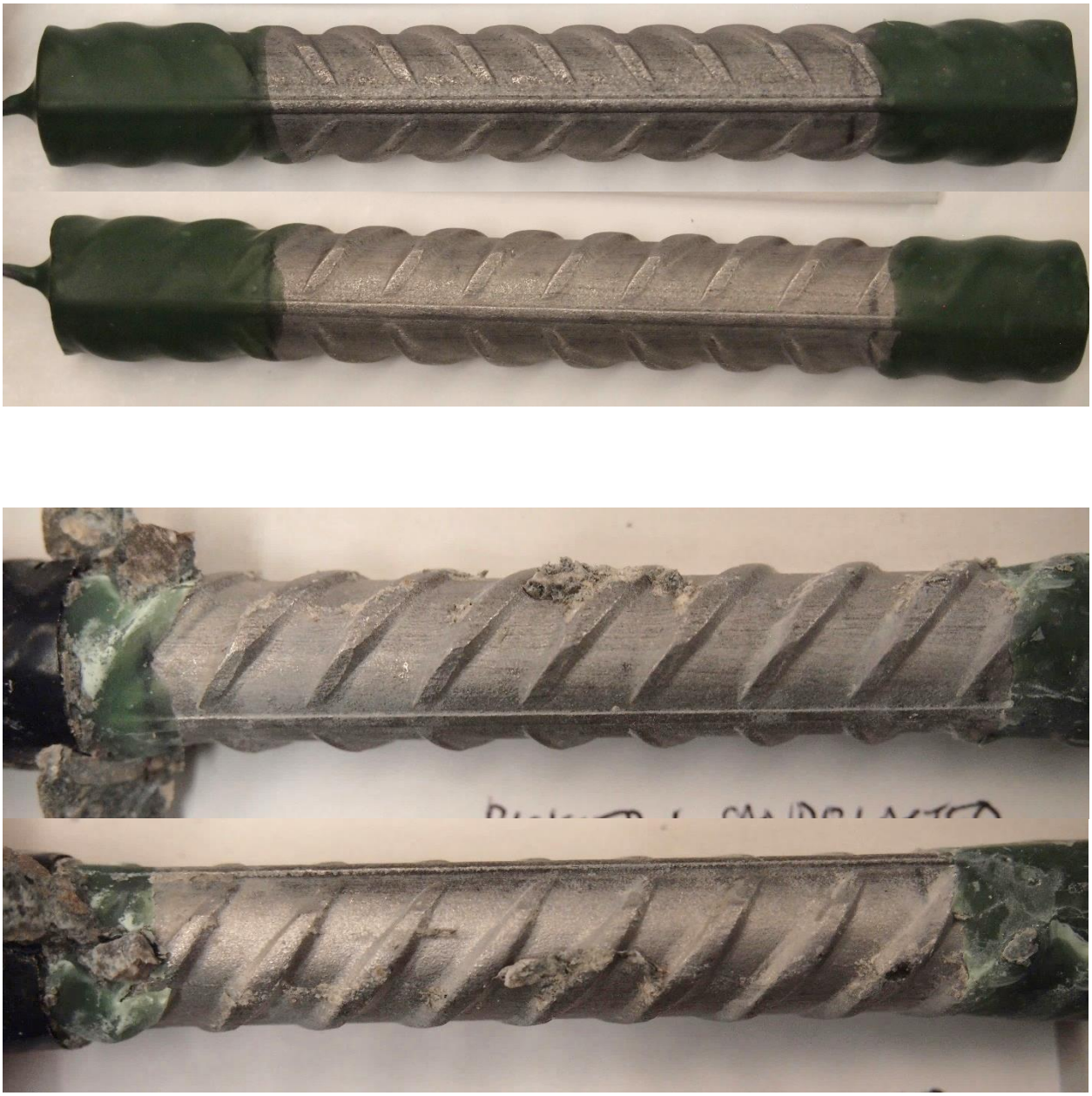

Figure C-9: Specimen PKSB-03 before testing (top) and after testing (bottom)

PKSB-04

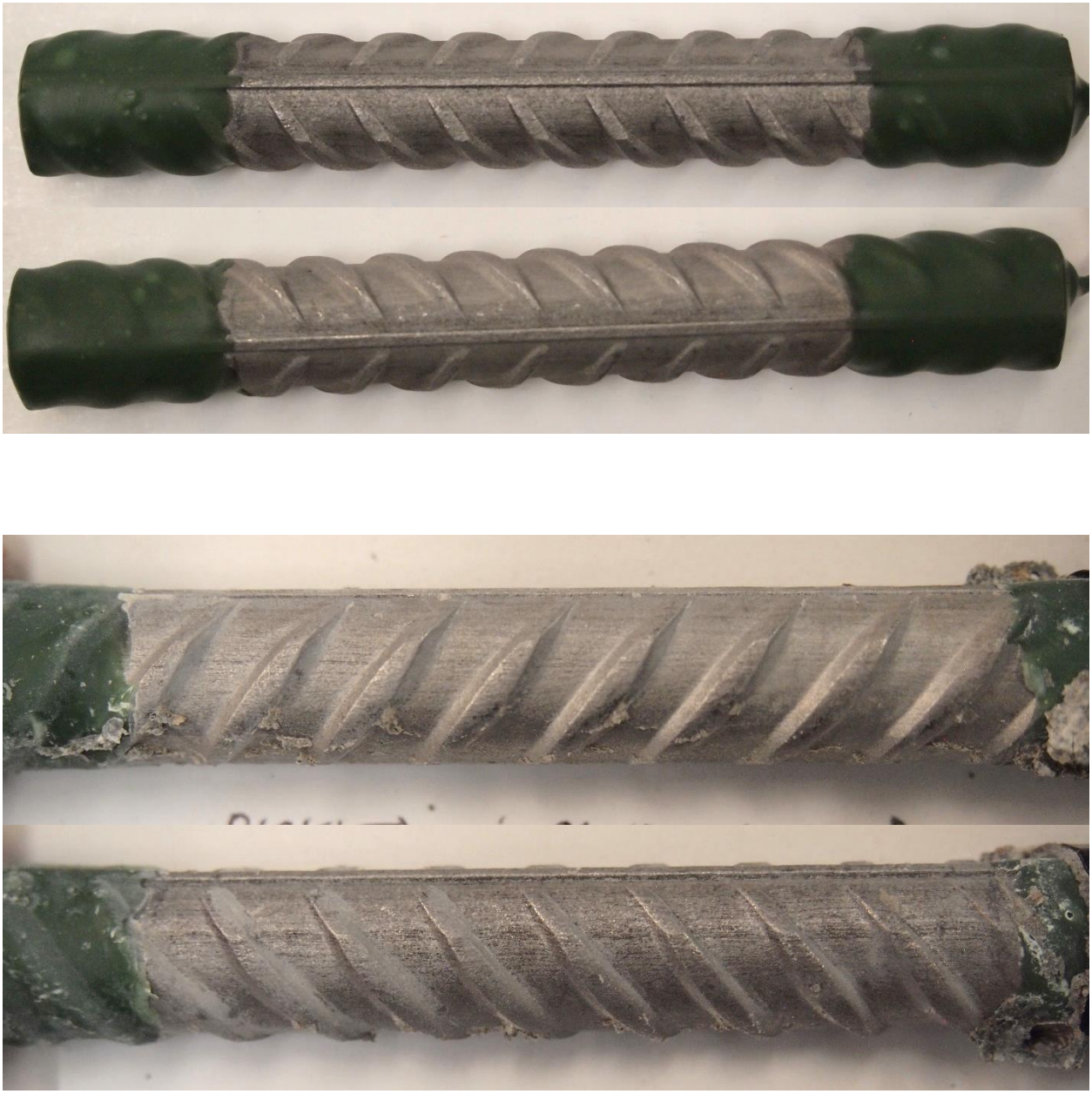

Figure C-10: Specimen PKSB-04 before testing (top) and after testing (bottom)

PKSB-05

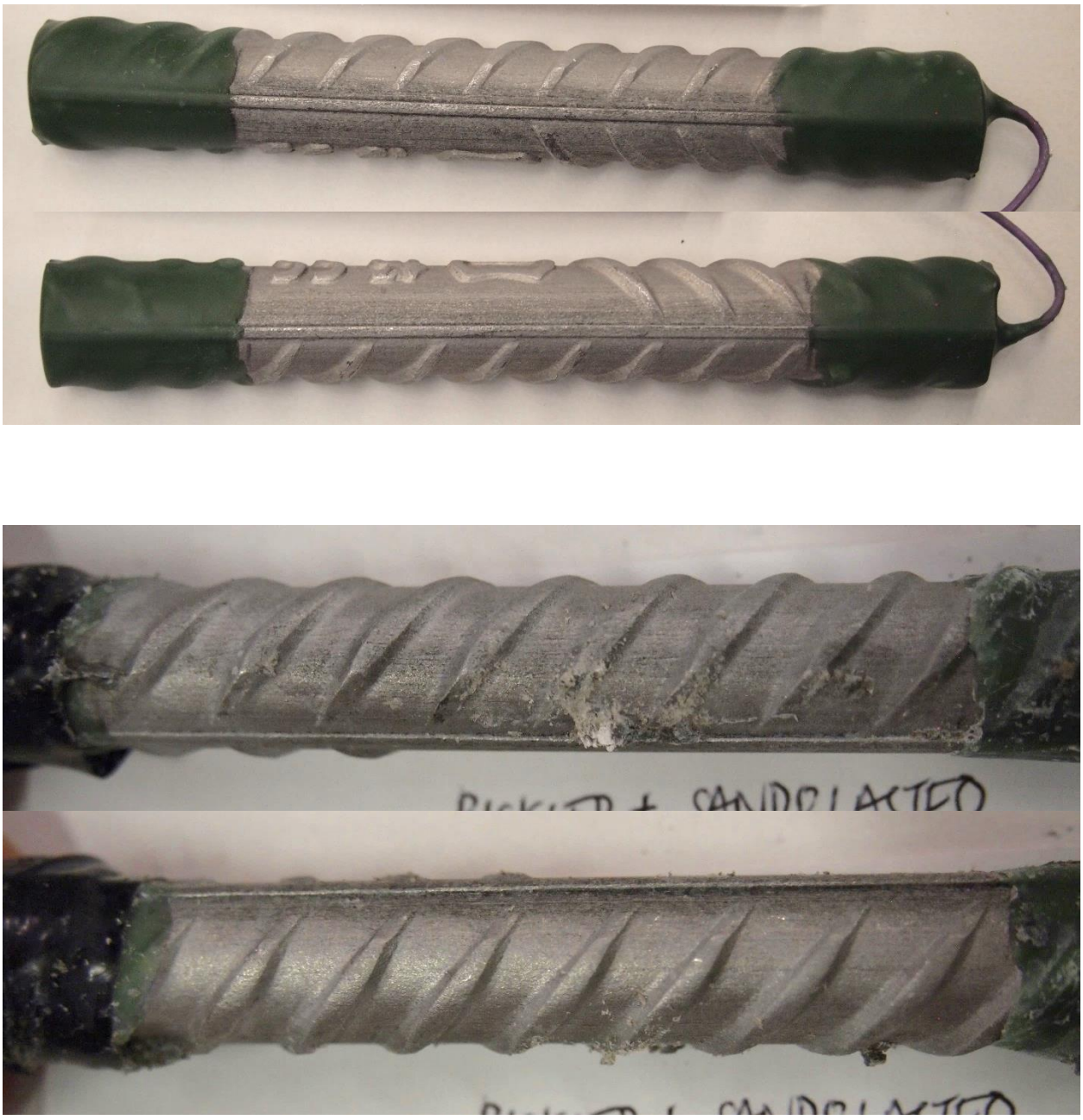

Figure C-11: Specimen PKSB-05 before testing (top) and after testing (bottom)

PKSB-06

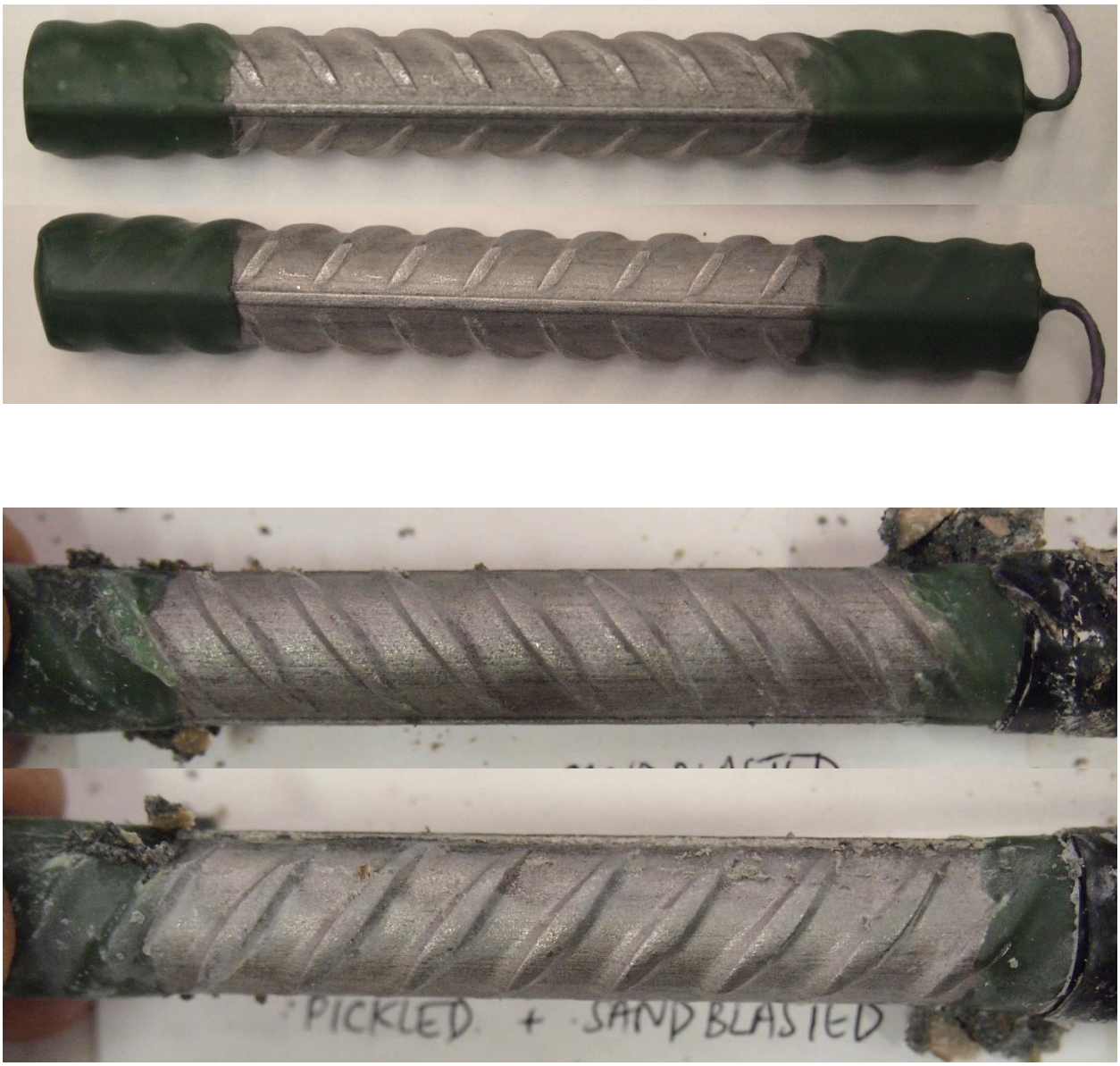

Figure C-12: Specimen PKSB-06 before testing (top) and after testing (bottom)

PKSBT-03

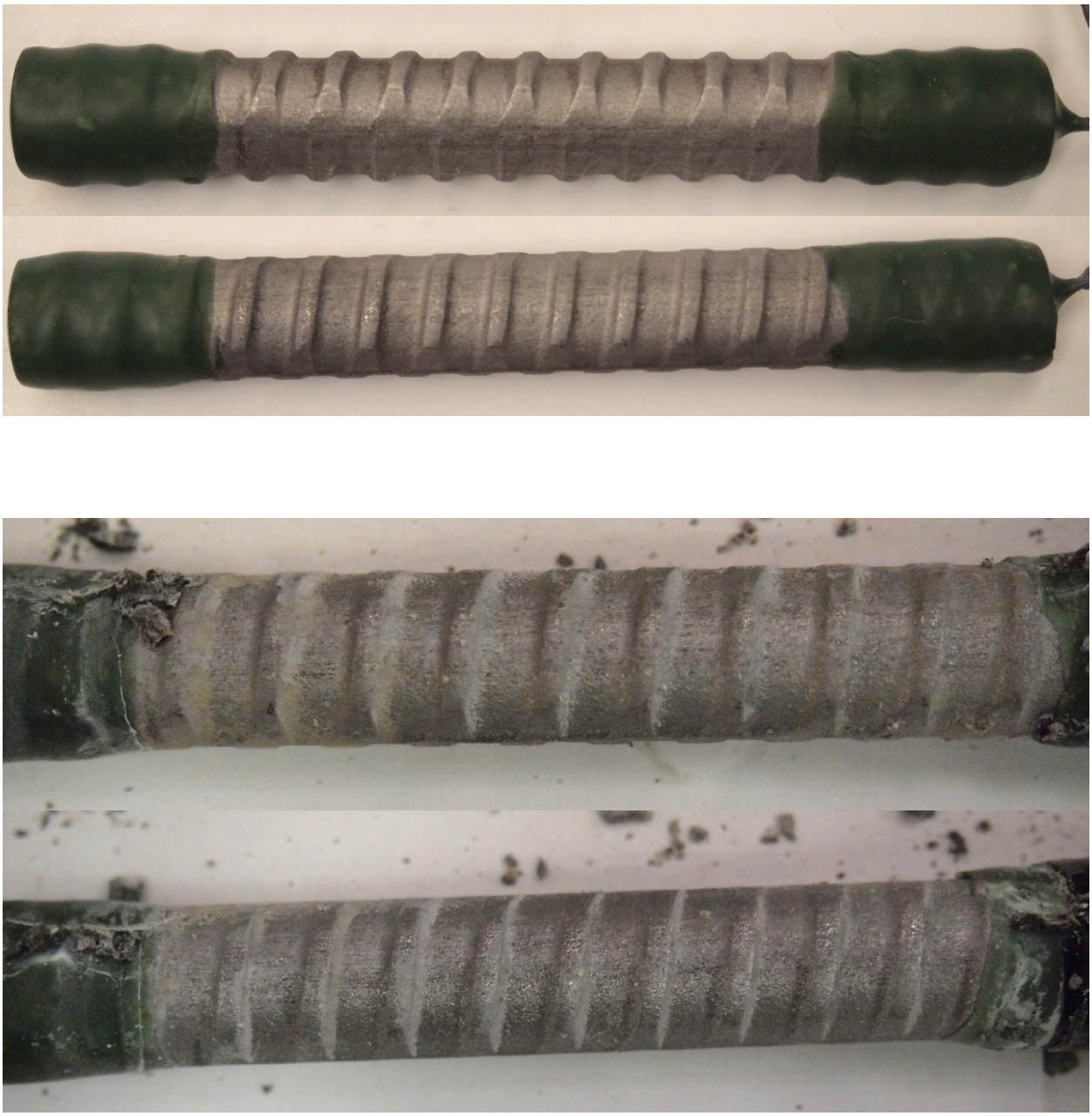

Figure C-13: Specimen PKSBT-03 before testing (top) and after testing (bottom)

PKSBT-04

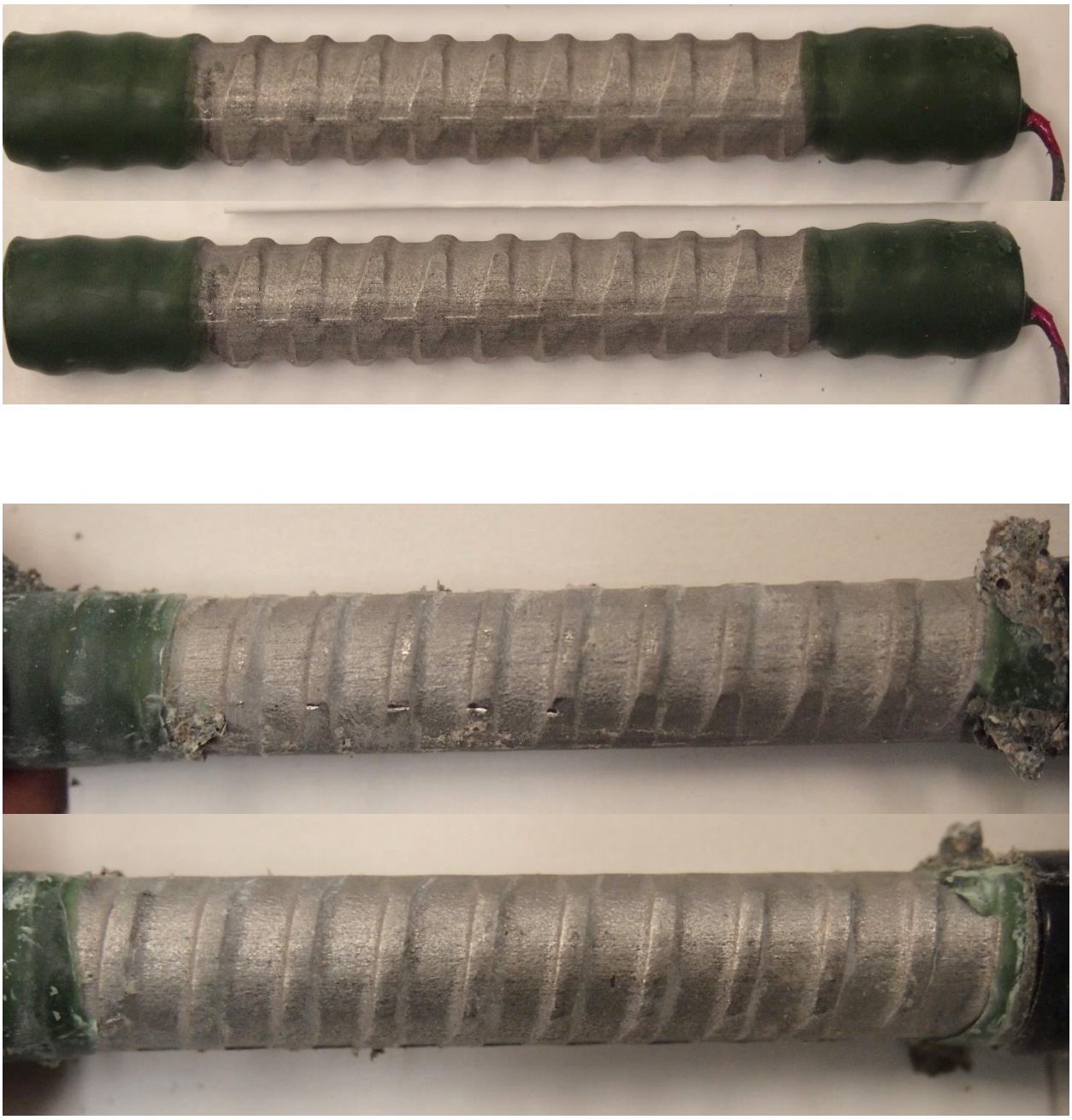

Figure C-14: Specimen PKSBT-04 before testing (top) and after testing (bottom)

PKSBT-05

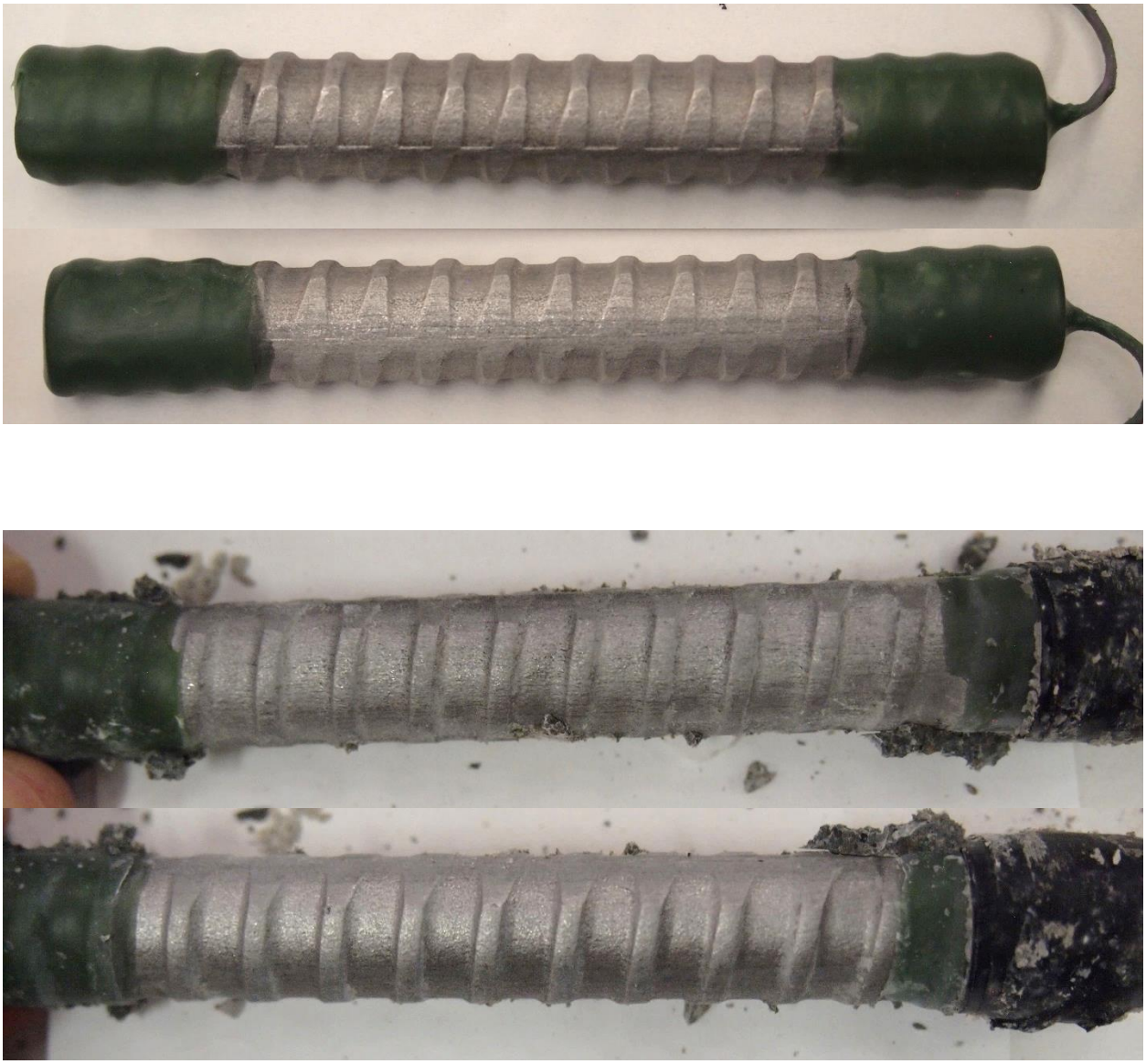

Figure C-15: Specimen PKSBT-05 before testing (top) and after testing (bottom)

PKSBT-06

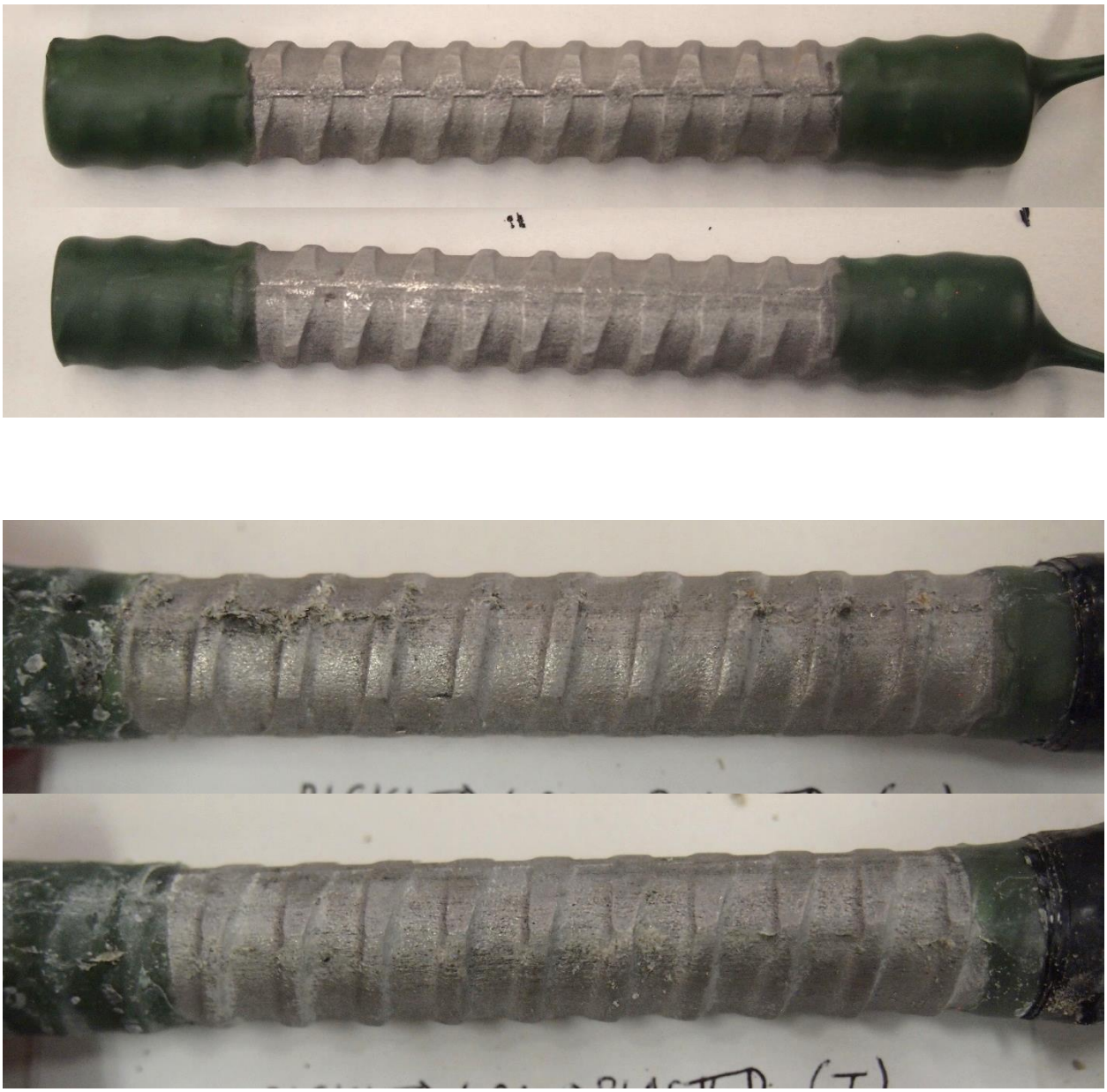

Figure C-16: Specimen PKSBT-06 before testing (top) and after testing (bottom)

SBO-03

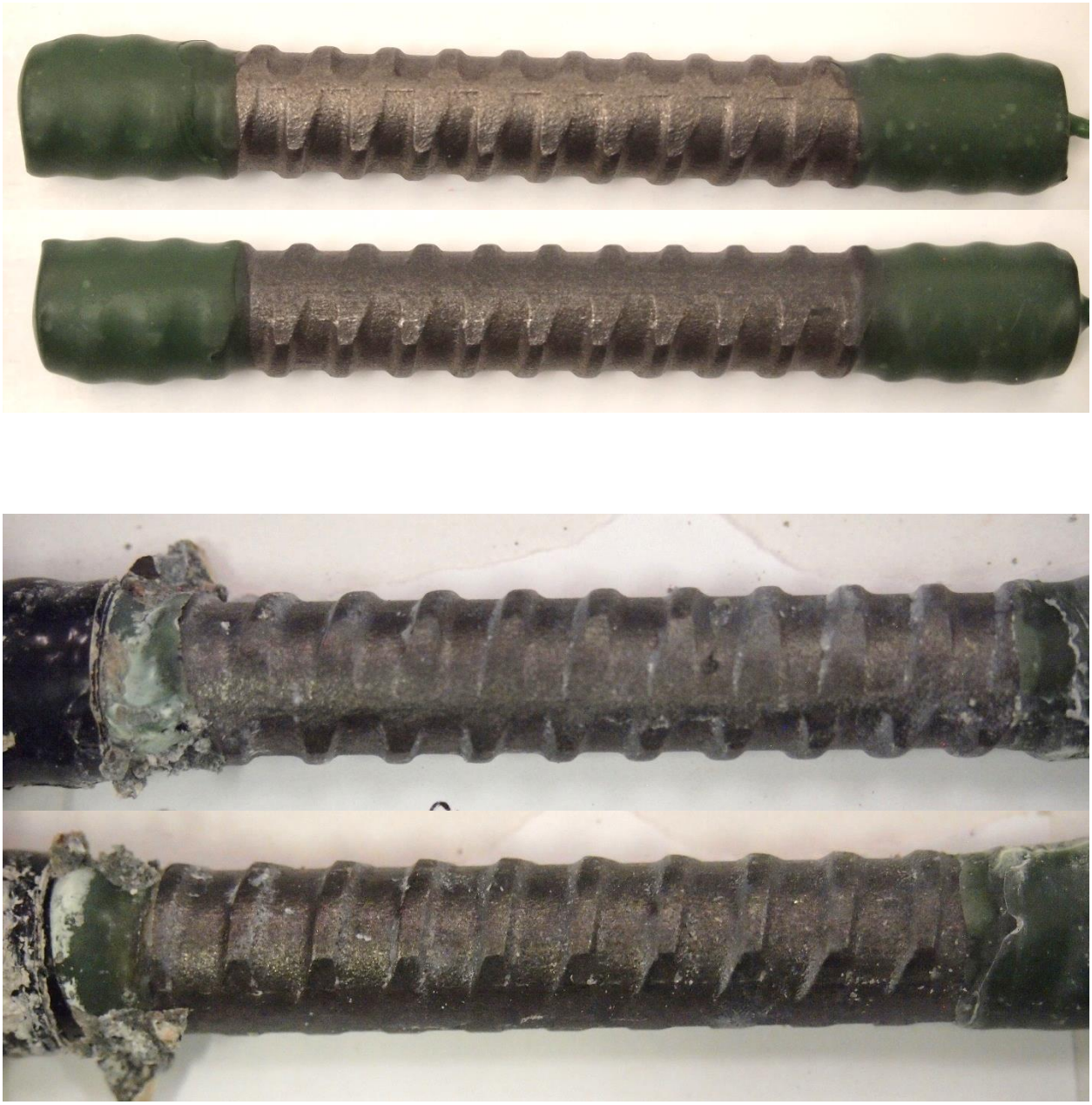

Figure C-17: Specimen SBO-03 before testing (top) and after testing (bottom)

SBO-04

Figure C-18: Specimen SBO-04 before testing (top) and after testing (bottom). Corrosion product observed on rebar surface after testing

Figure C-19: Corrosion product observed on SBO-04 (top) and (bottom) some corrosion product observed on concrete

Figure C-20: Corrosion product found under the lacquer at rebar ends on SBO-04 due to crevice corrosion

SBO-05

Figure C-21: Specimen SBO-05 before testing (top) and after testing (bottom)

SBO-06

Figure C-22: Specimen SBO-06 before testing (top) and after testing (bottom). Corrosion product observed on rebar and on concrete surface in contact with rebar

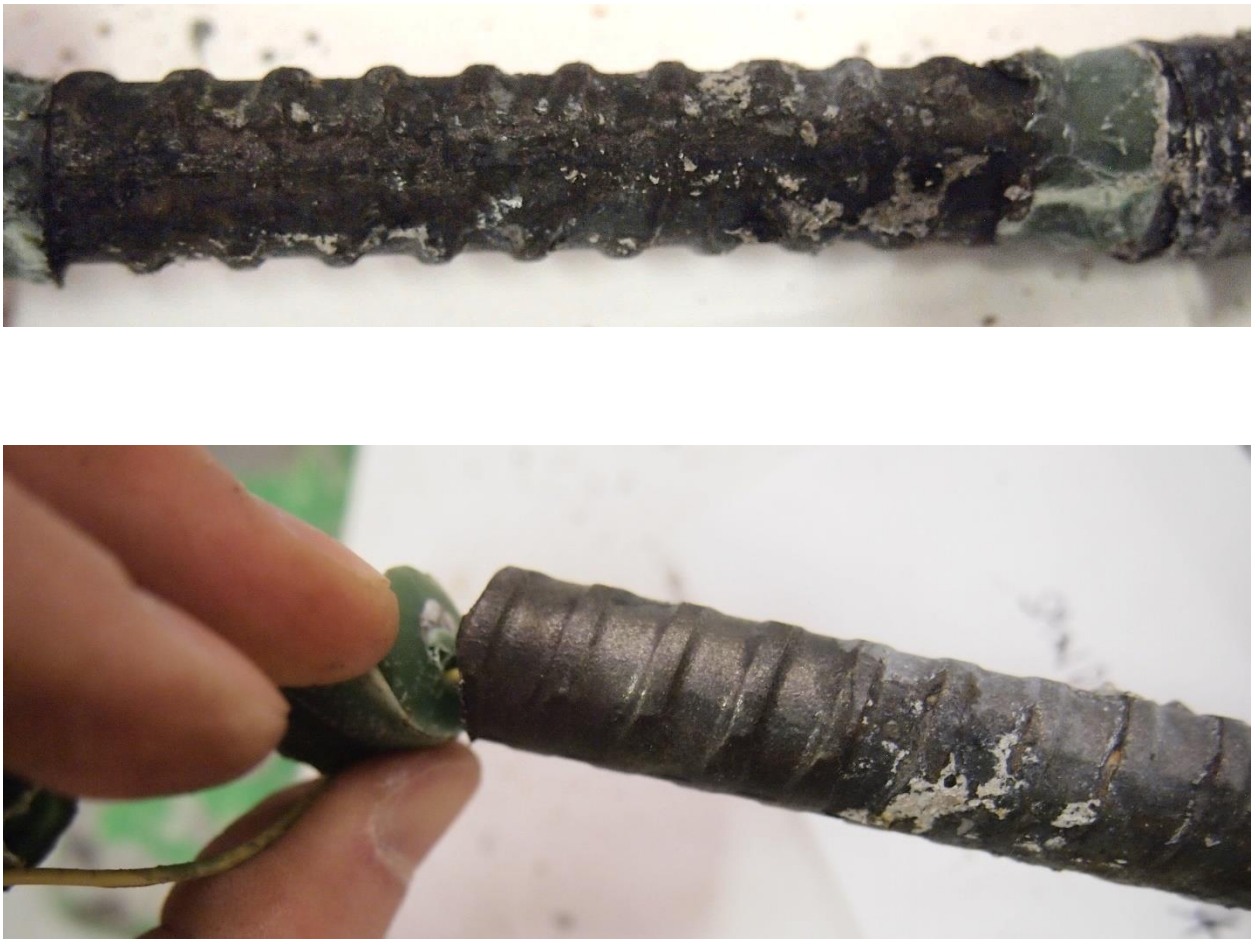

Figure C-23: Corrosion product observed on surface of SBO-06 (top). No corrosion product was found when lacquer at rebar ends were removed

D. Appendix D: Rebar Specimen Images Before and After Longer-Term Exposure Test

The following images show the condition of the rebar specimens before testing and after 440 days in mortar. The specimens were exposed to 15% by weight sodium chloride solution for final 240 days before autopsy.

For all specimens shown, the top image shows the condition of the rebar specimens before being cast into mortar, while the bottom shows the condition of the rebar after autopsy.

AR-(i)

AR-(iv)

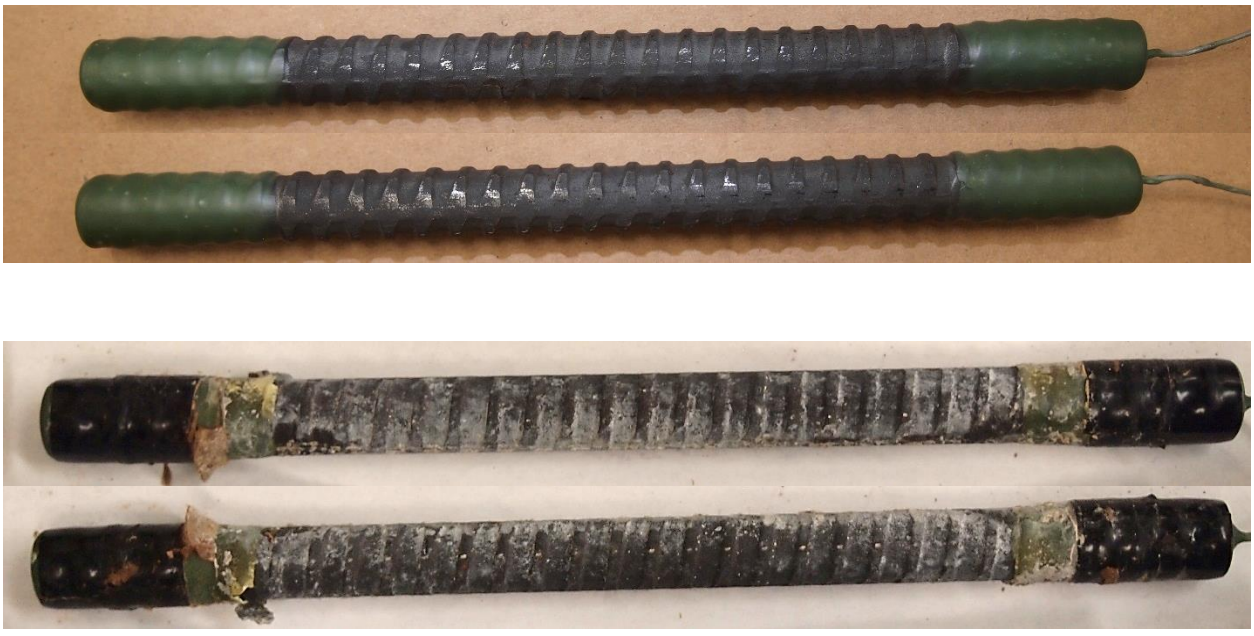

PK-(i)

PK-(iv)

PKSB-(i)

PKSB-(iv)

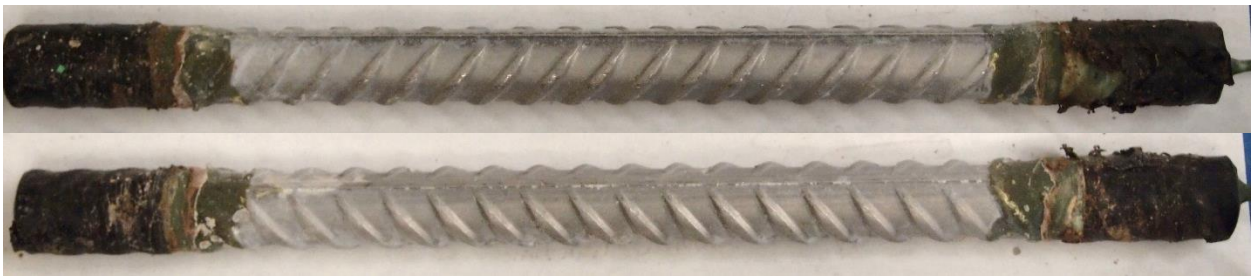

PKSBT-(i)

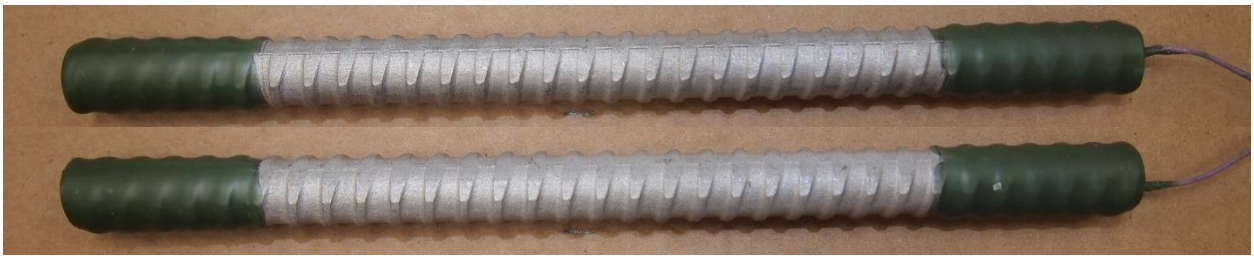

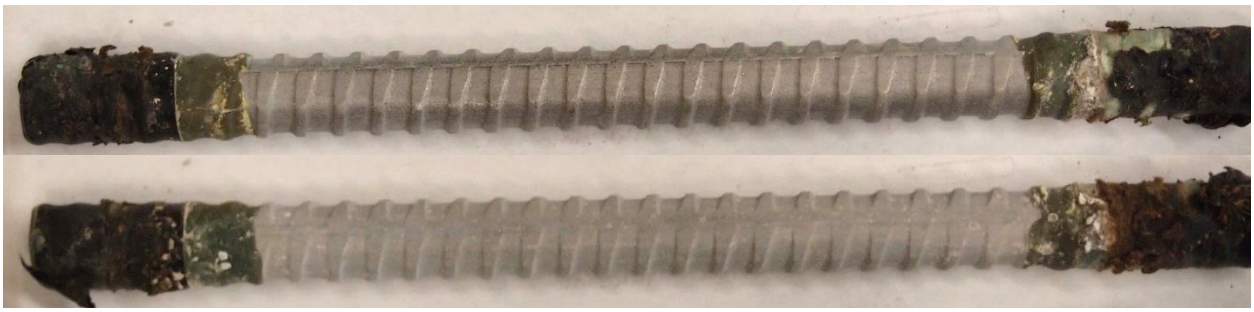

PKSBT-(iv)

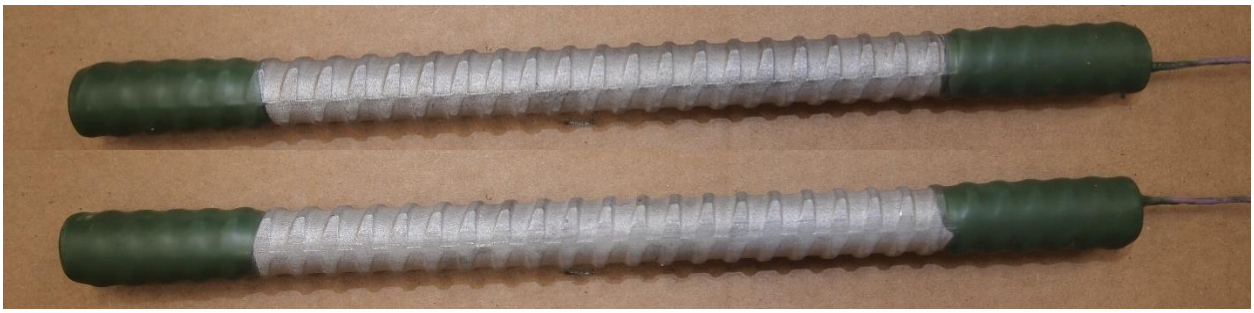

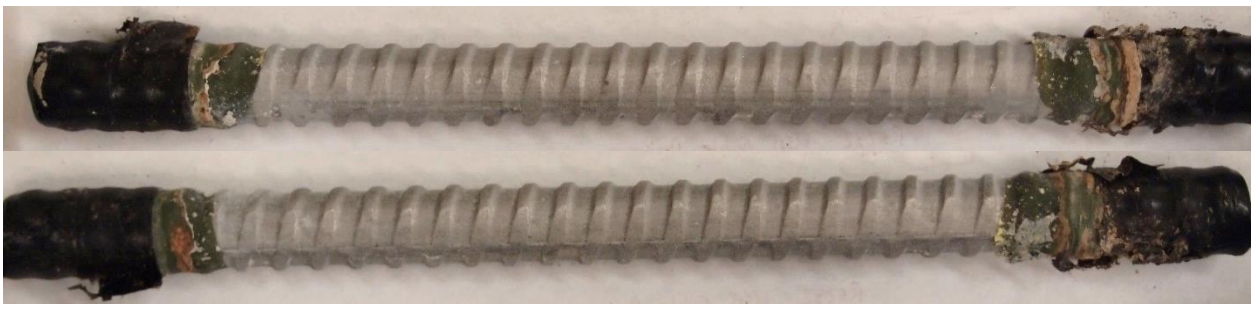

SBO-(i)

SBO-(iv)